FROM NIPAH VIRUS HOST INFECTION
TO THE PRODUCTION OF NEW VIRAL PARTICLES

A Dissertation

Presented to the Faculty of the Graduate School

of Cornell University

In Partial Fulfillment of the Requirements for the Degree of

Doctor of Philosophy

by

Gunner Pete Johnston

May 2019

FROM NIPAH VIRUS HOST INFECTION
TO THE PRODUCTION OF NEW VIRAL PARTICLES

Gunner Pete Johnston, Ph. D.

Cornell University 2019

ABSTRACT: Nipah virus (NiV) belongs to the viral family *Paramyxoviridae* and is a pathogen of significant threat to global human health and agriculture. The absence of approved vaccines or treatments for NiV, severe human mortality reaching 100% rates in recent outbreaks, and the identification of at least twenty related viruses, underlines the urgency with which NiV and related pathogens should be studied. Despite prior reports that the NiV matrix (M) protein is the only viral protein significantly involved in particle formation and budding, we report that the NiV fusion (F) protein supports budding by enriching incorporation of the NiV attachment (G) protein into particles. Further, we report that this novel function of NiV F is dependent on motifs within its cytoplasmic tail, indicating potential dependence on cellular machinery. These findings were expanded upon with isolation of viral particles produced from different combinations of F, G, and M and subsequent proteomic analysis of such particles. These analyses and validation identified F-driven budding as most associated with cellular machinery, particularly vesicular trafficking and the actin cytoskeleton. Cellular factors involved in regulating endocytosis and recycling as well as ESCRTs were highly modulatory of F budding whether F was expressed alone or co-expressed with G and

M. Finally, by broadening our use of high-throughput and bioinformatic technologies to “live” NiV infection at bio-safety level 4 conditions, we describe a novel study offering a comprehensive overview of infection. This multi-omics approach, combining transcriptomics, proteomics, metabolomics, and lipidomics indicated drastic changes to human cells affecting major processes including immune response, metabolism, and gene expression. Interestingly, we report substantial decreases in the abundance of proteins involved in translation, however, proteins associated with numerous, specific processes such as RNA processing exhibited dramatic enrichment. Interestingly, we also report major discrepancies between transcriptomics and proteomics, suggesting probable regulation of post-transcriptional protein expression during infection. Metabolic and lipidomic profiles supported shunting of glucose into nucleotide synthesis, the use of glutamine in anaplerosis, and the use of triglyceride catabolism to support cellular function. These findings have not been reported before for a henipavirus infection, begging further studies into their importance to infection.

BIOGRAPHICAL SKETCH

Gunner P. Johnston was born in Vancouver, Washington and started high school a year early at the local La Center High School. In the middle of his freshman year, he transferred to CAM High School. For the last two years of high school, Gunner enrolled in a dual-credit program that allowed him to attend the local community college full-time. After earning his A.A. *with honors* from Clark College, Gunner was accepted to study at Washington State University at Vancouver. In 2014, he earned his B.S. in Biology *summa cum laude* at the age of 19. Gunner then moved to Pullman, Washington where he was accepted into the Ph.D. of Molecular Biosciences program at Washington State University. After his first year, he began research with his advisor Dr. Hector Aguilar-Carreno. Halfway through his third year as a Ph.D. student at Washington State University, Dr. Aguilar-Carreno moved his laboratory to Cornell University and Gunner transferred to the Department of Microbiology and Immunology at Cornell University from where he earned his doctorate in 2019.

DEDICATION

For guiding me through this process, I give my sincerest thanks to my advisor, Dr. Hector Aguilar-Carreno and the members of my committee: Dr. Ruth Collins, Dr. Volker Vogt, and Dr. Gary Whitaker.

There are many people that I can think of who have been instrumental in getting me this far into my education. I want to thank my parents: Christina, Keith, and Dave as well as my grandmother Dorene for all of their support and love. I also want to thank my siblings: Tonya, Terry Jr., Keith Jr., Kevin, Kristen, Jonah, Benjamin, and Daniel for all the memories we share and how each of you have helped me grow as a person. I would never forget my oldest friends: Christopher, Alexander, and Brandon all of whom I consider my brothers. Thank you, Jewel, for all of your love, patience, and support. You carried me through the most difficult parts of this Ph.D.

I don't think I would have survived graduate school with my sanity intact if it weren't for the wonderful, dysfunctional band of people I refer to as my lab mates. Whether it was duck jokes with Jackie, philosophical conversations with Liz, dancing and silliness with Erik, dinner and board games with Daniel and Victoria, or fishing with David, I have come to care about each of you and wish you the best after graduate school. I fondly remember our times playing D&D and eating wings at the ZZU. Thank you to the post-docs and research faculty: Birgit, Abrrey, Duncan, Gaby, and Fikret for our meaningful scientific discussions, they have helped me expand my understanding. Finally, I want to thank my many co-authors and students who have helped me with the research described in this dissertation and have taught me how to be a teacher. To all of you and anyone I missed, thank you for making graduate school a family experience.

ACKNOWLEDGMENTS

The work described here was made possible through: the hard work of my co-authors, the guidance of my advisor and committee, the generous donation of materials by Drs. Ruth Collins (Cornell University) and Fuyuhiko Tamanoi (UCLA), and by our generous funding sources.

I would like to acknowledge the Journal of Virology of the American Society for Microbiology publishing group for publishing my first manuscript and for allowing its incorporation into this dissertation.

The studies described here were supported by several sources of funding. Among them were:

- NIH/NIAID grant AI109022 to Hector Aguilar-Carreno
- NIH/NIGMS training grant T32GM008336 to Gunner P. Johnston, Erik M. Contreras, and Victoria Ortega
- Department of Homeland Security (DHS) Science and Technology Directorate (S&T) under Contract HSHQPM-14-X-00238 to Joshua N. Adkins and Katrina Waters, with a sub-contract to Hector Aguilar-Carreno

TABLE OF CONTENTS

Biographical Sketch iii
Dedication iv
Acknowledgments v
Table of Contents vi
List of Figures vii
List of Tables viii

Chapter 1: Studying Nipah Virus through the Lens of Host-Pathogen Interaction 1
Nipah Virus: An Introduction 1
Nipah Virus Infection 3
Viral Budding 5
Budding and the Cell 7
The Proteomic Approach to Budding 9
Beyond Budding: High-throughput Analyses of NiV Infection 9

Chapter 2: Cytoplasmic Motifs in the Nipah Virus Fusion Protein Modulate Virus Particle Assembly and Egress 20
Introduction 23
Results 26
Discussion 38
Methods 42

Chapter 3: Nipah Virus-Like Particle Egress is Modulated by Cytoskeletal and Vesicular Trafficking Pathways: a Proteomics Analysis 51
Introduction 55
Methods 58
Results 65
Discussion 80

Chapter 4: Multi-platform 'omics' analyses of live Nipah virus infection of mammalian cells 93
Introduction 96
Methods 99
Results 107
Discussion 127

Conclusion: 142

LIST OF FIGURES

Chapter 1
Fig. 1.1 3
Fig. 1.2 5
Fig. 1.3 7
Fig. 1.4 11

Chapter 2
Fig. 2.1 27
Fig. 2.2 29
Fig. 2.3 30
Fig. 2.4 32
Fig. 2.5 34
Fig. 2.6 35
Fig. 2.7 36
Fig. 2.8 37

Chapter 3
Fig. 3.1 66
Fig. 3.2 68
Fig. 3.3 73
Fig. 3.4 75
Fig. 3.5 77
Fig. 3.6 79

Chapter 4
Fig. 4.1 108
Fig. 4.2 110
Fig. 4.3 112
Fig. 4.4 113
Fig. 4.5 115
Fig. 4.6 118
Fig. 4.7 121
Fig. 4.8 123
Fig. 4.9 125

LIST OF TABLES

Chapter 3
Table 3.1 70-71

Chapter 4
Table 4.1 ..... Included in a supplemental file
Table 4.2 ..... Included in a supplemental file

CHAPTER 1

STUDYING NIPAH VIRUS THROUGH THE LENS OF HOST-PATHOGEN INTERACTION

Nipah Virus: An Introduction

The viral family *Paramyxoviridae* includes several human pathogens with major impacts on human health such as measles, mumps, and the parainfluenza viruses. The deadliest paramyxoviruses, however, are Nipah virus (NiV) and Hendra virus (HeV), the founding members of the genus *Henipavirus* (1). The first henipavirus, HeV, was discovered in Queensland, Australia in 1994 after the deaths of more than a dozen horses and their trainer by a novel negative-sense single-stranded paramyxovirus (2). Four years after the discovery of HeV, a viral outbreak occurred in pigs and humans in Malaysia and was originally attributed to Japanese Encephalitis due to the widespread symptoms of encephalitis for people infected (3). After closer study, a new virus related to HeV, NiV, was found to be the causative agent for the 257 cases leading to 105 human deaths, carrying a mortality rate ~41% (4, 5). Together NiV and HeV would then serve as the foundation for the new genus Henipavirus. While pigs were infected easily by NiV but generally exhibited minimal mortality, significant coughing and their roles in spreading NiV to humans led to over 1 million being culled to quell the spread of the outbreak (5).

Since 1998, many more outbreaks of NiV have occurred in Southeast Asia, primarily in India, Bangladesh, and the Phillipines (6–11). Interestingly, the outbreaks since 1998 have primarily been associated with a second strain of NiV, which shares

nearly 92% genome sequence identity and has exhibited higher mortality rates (~75%) as compared to the 1998-1999 Malaysian outbreak (11). Since its discovery, NiV has been identified as capable of transmission between humans and as able to infect many species of mammals (8, 9, 12, 13). NiV is generally transmitted through bodily fluids, aerosols, and the ingestion of date palm sap infected by the fruit bat reservoirs of flying fox genus *Pteropus* (1, 7, 9, 14, 15).

Based on the absence of approved vaccines or treatments and the threat these viruses pose to human health, both NiV and HeV are classified as Priority Category C Pathogens requiring biosafety level 4 containment (16). Moreover, the World Health Organization recently listed NiV among the most likely pathogens to cause a major pandemic (17). Importantly, at least 20 new, related viruses have been discovered across Africa and the Americas in the last decade, highlighting the importance of research into the lifecycles of henipaviruses as well as development of new methods, vaccines, and therapeutics to combat future outbreaks (18–20). The locations of known outbreaks of NiV and HeV, countries with evidence of henipaviruses, and the ecological ranges for bat henipavirus reservoirs are summarized below (Fig. 1). The studies described in the next several chapters here comprise approaches to understanding how several NiV proteins produce viral particles (Chapter 2), how these proteins may interact with cellular machinery to support particle egress (Chapter 3), and a multi-omics bioinformatics analysis of a “live” bio-safety level 4 infection across several time points in human cells (Chapter 4).

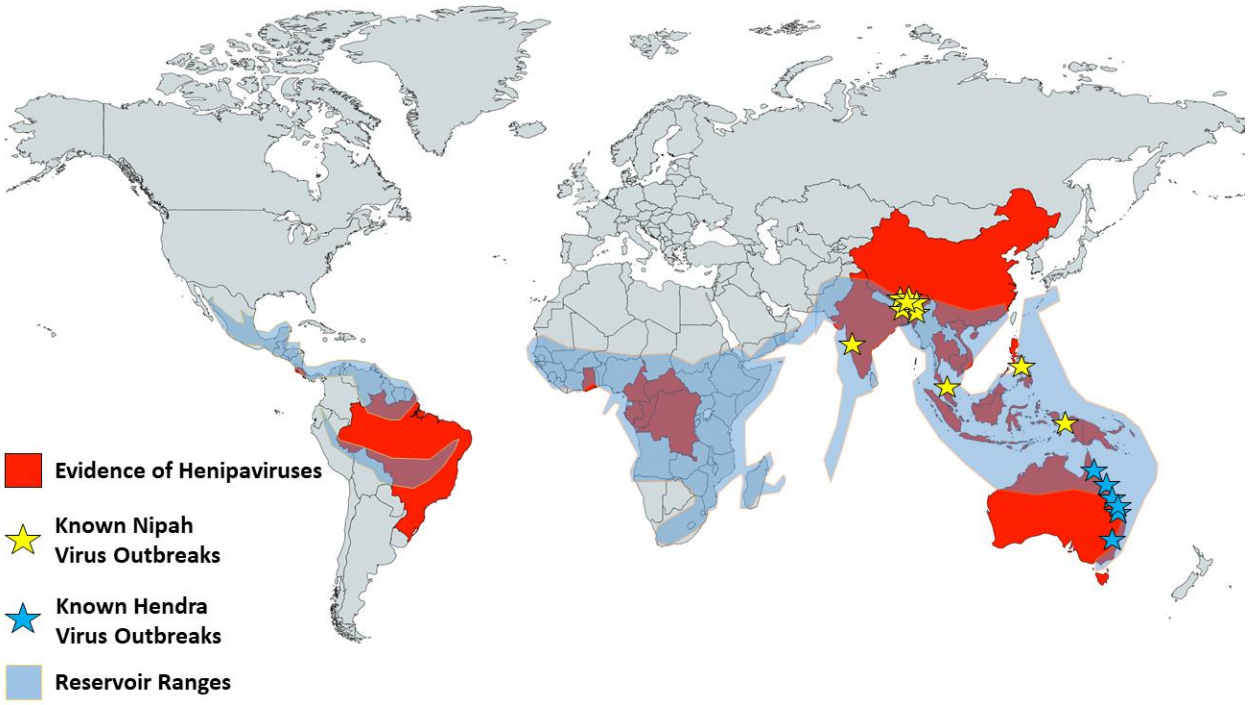

Fig. 1.1: The Global Distribution of Henipaviruses
Pathogens officially categorized as henipaviruses and newly discovered related viruses have been identified on almost every continent. The broad ecological ranges of henipavirus flying fox reservoirs and wide host tropisms support continual outbreaks of these viruses.

Nipah Virus Infection

As mentioned in the previous section, NiV infections are generally transmitted through bodily fluids, contaminated food or water, or potentially through aerosols (9, 12, 14, 15). Based on infections in animal models, NiV infects lung respiratory epithelial cells and lung microvascular endothelial cells, supporting vasculitis and eventual viremia (15, 21, 22). The permissiveness of microvascular endothelia to NiV also frequently supports infection of the vasculature of organs, particularly the spleen and kidneys (6, 12, 23, 24). Infection of nerve cells of the olfactory bulb can also occur, supporting greater infection of neurons of the brain and ultimately, encephalitis (15, 25).

Other cell types such as dendritic cells have been shown to be permissive to NiV infection, however, the importance of such infections in overall pathology remains unclear (26, 27).

In all these cases, infection is thought primarily to occur through entry of NiV particles into the cell. As NiV is an enveloped virus, entry events require fusion of the viral and cellular membranes (28). Dr. Aguilar-Carreno and his colleagues identified that the NiV attachment glycoprotein (G) binds to the cellular protein, ephrinB2, using it as the host receptor for entry (29). A related protein, ephrinB3 was also found to act as an entry receptor though this protein exhibited much less binding affinity for NiV G (30). After receptor binding, NiV G undergoes conformational changes that eventually lead to exposure of its stalk domain to the only other integral NiV protein, the fusion (F) glycoprotein (31). Studies so far into this process indicate that the exposure of the NiV G stalk induces major conformational changes in F that lead to its partial insertion into the host membrane followed by further conformational changes resulting in fusion of the viral and cellular membranes (32, 33). Thus, the close coordination of NiV F and G drives an essential aspect of the NiV life cycle: viral entry.

After fusion of the viral and cellular membranes, the 18,246-nucleotide negative-sense single-stranded genome is enabled to enter the cell where transcription begins (34). While there are only six genes, NiV produces nine total proteins (Fig. 2). Transcription as well as genome replication, occurring later in infection, depend on several NiV proteins, namely the Nucleoprotein (N), Phosphoprotein (P), and Large polymerase (L) (35). Two of the additional proteins produced from the P gene, V and W, have generally been identified as inhibitors of several anti-viral immune response

pathways within the cells infected including the Jak-STAT and Interferon pathways (36, 37, 38). During the course of infection in a cell, NiV G as well as NiV F, activated after cleavage from the cellular proteases cathepsin L or B, accumulate on the cellular surface (39, 40). The presence of these proteins together supports fusion of infected cells with neighboring cells expressing the viral receptor ephrinB2 or ephrinB3 to form multi-nucleated syncytia, a hallmark of paramyxovirus infection and a major contributing factor to pathogenesis (41).

Paramyxoviruses additionally produce a matrix (M) protein which is thought to be central to the assembly and budding of viral components into new particles (42, 43). The M protein as well as the final P gene product, C, will be discussed in the next section.

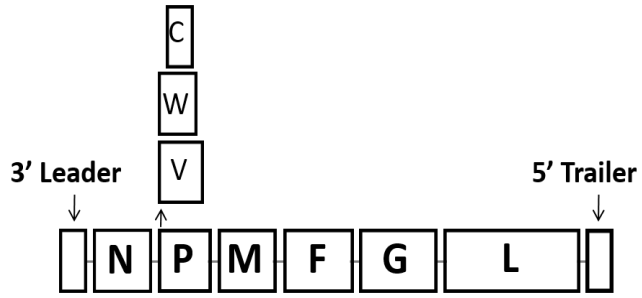

Fig. 1.2: The Nipah Virus Genome The 18,246 nucleotide RNA genome is flanked by a leader and a trailer region important for transcription and replication. While the genome contains only six genes (N, P, M, F, G, L), the P gene is also used to produce three additional proteins: C, V, and W.

Viral Budding

Virus budding or egress from infected cells has been studied in many membrane enveloped viruses of all shapes and sizes (43–45). Numerous mechanisms of viral budding have been or are beginning to be unearthed, each with a set of working parts involved in forming the end products – infectious units to expand and spread infection (46–48). While significant work has been done to understand these mechanisms of viral egress, leading to the developments of many useful technologies not limited to vaccines

and tools for research in transgenics and molecular biology, how many viruses produce particles during infection remains unclear. Further, many viruses have been observed to form large numbers of non-infectious virus-like particles (VLPs) during infection. Whether VLPs are simply produced as incomplete biproducts of messy mechanisms driving egress or whether they serve a purpose beneficial to a virus remains a major question of ongoing study (49, 50). In either case, VLPs are observed for many different viruses and are often used to identify if and how particular viral proteins drive budding (43, 51–53). This makes VLPs useful models for studying the mechanisms that drive or modulate assembly and budding and in the case of bio-safety level 4 agents such as NiV and HeV, the study of VLPs and how they are produced can serve to yield insights into a crucial step in the lifecycles of viruses that normally present high thresholds of difficulty to study due to bio-safety constraints.

Formation of infectious paramyxovirus particles (Fig. 3) must include incorporation of both glycoproteins (F and G for NiV) for entry as well as the viral ribonucleoprotein complex (vRNP) comprised of the genome, N, P, and L for transcription and replication. As mentioned briefly, the M protein is thought to act as the central factor that coordinates coalescence of these viral components during paramyxovirus budding (43). M is thought to do this through interactions with the vRNP via the N protein as well as a strong capability to deform the host membrane into particle structures (42, 54, 55). Specifically, several paramyxovirus M proteins drive budding largely through oligomerization into a scaffolding array capable of inducing membrane curvature (56, 56, 57). To say that paramyxovirus budding is dependent on M, however, is far from the truth since numerous other viral proteins have been shown

to be either supportive or required for budding (52, 53, 58). Among these proteins, the C protein produced from the P gene, has been reported for Sendai and Nipah virus to support M budding by recruiting cellular factors involved in membrane deformation and abscission (59, 60). While for some paramyxoviruses, glycoproteins appear not to support egress, for Sendai, mumps, and simian virus 5, one or both glycoproteins are supportive or essential for particle formation (52, 53, 58). The importance of other viral components was recently made clearer for NiV since live virus with a deletion of the M gene demonstrated a substantial reduction but not loss of infectious particle formation (61). In Chapter 2, we will describe a new role for NiV F as important in NiV budding, in addition to M, particularly for its support of G incorporation into particles (62).

Budding and the Cell

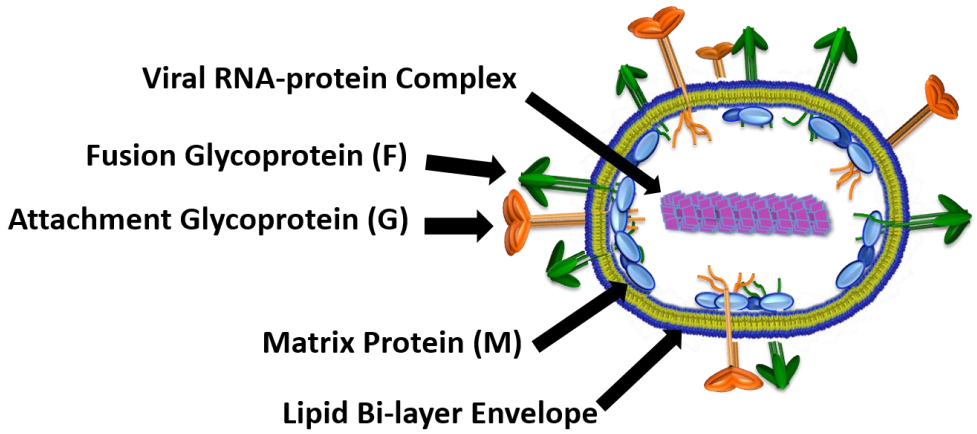

Fig. 1.3: Nipah Virus Particles
Infectious particles of NiV are generally spherical or pleomorphic. As an enveloped virus, NiV particles contain a lipid bi-layer in which the attachment and fusion glycoproteins, both required for membrane fusion leading to viral entry, are embedded. Inside the virion is the matrix protein, important for particle production, as well as the viral genome in complex with viral replication machinery.

While many different mechanisms exist for enveloped virus budding, most if not all depend on the actions of both viral and cellular proteins (44, 47). While many proteins such as NiV M are capable of inducing membrane curvature innately, the actions of many other proteins with roles in egress are dependent on recruitment of cellular factors (63). Many different cellular proteins are targeted by such recruitment; however, there are several groups or machineries of consistent interest for many, unrelated viruses. Cellular factors involved in and associated with the Endosomal Sorting Complexes Required for Transport (ESCRTs) top the list for many viruses (45, 59, 59, 60, 64–66). ESCRTs include four complexes (0-III) as well as a centrally important ATPase, Vps4 (45, 67). ESCRT proteins either directly or through ESCRT recruiting proteins have been observed to be important for egress of viruses in many families not limited to retroviruses, arenaviruses, filoviruses, and paramyxoviruses, often through conserved sequence motifs (68, 69). These motifs are frequently termed late motifs or late domains because their removal often leads to abrogation of viral budding in late steps such as membrane abscission (70–74). Thus, one common approach to elucidating the budding mechanism of a newly discovered virus is to identify and mutate such motifs in proteins found to have the capability to drive particle formation (68, 70, 73).

Not all viruses are dependent on ESCRT function, however, and in viruses that utilize this machinery, not all proteins capable of supporting budding need require it (44, 75, 76). The NiV M protein, for example was shown not to utilize ESCRT machinery for its ability to drive egress (77). Further, a study of NiV published around the time of publication for Chapter 2, for example, demonstrated that while M does not use

ESCRTs, live NiV particle formation is strongly affected by their down-regulation (59). Another emerging group of proteins shown to be involved in budding are the Rab11 GTPase family interacting proteins. Specifically, several reports have indicated their involvement in driving influenza A and respiratory syncytial virus budding (75, 76). Other cellular components, particularly the cytoskeleton and associated factors, have also been shown to have roles in the assembly and egress of numerous viruses, though these roles are not well understood in many cases (78–81)

The Proteomic Approach to Budding

Since so many cellular proteins have been shown to be involved in viral assembly and budding, there have been numerous attempts to make their identification easier. One of the more intuitive approaches to identifying these cellular factors is to isolate viral particles and analyze them proteomically using mass spectrometry (82–86). Since previous literature indicated that NiV F, M, and to a lesser degree G all exhibited abilities to induce particle formation when expressed alone and that F is supportive of G incorporation into particles, we became interested in the identification of cellular factors used by each protein (87). Thus, we used a proteomic approach to assess VLPs produced from different combinations of F, G, and M for incorporated cellular factors (Chapter 3).

Beyond Budding: High-throughput Analyses of NiV Infection

While the last section covered the use of mass spectrometric approaches to uncovering mechanisms of viral budding and the identification of cellular factors

involved, developments in proteomics and other high-throughput methods are proving increasingly useful for understanding other aspects of viral lifecycles (88). Interactome studies have been conducted for several viruses, with the aim of identifying cellular factors that bind individual viral proteins (89–91). Other techniques such as RNA sequencing and microarrays are frequently used to understand how gene expression in cells infected with a given virus changes (92–95). These transcriptomic studies can offer much insight into the interplay between viral manipulation of cellular processes and the cell's own response to infection. However, the major limitation of transcriptomics is that many conclusions made from it are often dependent on patterns of protein levels being consistent with those of transcripts (96).

While changes to metabolism and lipid profiles have been identified for several chronic viruses through metabolomic and lipidomic approaches, very little is understood about the dynamics of these molecules during acute infections such as NiV (97–100). A new 'multi-omic' approach, combining several high-throughput methods to capture cellular changes in response to infection, however, is emerging and has great potential in overcoming the drawbacks of each technology and giving a more complete picture of infection (101–103). Such an approach has been used to better understand Ebola virus pathology in humans, leading to the identification of important roles for pancreatic enzymes and neutrophils in tissue damage and immune response (104).

In Chapter 4, we will describe the use of such an approach to a time-course of human cells infected with NiV in bio-safety level 4 conditions. Despite the difficulty of transitioning many samples from bio-safety level 4 conditions and preparing them for omics analyses at bio-safety level 2, these experiments yield many new insights into the

changes a cell undergoes during NiV infection (Fig. 4). While biochemical studies emerging from 'omics' studies will always be valuable for uncovering the mechanisms and dynamics of processes during infections, the increasing capabilities of bioinformatics and high-throughput technologies lend much promise for our future understanding of viral infections and in a broader sense, all of biology.

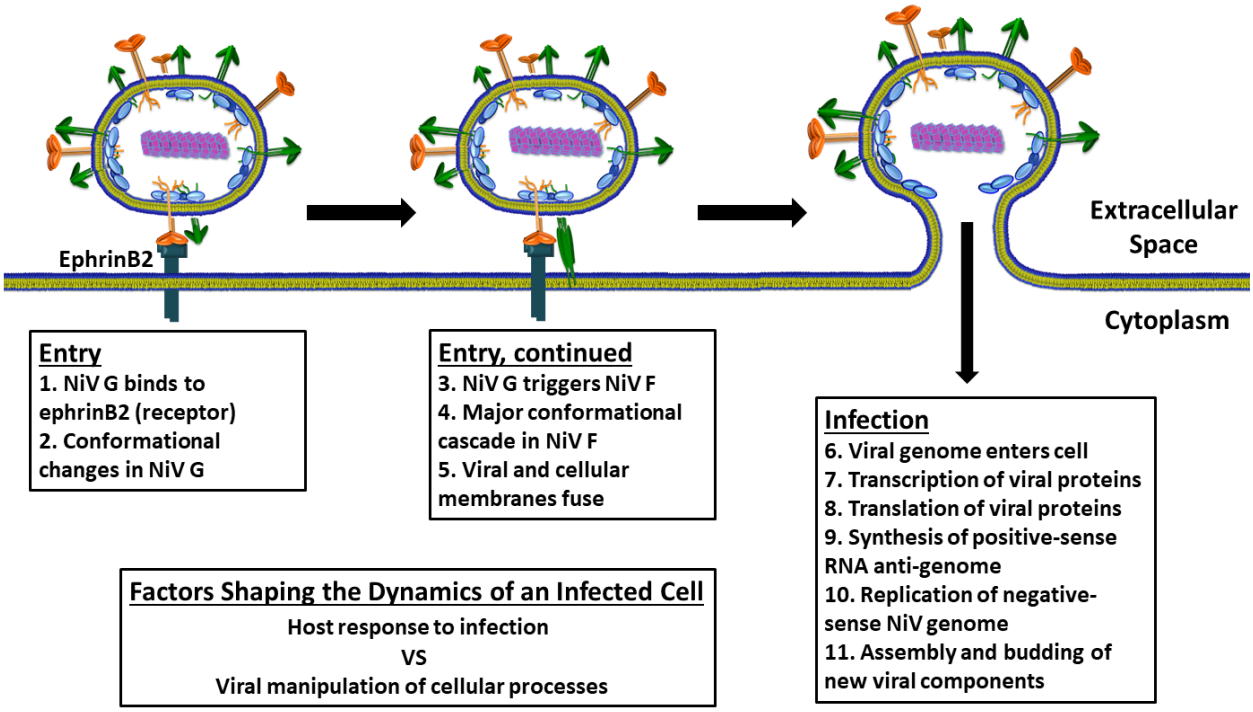

Fig. 1.4: Nipah virus Infection
NiV particles enter cells after binding the conserved cellular protein, ephrinB2, with the viral attachment glycoprotein. Conformational changes in the attachment protein then induce a major conformational cascade in the viral fusion protein, which fuses the viral and cellular membranes. After entry, the viral genome and the replication proteins N, P, and L, enter the cell. Based on related viruses, the viral genome is first used for transcription of viral genes to support synthesis of viral proteins but is later used to create full-length positive-sense antigenomes. These antigenomes are used as templates to replicate the negative-sense viral genome. Upon successful genome replication and viral protein synthesis, the new components coalesce at the plasma membrane and bud to form new virions. Throughout infection, cellular changes are caused both by the actions of viral proteins and by cellular response to infection.

REFERENCES

1. Field HE, Mackenzie JS, Daszak P. 2007. Henipaviruses: emerging paramyxoviruses associated with fruit bats. Curr Top Microbiol Immunol 315:133–159.
2. Murray K, Selleck P, Hooper P, Hyatt A, Gould A, Gleeson L, Westbury H, Hiley L, Selvey L, Rodwell B. 1995. A morbillivirus that caused fatal disease in horses and humans. Science 268:94–97.
3. Lim CC, Sitoh YY, Hui F, Lee KE, Ang BS, Lim E, Lim WE, Oh HM, Tambyah PA, Wong JS, Tan CB, Chee TS. 2000. Nipah viral encephalitis or Japanese encephalitis? MR findings in a new zoonotic disease. AJNR Am J Neuroradiol 21:455–461.
4. Chua KB. 2000. Nipah Virus: A Recently Emergent Deadly Paramyxovirus. Science 288:1432–1435.
5. Lam SK, Chua KB. 2002. Nipah Virus Encephalitis Outbreak in Malaysia. Clin Infect Dis 34:S48–S51.
6. DeBuysscher BL, de Wit E, Munster VJ, Scott D, Feldmann H, Prescott J. 2013. Comparison of the Pathogenicity of Nipah Virus Isolates from Bangladesh and Malaysia in the Syrian Hamster. PLoS Negl Trop Dis 7:e2024.
7. Islam MS, Sazzad HMS, Satter SM, Sultana S, Hossain MJ, Hasan M, Rahman M, Campbell S, Cannon DL, Ströher U, Daszak P, Luby SP, Gurley ES. 2016. Nipah Virus Transmission from Bats to Humans Associated with Drinking Traditional Liquor Made from Date Palm Sap, Bangladesh, 2011–2014. Emerg Infect Dis 22:664–670.
8. Luby SP, Hossain MJ, Gurley ES, Ahmed B-N, Banu S, Khan SU, Homaira N, Rota PA, Rollin PE, Comer JA, Kenah E, Ksiazek TG, Rahman M. 2009. Recurrent Zoonotic Transmission of Nipah Virus into Humans, Bangladesh, 2001–2007. Emerg Infect Dis 15:1229–1235.
9. Gurley ES, Hegde ST, Hossain K, Sazzad HMS, Hossain MJ, Rahman M, Sharker MAY, Salje H, Islam MS, Epstein JH, Khan SU, Kilpatrick AM, Daszak P, Luby SP. 2017. Convergence of Humans, Bats, Trees, and Culture in Nipah Virus Transmission, Bangladesh. Emerg Infect Dis 23:1446–1453.
10. Ching PKG, de los Reyes VC, Sucaldito MN, Tayag E, Columna-Vingno AB, Malbas FF, Bolo GC, Sejvar JJ, Eagles D, Playford G, Dueger E, Kaku Y, Morikawa S, Kuroda M, Marsh GA, McCullough S, Foxwell AR. 2015. Outbreak of Henipavirus Infection, Philippines, 2014. Emerg Infect Dis 21:328–331.
11. Paul L. 2018. Nipah virus in Kerala : A deadly Zoonosis. Clin Microbiol Infect.
12. de Wit E, Munster VJ. 2015. Animal models of disease shed light on Nipah virus pathogenesis and transmission: Nipah virus pathogenesis and transmission. J Pathol 235:196–205.

13. Mills JN, Alim ANM, Bunning ML, Lee OB, Wagoner KD, Amman BR, Stockton PC, Ksiazek TG. 2009. Nipah Virus Infection in Dogs, Malaysia, 1999. Emerg Infect Dis 15:950–952.

14. de Wit E, Prescott J, Falzarano D, Bushmaker T, Scott D, Feldmann H, Munster VJ. 2014. Foodborne Transmission of Nipah Virus in Syrian Hamsters. PLoS Pathog 10:e1004001.

15. Escaffre O, Hill T, Ikegami T, Juelich TL, Smith JK, Zhang L, Perez DE, Atkins C, Park A, Lawrence WS, Sivasubramani SK, Peel JE, Peterson JW, Lee B, Freiberg AN. 2018. Experimental Infection of Syrian Hamsters With Aerosolized Nipah Virus. J Infect Dis 218:1602–1610.

16. Satterfield BA, Dawes BE, Milligan GN. 2016. Status of vaccine research and development of vaccines for Nipah virus. Vaccine 34:2971–2975.

17. 2015. Blueprint for R&D preparedness and response to public health emergencies due to highly infectious pathogens.

18. Wu Z, Yang L, Yang F, Ren X, Jiang J, Dong J, Sun L, Zhu Y, Zhou H, Jin Q. 2014. Novel Henipa-like Virus, Mojiang Paramyxovirus, in Rats, China, 2012. Emerg Infect Dis 20.

19. Marsh GA, de Jong C, Barr JA, Tachedjian M, Smith C, Middleton D, Yu M, Todd S, Foord AJ, Haring V, Payne J, Robinson R, Broz I, Crameri G, Field HE, Wang L-F. 2012. Cedar Virus: A Novel Henipavirus Isolated from Australian Bats. PLoS Pathog 8:e1002836.

20. Pernet O, Schneider BS, Beaty SM, LeBreton M, Yun TE, Park A, Zachariah TT, Bowden TA, Hitchens P, Ramirez CM, Daszak P, Mazet J, Freiberg AN, Wolfe ND, Lee B. 2014. Evidence for henipavirus spillover into human populations in Africa. Nat Commun 5:5342.

21. Casola A, Rockx B, Halliday H, Escaffre O, Borisevich V. 2015. Oxidative stress in Nipah virus-infected human small airway epithelial cells. J Gen Virol 96:2961–2970.

22. Escaffre O, Borisevich V, Carmical JR, Prusak D, Prescott J, Feldmann H, Rockx B. 2013. Henipavirus Pathogenesis in Human Respiratory Epithelial Cells. J Virol 87:3284–3294.

23. Escaffre O, Borisevich V, Rockx B. 2013. Pathogenesis of Hendra and Nipah virus infection in humans. J Infect Dev Ctries 7.

24. Geisbert TW, Daddario-DiCaprio KM, Hickey AC, Smith MA, Chan Y-P, Wang L-F, Mattapallil JJ, Geisbert JB, Bossart KN, Broder CC. 2010. Development of an Acute and Highly Pathogenic Nonhuman Primate Model of Nipah Virus Infection. PLoS ONE 5:e10690.

25. Munster VJ, Prescott JB, Bushmaker T, Long D, Rosenke R, Thomas T, Scott D, Fischer ER, Feldmann H, de Wit E. 2012. Rapid Nipah virus entry into the central nervous system of hamsters via the olfactory route. Sci Rep 2.

26. Tiong V, Shu M-H, Wong WF, AbuBakar S, Chang L-Y. 2018. Nipah Virus Infection of Immature Dendritic Cells Increases Its Transendothelial Migration Across Human Brain Microvascular Endothelial Cells. Front Microbiol 9.

27. Gupta M, Lo MK, Spiropoulou CF. 2013. Activation and cell death in human dendritic cells infected with Nipah virus. Virology 441:49–56.

28. Aguilar HC, Iorio RM. 2012. Henipavirus Membrane Fusion and Viral Entry, p. 79–94. *In* Lee, B, Rota, PA, Lee, B, Rota, PA (eds.), Henipavirus. Berlin, Heidelberg.

29. Negrete OA, Levroney EL, Aguilar HC, Bertolotti-Ciarlet A, Nazarian R, Tajyar S, Lee B. 2005. EphrinB2 is the entry receptor for Nipah virus, an emergent deadly paramyxovirus. Nature 436:401–405.

30. Xu K, Broder CC, Nikolov DB. 2012. Ephrin-B2 and ephrin-B3 as functional henipavirus receptors. Semin Cell Dev Biol 23:116–123.

31. Liu Q, Stone JA, Bradel-Tretheway B, Dabundo J, Benavides Montano JA, Santos-Montanez J, Biering SB, Nicola AV, Iorio RM, Lu X, Aguilar HC. 2013. Unraveling a Three-Step Spatiotemporal Mechanism of Triggering of Receptor-Induced Nipah Virus Fusion and Cell Entry. PLoS Pathog 9:e1003770.

32. Liu Q, Bradel-Tretheway B, Monreal AI, Saludes JP, Lu X, Nicola AV, Aguilar HC. 2015. Nipah Virus Attachment Glycoprotein Stalk C-Terminal Region Links Receptor Binding to Fusion Triggering. J Virol 89:1838–1850.

33. Aguilar HC, Henderson BA, Zamora JL, Johnston GP. 2016. Paramyxovirus Glycoproteins and the Membrane Fusion Process. Curr Clin Microbiol Rep 3:142–154.

34. Lim ME, Lam SK, Chan YP, Chua KB, Koh CL. 2001. Complete nucleotide sequences of Nipah virus isolates from Malaysia. J Gen Virol 82:2151–2155.

35. Arankalle VA, Bandyopadhyay BT, Ramdasi AY, Jadi R, Patil DR, Rahman M, Majumdar M, Banerjee PS, Hati AK, Goswami RP, Neogi DK, Mishra AC. 2011. Genomic Characterization of Nipah Virus, West Bengal, India. Emerg Infect Dis 17:907–909.

36. Basler CF. 2012. Nipah and Hendra Virus Interactions with the Innate Immune System, p. 123–152. *In* Lee, B, Rota, PA, Lee, B, Rota, PA (eds.), Henipavirus. Berlin, Heidelberg.

37. Seto J, Qiao L, Guenzel CA, Xiao S, Shaw ML, Hayot F, Sealfon SC. 2010. Novel Nipah Virus Immune-Antagonism Strategy Revealed by Experimental and Computational Study. J Virol 84:10965–10973.

38. Shaw ML, Garcia-Sastre A, Palese P, Basler CF. 2004. Nipah Virus V and W Proteins Have a Common STAT1-Binding Domain yet Inhibit STAT1 Activation from the Cytoplasmic and Nuclear Compartments, Respectively. J Virol 78:5633–5641.

39. Diederich S, Sauerhering L, Weis M, Altmeppen H, Schaschke N, Reinheckel T, Erbar S, Maisner A. 2012. Activation of the Nipah Virus Fusion Protein in MDCK

Cells Is Mediated by Cathepsin B within the Endosome-Recycling Compartment. J Virol 86:3736–3745.

40. Vogt C, Eickmann M, Diederich S, Moll M, Maisner A. 2005. Endocytosis of the Nipah virus glycoproteins. J Virol 79:3865–3872.
41. Wong KT, Shieh W-J, Kumar S, Norain K, Abdullah W, Guarner J, Goldsmith CS, Chua KB, Lam SK, Tan CT, Goh KJ, Chong HT, Jusoh R, Rollin PE, Ksiazek TG, Zaki SR, Nipah Virus Pathology Working Group. 2002. Nipah virus infection: pathology and pathogenesis of an emerging paramyxoviral zoonosis. Am J Pathol 161:2153–2167.
42. Battisti AJ, Meng G, Winkler DC, McGinnes LW, Plevka P, Steven AC, Morrison TG, Rossmann MG. 2012. Structure and assembly of a paramyxovirus matrix protein. Proc Natl Acad Sci 109:13996–14000.
43. Harrison MS, Sakaguchi T, Schmitt AP. 2010. Paramyxovirus assembly and budding: building particles that transmit infections. Int J Biochem Cell Biol 42:1416–1429.
44. Chen BJ, Lamb RA. 2008. Mechanisms for enveloped virus budding: Can some viruses do without an ESCRT? Virology 372:221–232.
45. Votteler J, Sundquist WI. 2013. Virus Budding and the ESCRT Pathway. Cell Host Microbe 14:232–241.
46. Garoff H, Hewson R, Opstelten DJ. 1998. Virus maturation by budding. Microbiol Mol Biol Rev MMBR 62:1171–1190.
47. Pornillos O, Garrus JE, Sundquist WI. 2002. Mechanisms of enveloped RNA virus budding. Trends Cell Biol 12:569–579.
48. Simons K, Garoff H. 1980. The Budding Mechanisms of Enveloped Animal Viruses. J Gen Virol 50:1–21.
49. Heilingloh CS, Krawczyk A. 2017. Role of L-Particles during Herpes Simplex Virus Infection. Front Microbiol 8.
50. Brooke CB. 2014. Biological activities of “noninfectious” influenza A virus particles. Future Virol 9:41–51.
51. Luo L, Li Y, Yong Kang C. 2003. Budding and secretion of HIV Gag-Env virus-like particles from recombinant human adenovirus infected cells. Virus Res 92:75–82.
52. Schmitt AP, Leser GP, Waning DL, Lamb RA. 2002. Requirements for budding of paramyxovirus simian virus 5 virus-like particles. J Virol 76:3952–3964.
53. Takimoto T, Murti KG, Bousse T, Scroggs RA, Portner A. 2001. Role of matrix and fusion proteins in budding of Sendai virus. J Virol 75:11384–11391.
54. Coronel EC, Murti KG, Takimoto T, Portner A. 1999. Human parainfluenza virus type 1 matrix and nucleoprotein genes transiently expressed in mammalian cells induce the release of virus-like particles containing nucleocapsid-like structures. J Virol 73:7035–7038.

55. Ray G, Schmitt PT, Schmitt AP. 2016. C-Terminal DxD-Containing Sequences within Paramyxovirus Nucleocapsid Proteins Determine Matrix Protein Compatibility and Can Direct Foreign Proteins into Budding Particles. J Virol 90:3650–3660.

56. Ke Z, Strauss JD, Hampton CM, Brindley MA, Dillard RS, Leon F, Lamb KM, Plemper RK, Wright ER. 2018. Promotion of virus assembly and organization by the measles virus matrix protein. Nat Commun 9:1736.

57. Liu YC, Grusovin J, Adams TE. 2018. Electrostatic Interactions between Hendra Virus Matrix Proteins Are Required for Efficient Virus-Like-Particle Assembly. J Virol 92:e00143-18.

58. Li M, Schmitt PT, Li Z, McCrory TS, He B, Schmitt AP. 2009. Mumps virus matrix, fusion, and nucleocapsid proteins cooperate for efficient production of virus-like particles. J Virol 83:7261–7272.

59. Park A, Yun T, Vigant F, Pernet O, Won ST, Dawes BE, Bartkowski W, Freiberg AN, Lee B. 2016. Nipah Virus C Protein Recruits Tsg101 to Promote the Efficient Release of Virus in an ESCRT-Dependent Pathway. PLOS Pathog 12:e1005659.

60. Irie T, Nagata N, Yoshida T, Sakaguchi T. 2008. Recruitment of Alix/AIP1 to the plasma membrane by Sendai virus C protein facilitates budding of virus-like particles. Virology 371:108–120.

61. Dietzel E, Kolesnikova L, Sawatsky B, Heiner A, Weis M, Kobinger GP, Becker S, von Messling V, Maisner A. 2016. Nipah Virus Matrix Protein Influences Fusogenicity and Is Essential for Particle Infectivity and Stability. J Virol 90:2514–2522.

62. Johnston GP, Contreras EM, Dabundo J, Henderson BA, Matz KM, Ortega V, Ramirez A, Park A, Aguilar HC. 2017. Cytoplasmic Motifs in the Nipah Virus Fusion Protein Modulate Virus Particle Assembly and Egress. J Virol 91:e02150-16.

63. Harty RN, Schmitt AP, Bouamr F, Lopez CB, Krummenacher C. 2011. Virus Budding/Host Interactions. Adv Virol 2011:1–2.

64. Mercenne G, Alam SL, Arii J, Lalonde MS, Sundquist WI. 2015. Angiomotin functions in HIV-1 assembly and budding. eLife 4.

65. Sakaguchi T, Kato A, Sugahara F, Shimazu Y, Inoue M, Kiyotani K, Nagai Y, Yoshida T. 2005. AIP1/Alix is a binding partner of Sendai virus C protein and facilitates virus budding. J Virol 79:8933–8941.

66. Strack B, Calistri A, Craig S, Popova E, Göttlinger HG. 2003. AIP1/ALIX Is a Binding Partner for HIV-1 p6 and EIAV p9 Functioning in Virus Budding. Cell 114:689–699.

67. Fujita H. 2003. A dominant negative form of the AAA ATPase SKD1/VPS4 impairs membrane trafficking out of endosomal/lysosomal compartments: class E vps phenotype in mammalian cells. J Cell Sci 116:401–414.

68. Bieniasz PD. 2006. Late budding domains and host proteins in enveloped virus release. Virology 344:55–63.

69. Freed EO. 2002. Viral Late Domains. J Virol 76:4679–4687.

70. Dilley KA, Gregory D, Johnson MC, Vogt VM. 2010. An LYPSL Late Domain in the Gag Protein Contributes to the Efficient Release and Replication of Rous Sarcoma Virus. J Virol 84:6276–6287.

71. Dolnik O, Kolesnikova L, Stevermann L, Becker S. 2010. Tsg101 Is Recruited by a Late Domain of the Nucleocapsid Protein To Support Budding of Marburg Virus-Like Particles. J Virol 84:7847–7856.

72. Heidecker G, Lloyd PA, Fox K, Nagashima K, Derse D. 2004. Late Assembly Motifs of Human T-Cell Leukemia Virus Type 1 and Their Relative Roles in Particle Release. J Virol 78:6636–6648.

73. Licata JM, Simpson-Holley M, Wright NT, Han Z, Paragas J, Harty RN. 2003. Overlapping motifs (PTAP and PPEY) within the Ebola virus VP40 protein function independently as late budding domains: involvement of host proteins TSG101 and VPS-4. J Virol 77:1812–1819.

74. Schmitt AP, Leser GP, Morita E, Sundquist WI, Lamb RA. 2005. Evidence for a New Viral Late-Domain Core Sequence, FPIV, Necessary for Budding of a Paramyxovirus. J Virol 79:2988–2997.

75. Rossman JS, Jing X, Leser GP, Lamb RA. 2010. Influenza Virus M2 Protein Mediates ESCRT-Independent Membrane Scission. Cell 142:902–913.

76. Utley TJ, Ducharme NA, Varthakavi V, Shepherd BE, Santangelo PJ, Lindquist ME, Goldenring JR, Crowe JE. 2008. Respiratory syncytial virus uses a Vps4-independent budding mechanism controlled by Rab11-FIP2. Proc Natl Acad Sci U S A 105:10209–10214.

77. Patch JR, Han Z, McCarthy SE, Yan L, Wang L-F, Harty RN, Broder CC. 2008. The YPLGVG sequence of the Nipah virus matrix protein is required for budding. Virol J 5:137.

78. Dietzel E, Kolesnikova L, Maisner A. 2013. Actin filaments disruption and stabilization affect measles virus maturation by different mechanisms. Virol J 10:249.

79. Gladnikoff M, Shimoni E, Gov NS, Rousso I. 2009. Retroviral Assembly and Budding Occur through an Actin-Driven Mechanism. Biophys J 97:2419–2428.

80. Miazza V, Mottet-Osman G, Startchick S, Chaponnier C, Roux L. 2011. Sendai virus induced cytoplasmic actin remodeling correlates with efficient virus particle production. Virology 410:7–16.

81. Taylor MP, Koyuncu OO, Enquist LW. 2011. Subversion of the actin cytoskeleton during viral infection. Nat Rev Microbiol 9:427–439.

82. Chan EY, Qian W-J, Diamond DL, Liu T, Gritsenko MA, Monroe ME, Camp DG, Smith RD, Katze MG. 2007. Quantitative Analysis of Human Immunodeficiency

Virus Type 1-Infected CD4+ Cell Proteome: Dysregulated Cell Cycle Progression and Nuclear Transport Coincide with Robust Virus Production. J Virol 81:7571–7583.

83. Chertova E, Chertov O, Coren LV, Roser JD, Trubey CM, Bess JW, Sowder RC, Barsov E, Hood BL, Fisher RJ, Nagashima K, Conrads TP, Veenstra TD, Lifson JD, Ott DE. 2006. Proteomic and Biochemical Analysis of Purified Human Immunodeficiency Virus Type 1 Produced from Infected Monocyte-Derived Macrophages. J Virol 80:9039–9052.

84. Radhakrishnan A, Yeo D, Brown G, Myaing MZ, Iyer LR, Fleck R, Tan B-H, Aitken J, Sanmun D, Tang K, Yarwood A, Brink J, Sugrue RJ. 2010. Protein Analysis of Purified Respiratory Syncytial Virus Particles Reveals an Important Role for Heat Shock Protein 90 in Virus Particle Assembly. Mol Cell Proteomics 9:1829–1848.

85. Ren X, Xue C, Kong Q, Zhang C, Bi Y, Cao Y. 2012. Proteomic analysis of purified Newcastle disease virus particles. Proteome Sci 10:32.

86. Vera-Velasco NM, García-Murria MJ, Sánchez del Pino MM, Mingarro I, Martinez-Gil L. 2018. Proteomic composition of Nipah virus -like particles. J Proteomics 172:190–200.

87. Patch JR, Crameri G, Wang L-F, Eaton BT, Broder CC. 2007. Quantitative analysis of Nipah virus proteins released as virus-like particles reveals central role for the matrix protein. Virol J 4:1.

88. Lum KK, Cristea IM. 2016. Proteomic approaches to uncovering virus–host protein interactions during the progression of viral infection. Expert Rev Proteomics 13:325–340.

89. Coyaud E, Ranadheera C, Cheng DT, Goncalves J, Dyakov B, Laurent E, St-Germain JR, Pelletier L, Gingras A-C, Brumell JH, Kim PK, Safronetz D, Raught B. 2018. Global interactomics uncovers extensive organellar targeting by Zika virus. Mol Cell Proteomics mcp.TIR118.000800.

90. Hafirassou ML, Meertens L, Umaña-Diaz C, Labeau A, Dejarnac O, Bonnet-Madin L, Kümmerer BM, Delaugerre C, Roingeard P, Vidalain P-O, Amara A. 2017. A Global Interactome Map of the Dengue Virus NS1 Identifies Virus Restriction and Dependency Host Factors. Cell Rep 21:3900–3913.

91. Martinez-Gil L, Vera-Velasco NM, Mingarro I. 2017. Exploring the Human-Nipah Virus Protein-Protein Interactome. J Virol 91:e01461-17.

92. Depledge DP, Mohr I, Wilson AC. 2019. Going the Distance: Optimizing RNA-Seq Strategies for Transcriptomic Analysis of Complex Viral Genomes. J Virol 93:e01342-18.

93. Glennon NB, Jabado O, Lo MK, Shaw ML. 2015. Transcriptome Profiling of the Virus-Induced Innate Immune Response in Pteropus vampyrus and Its Attenuation by Nipah Virus Interferon Antagonist Functions. J Virol 89:7550–7566.

94. Lan X, Wang Y, Tian K, Ye F, Yin H, Zhao X, Xu H, Huang Y, Liu H, Hsieh JCF, Lamont SJ, Zhu Q. 2017. Integrated host and viral transcriptome analyses reveal

pathology and inflammatory response mechanisms to ALV-J injection in SPF chickens. Sci Rep 7.

95. Wynne JW, Shiell BJ, Marsh GA, Boyd V, Harper JA, Heesom K, Monaghan P, Zhou P, Payne J, Klein R, Todd S, Mok L, Green D, Bingham J, Tachedjian M, Baker ML, Matthews D, Wang L-F. 2014. Proteomics informed by transcriptomics reveals Hendra virus sensitizes bat cells to TRAIL mediated apoptosis. Genome Biol 15:532.

96. Feder ME, Walser J-C. 2005. The biological limitations of transcriptomics in elucidating stress and stress responses. J Evol Biol 18:901–910.

97. Diop F, Vial T, Ferraris P, Wichit S, Bengue M, Hamel R, Talignani L, Liegeois F, Pompon J, Yssel H, Marti G, Missé D. 2018. Zika virus infection modulates the metabolomic profile of microglial cells. PLOS ONE 13:e0206093.

98. Manchester M, Anand A. 2017. Metabolomics: Strategies to Define the Role of Metabolism in Virus Infection and Pathogenesis. Adv Virus Res 98:57–81.

99. Roe B, Kensicki E, Mohney R, Hall WW. 2011. Metabolomic Profile of Hepatitis C Virus-Infected Hepatocytes. PLOS ONE 6:e23641.

100. Sun H, Zhang A, Yan G, Piao C, Li W, Sun C, Wu X, Li X, Chen Y, Wang X. 2013. Metabolomic Analysis of Key Regulatory Metabolites in Hepatitis C Virus–infected Tree Shrews. Mol Cell Proteomics MCP 12:710–719.

101. Hasin Y, Seldin M, Lusis A. 2017. Multi-omics approaches to disease. Genome Biol 18:83.

102. Söderholm S, Fu Y, Gaelings L, Belanov S, Yetukuri L, Berlinkov M, Cheltsov AV, Anders S, Aittokallio T, Nyman TA, Matikainen S, Kainov DE. 2016. Multi-Omics Studies towards Novel Modulators of Influenza A Virus-Host Interaction. Viruses 8.

103. Xie Q, Fan F, Wei W, Liu Y, Xu Z, Zhai L, Qi Y, Ye B, Zhang Y, Basu S, Zhao Z, Wu J, Xu P. 2017. Multi-omics analyses reveal metabolic alterations regulated by hepatitis B virus core protein in hepatocellular carcinoma cells. Sci Rep 7:41089.

104. Eisfeld AJ, Halfmann PJ, Wendler JP, Kyle JE, Burnum-Johnson KE, Peralta Z, Maemura T, Walters KB, Watanabe T, Fukuyama S, Yamashita M, Jacobs JM, Kim Y-M, Casey CP, Stratton KG, Webb-Robertson B-JM, Gritsenko MA, Monroe ME, Weitz KK, Shukla AK, Tian M, Neumann G, Reed JL, Bakel H van, Metz TO, Smith RD, Waters KM, N'jai A, Sahr F, Kawaoka Y. 2017. Multi-platform 'Omics Analysis of Human Ebola Virus Disease Pathogenesis. Cell Host Microbe 22:817-829.e8.

CHAPTER 2

Cytoplasmic Motifs in the Nipah Virus Fusion Protein Modulate Virus Particle Assembly and Egress

Gunner P. Johnston[a], Erik M. Contreras[b], Jeffrey Dabundo[b], Bryce A. Henderson[a,b], Keesha M. Matz[a], Victoria Ortega[a], Alfredo Ramirez[b], Arnold Park,[c] Hector C. Aguilar[a,b]

School of Molecular Biosciences, Washington State University, Pullman, Washington, USA[a]

Paul G. Allen School for Global Animal Health, Washington State University, Pullman, Washington, USA[b]

Department of Microbiology, Icahn School of Medicine at Mount Sinai, New York, New York, USA[c]

*This manuscript was published by the Journal of Virology (DOI:10.1128/JVI.02150-16) in 2017.

ABSTRACT

Nipah virus (NiV), a paramyxovirus in the genus *Henipavirus*, has a mortality rate in humans of approximately 75%. While several studies have begun our understanding of NiV particle formation, the mechanism of this process remains to be fully elucidated. For many paramyxoviruses, M proteins drive viral assembly and egress; however, some paramyxoviral glycoproteins have been reported as important or essential in budding. For NiV the matrix protein (M), the fusion glycoprotein (F) and, to a much lesser extent, the attachment glycoprotein (G) autonomously induce the formation of virus-like particles (VLPs). However, functional interactions between these proteins during assembly and egress remain to be fully understood. Moreover, if the F-driven formation of VLPs occurs through interactions with host cell machinery, the cytoplasmic tail (CT) of F is a likely interactive domain. Therefore, we analyzed NiV F CT deletion and alanine mutants and report that several but not all regions of the F CT are necessary for efficient VLP formation. Two of these regions contain YXXØ or dityrosine motifs previously shown to interact with cellular machinery involved in F endocytosis and transport. Importantly, our results showed that F-driven, M-driven, and M/F-driven viral particle formation enhanced the recruitment of G into VLPs. By identifying key motifs, specific residues, and functional viral protein interactions important for VLP formation, we improve our understanding of the viral assembly/egress process and point to potential interactions with host cell machinery.

IMPORTANCE

Henipaviruses can cause deadly infections of medical, veterinary, and agricultural importance. With recent discoveries of new henipa-like viruses, understanding the mechanisms by which these viruses reproduce is paramount. We have focused this study on identifying the functional interactions of three Nipah virus proteins during viral assembly and particularly on the role of one of these proteins, the fusion glycoprotein, in the incorporation of other viral proteins into viral particles. By identifying several regions in the fusion glycoprotein that drive viral assembly, we further our understanding of how these viruses assemble and egress from infected cells. The results presented will likely be useful toward designing treatments targeting this aspect of the viral life cycle and for the production of new viral particle-based vaccines.

KEYWORDS

paramyxovirus, *Paramyxoviridae*, viral assembly, budding, Nipah virus, cytoplasmic tail, fusion protein, matrix, attachment, glycoprotein

INTRODUCTION

The *Paramyxoviridae* family includes a wide array of medically relevant pathogens, including but not limited to measles (MeV), mumps, and parainfluenza viruses. The deadliest members of this family belong to the genus *Henipavirus*, with two of its members, Nipah virus (NiV) and Hendra virus capable of causing encephalitis, respiratory disease, and approximately 40 to 75% mortality rates in humans (1). Moreover, new henipa-like viruses have been discovered recently, such as Mojiang virus, which is suspected for three deaths in China (2), and close to 20 new bat viral species (3). Further, henipaviruses (HNVs) are zoonotic and can infect many mammalian orders (4). During its first outbreak in 1998 and 1999, NiV caused over 100 human deaths and prompted the culling of over one million Malaysian pigs (5, 6). There are no approved human treatments or vaccines for NiV infections, leading to its classification as a biosafety level 4 (BSL-4) agent and a potential threat to international security (7). Furthermore, the World Health Organization has recently listed Nipah virus as one of the top pathogens most likely to cause major epidemics in the future (8).

Paramyxoviruses carry negative-sense, single-stranded RNA genomes 15 to 19 kb in size. While the exact number of protein products made from the genome varies from 6 to 10 among viral species, all paramyxoviruses produce a matrix (M), fusion (F), and attachment glycoprotein (G in the case of HNVs) (9). For HNVs, the F and G glycoproteins are both necessary for viral entry (viral-cell membrane fusion) and are responsible for cell-cell fusion events (syncytia) between infected and naive cells (10, 11). On the other hand, the M protein is generally the main driver in paramyxoviral assembly and budding (12). F and G operate together to mediate viral entry and

syncytium formation. G recognizes the host cell receptor ephrinB2 or ephrinB3, triggering F to induce virus-cell or cell-cell membrane fusion (13–18). Although the presence of NiV M has been shown to affect the transport of F and G in polarized epithelia, the mechanism(s) of these effects remains to be elucidated (19). The glycoproteins F and G have also been shown to affect the transport of each other; however, these functional interactions appear to be dependent on cell type (19–21). While NiV M has important roles in protein transport and, ultimately, particle formation, attempts so far to show physical interactions of M with either of the glycoproteins have failed.

The mechanisms of viral particle formation vary considerably between paramyxoviruses (12). M is generally considered essential for these processes, since it acts to incorporate other viral components and create an infectious virion. In support of this central role, M proteins of most paramyxoviruses have the ability to form virus-like particles (VLPs) without any other viral factors present (22–29). Despite assembly and budding for most paramyxoviruses being driven largely by the M protein, other proteins, including the glycoproteins, have been shown to support and in some cases be required for these processes. For example, the particle formation of mumps virus is considerably enhanced by expression of the fusion glycoprotein but not the hemagglutinin-neuraminidase (HN) attachment glycoprotein (30). Similarly, the fusion glycoprotein but not the attachment glycoprotein of Sendai virus can significantly enhance particle formation (29).

Interestingly, for parainfluenza virus 5, either F or HN but not both are required for viral budding (31). This is in contrast to some paramyxoviruses, where the F protein

likely does not have an important, or at least a driving function in budding, as is the case for MeV and Newcastle disease virus (24, 26, 27). Previous findings for NiV suggest that F, G, and M can each induce VLP formation when expressed alone, albeit at different efficiencies (25, 32). Specifically, one study showed that while M and F exhibited high abilities to bud autonomously, G did so with much lower efficiency (25). Although it is known that these proteins can induce particle formation, there is very limited knowledge on how NiV F, G, and M functionally interact during viral assembly and whether they influence incorporation of each other into viral particles (25).

In support of an important role for NiV F during particle formation, one study using a new flow virometric tool suggested that incorporation of G into VLPs was considerably more efficient when F in addition to M was expressed (33). Overall, the involvement of F with G and M during particle assembly remains unclear and the functions and mechanism(s) for the autonomous budding of F is unknown. In this study, we quantitatively show that either F or M can enhance the incorporation of G into VLPs severalfold more efficiently than G can do autonomously. In addition, we demonstrate that the ability of NiV F to form VLPs is principally dependent on three regions of its cytoplasmic tail, including a polybasic motif and two tyrosine motifs known to be important for F trafficking or surface expression (20, 21, 34–36). Some of these functions may be dependent on interactions with clathrin adaptor protein (AP) complexes (21, 37).

RESULTS

NiV F and M support incorporation of NiV G into VLPs. By expressing the NiV F, G, and M proteins in different combinations, we first aimed to understand the roles and relative importance of each of these proteins during assembly and incorporation of one another into viral particles. All combinations of F, G, and M (4:1:1 ratio of their expression plasmids, respectively) were assessed for levels of whole-cell expression by Western blotting and at the cellular surface (for F or G) by flow cytometry. In addition, levels of each protein incorporated into VLPs were determined by sucrose cushion ultracentrifugation of cleared supernatants, followed by Western blotting. In agreement with a previous study, when expressed in HEK293T cells, F and M efficiently formed VLPs autonomously, whereas G did so less efficiently (Fig. 1A) (25) . In addition, both F and M showed the ability to incorporate G into VLPs roughly five times more efficiently than when G was expressed alone (Fig. 1B; both are $P < 0.01$). Interestingly, coexpression of F, G, and M led to a >8-fold increase in G incorporation ($P < 0.05$) while maintaining a nonsignificant difference in F or M incorporation (Fig. 1B). This finding supports cooperation between F and M in the incorporation of NiV G. We also report that, at least in the case of coexpression of M and G, the incorporation of M was reduced by about 20% (Fig. 1B; $P < 0.01$) compared to the single expression of M, suggesting that there may be some cost of incorporating G into viral particles. Possible explanations for this observation include competition for M binding between G and host cellular factors that support particle egress or that G can alter M trafficking to assembly sites. Although cellular surface expression (CSE) data showed that the levels of F CSE are higher when F was coexpressed with G (with or without M present) (Fig. 1C; $P < 0.05$), this did not

increase the incorporation of F into VLPs (Fig. 1B).

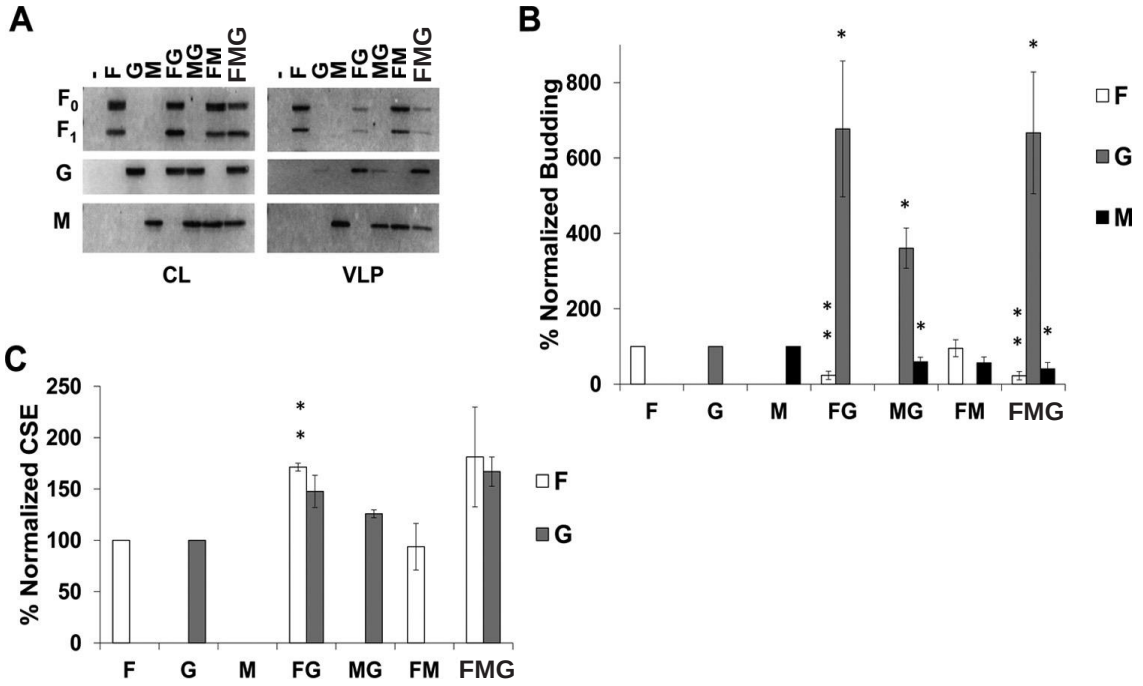

FIG 2.1 NiV F and M support incorporation of NiV G into VLPs. (A) Cell lysates (CL) and virus-like particles (VLPs) were isolated from HEK293T cells transfected for 24 h with the corresponding combinations of NiV F, G, and M. Transfections were done with F:G:M ratios of 4:1:1, with pcDNA3.1 as an empty vector. All samples were run through SDS-PAGE and Western blotting. For NiV F, the uncleaved form is designated F0, and part of the cleaved form is designated F1. (B) Densitometric analysis was used to quantify all bands and budding indices were calculated by dividing the band intensity of each VLP band by their corresponding band in CL. This was normalized to the ratio of individually expressed F, G, or M and is shown as a percentage of that ratio. (C) Flow cytometric analysis was used to assess cellular surface expression of F and G and these values were normalized to corresponding single expression values after removal of background. Error bars designate values for standard errors of the mean. Three or more independent experiments were used for each ratio, and the statistical significance was evaluated with one-sample t tests. Statistical significance is indicated by asterisks: *, $P < 0.05$; and **, $P < 0.01$.

NiV G can reduce incorporation of F and M into VLPs. We have shown that coexpression of NiV F or M with G significantly increased the incorporation efficiency of NiV G into VLPs (Fig. 1). Since it also appeared that the expression of G reduced the incorporation of F and/or M into VLPs, we next sought to determine whether increasing the

levels of NiV G expression would more clearly reduce incorporation of F and M into VLPs. We report that transfection of F, G, and M expression plasmids at a 4:2:1 ratio instead of 4:1:1 (Fig. 1) (while maintaining a total of 3 μg of DNA per well) significantly altered the levels of F and M in VLPs relative to their individual expression (Fig. 2A and B). Specifically, we show that F incorporation was reduced by almost 80% when co-expressed with G (Fig. 2B; $P < 0.01$). Importantly, this was not due to a decrease in F CSE when G is coexpressed. In fact, in the presence of G, NiV F cell surface expression maintained the ~70% increase as seen with the 4:1:1 ratio (Fig. 2C; $P < 0.01$). Interestingly, we saw the same reduction of F in VLPs even when M was expressed in addition to G, indicating that M could not rescue the incorporation of F into VLPs (Fig. 2B; $P < 0.01$).

In addition, M incorporation was significantly reduced by expression of G. Specifically, M levels in VLPs decreased by about 40% ($P < 0.05$) and 60% ($P < 0.05$) when coexpressed with G or both F and G, respectively (Fig. 2B). These findings, in conjunction with those of Fig. 1, support a mechanism of F, G, and M budding that requires a delicate balance among the relative expression levels of each of these viral proteins.

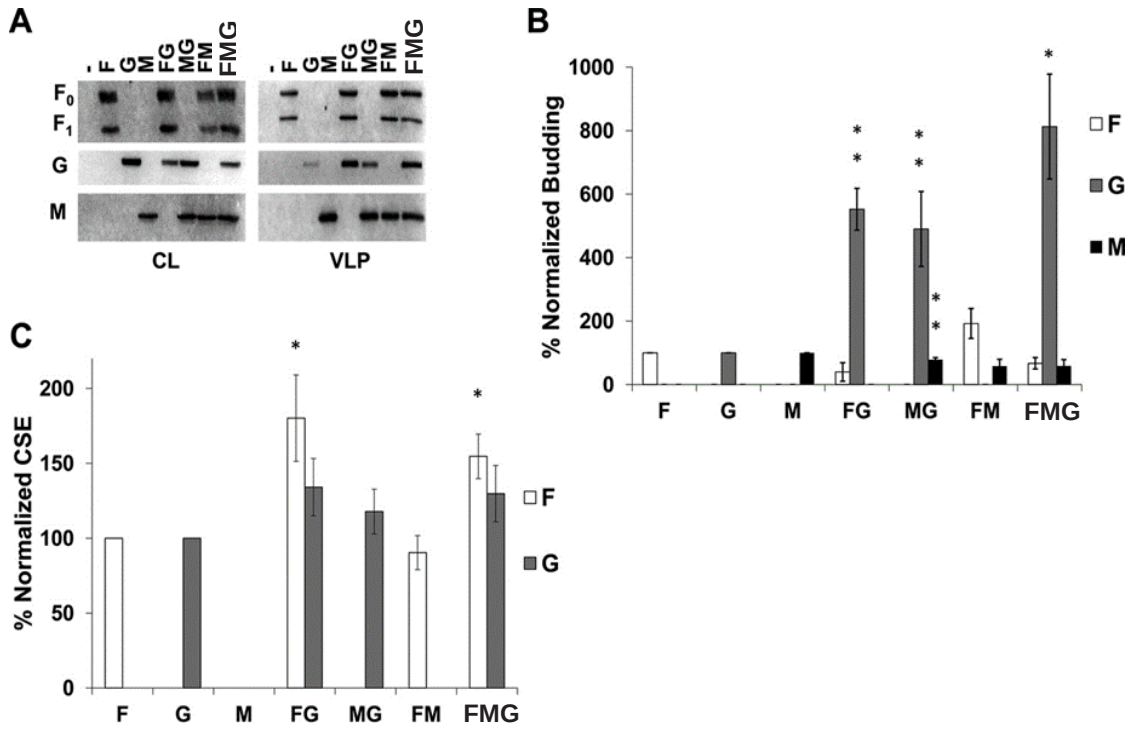

FIG 2.2 NiV G can reduce incorporation of F and M into VLPs. The same experiments and analyses were completed as in Fig. 1 except the F:G:M ration was changed to 4:2:1. Error bars designate values for standard errors of the mean. Three or more independent experiments were used for each ratio, and the statistical significance was evaluated with one-sample t tests. Statistical significance is indicated by asterisks: *, $P < 0.05$; and **, $P < 0.01$.

Specific regions of the NiV F cytoplasmic tail drive its ability to form VLPs. The functions of paramyxoviral glycoproteins during assembly and budding are usually associated with motifs in the cytoplasmic tails (CTs) of these proteins (38). We have shown an important role for NiV F during particle formation (Fig. 1) and now look to elaborate on the mechanism of this behavior by identifying what drives the budding capabilities of F. The NiV F CT has been previously studied in the context of viral entry and membrane fusion; thus, we have assessed the budding capacities of previously studied mutants harboring deletions of regions in the CT (Fig. 3A) (35). Based on total expression and corresponding presence in VLPs (Fig. 3B and C), we calculated budding indexes for

these deletion mutants as the ratio of normalized VLP signals to normalized cell lysate signals, so that the index for wild-type (WT) F would be 1.00. Interestingly, the T1, T2, and T4 mutants exhibited budding indices of 0.23 ($P < 0.01$), 0.20 ($P < 0.01$), and 0.22 ($P < 0.01$), respectively (Fig. 3D). This was in direct contrast to the budding index of the T3 deletion mutant, which was not significantly different from that of WT F (Fig. 3D). In addition, we report that the T1 and T2 mutants exhibited levels of CSE that appeared to be higher than would be expected from their total cell expression (CL versus CSE values, Fig. 3C). Thus, relative budding indexes were also calculated based on expression of each mutant with their corresponding levels of CSE (Fig. 3D). The marked decrease in budding by deleting regions T1, T2, or T4 suggest that these regions are functionally important for the budding ability of NiV.

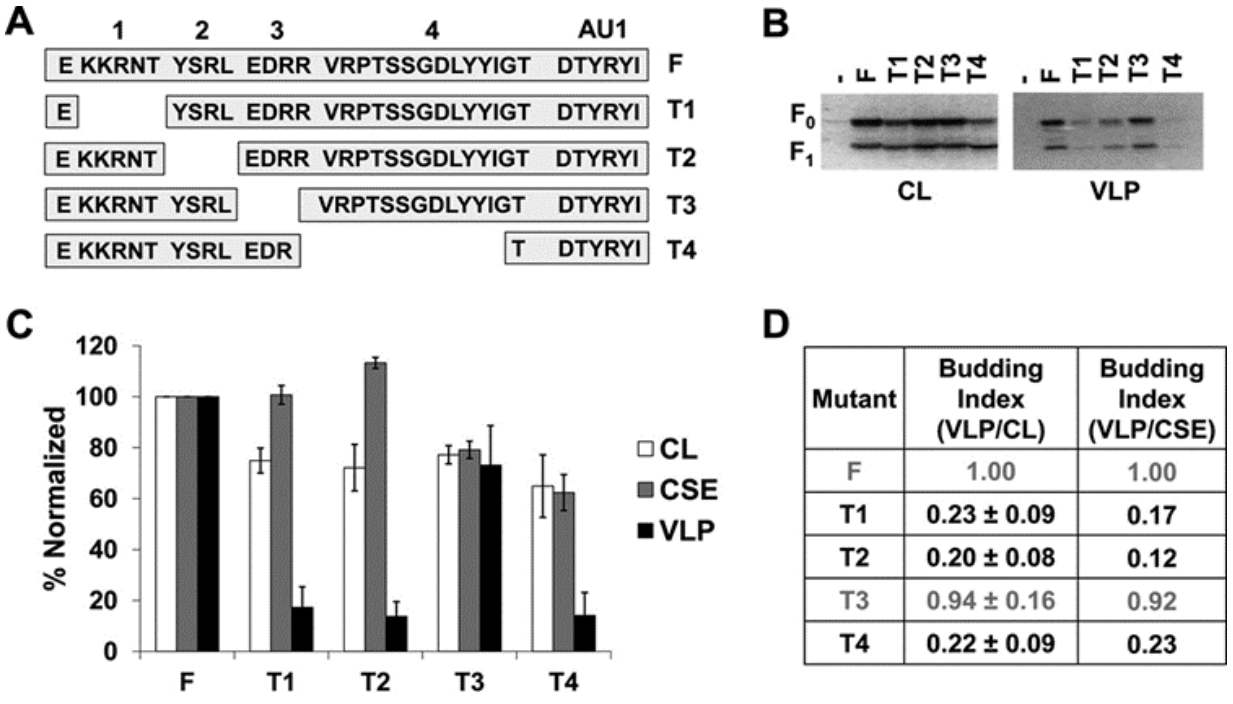

Mutant	Budding Index (VLP/CL)	Budding Index (VLP/CSE)
F	1.00	1.00
T1	0.23 ± 0.09	0.17
T2	0.20 ± 0.08	0.12
T3	0.94 ± 0.16	0.92
T4	0.22 ± 0.09	0.23

FIG 2.3 Specific regions of the NiV F cytoplasmic tail drive its ability to form VLPs. (A) Schematic designating regions of the NiV F CT and showing the sequence for four deletion mutants made. (B) HEK293T cells were transfected for 24 h with an empty vector, wild-type NiV F, or one of the four CT mutants. Both cell lysates and VLPs were harvested and subjected SDS-PAGE, followed by Western blot analysis. (C) Densitometry was used to quantify band intensity for cell lysates and VLPs. In addition, flow cytometric analyses were used to evaluate the levels of cell-surface expression (CSE) for each of the mutants relative to the wild-type F. (D) As in Fig. 1, the cell lysate and VLP band intensities were used to calculate budding indices, and all were normalized to wild-type F. A similar index is also shown using values for VLP intensity and corresponding CSE values. Mutants exhibiting budding at levels significantly below those of wild-type F have their values in black. Error bars designate values for standard errors of the mean. Three or more independent experiments were used for each ratio, and the statistical significance was evaluated with one-sample t tests.

A region including a membrane-proximal polybasic cluster mildly modulates the budding of F. Polybasic motifs, such as that in KKRNT of the NiV F CT, are sometimes associated with host cellular factors such as members of the actin cytoskeleton (39). To test which residues of this region may be responsible for the phenotype associated with deletion of the T1 region, we used alanine mutation screening and tested these mutants for any budding phenotypes (Fig. 4A). For both total expression and CSE, all five single-alanine mutants in T1 exhibited levels roughly consistent with those of wild-type F (Fig. 4B and C). In contrast to the substantial decrease in particle formation seen with deleting all of T1 (Fig. 3), single alanine mutations did not show any significant residues that indicate responsibility for this phenotype. While not at, but approaching, statistical significance, the N4A and T5A mutants appeared interesting as potential contributing factors in the T1 deletion budding phenotype (Fig. 4B and C). To further test this, an N4A/T5A double mutant was generated; however, this mutant also failed to produce the budding phenotype seen when the entire T1 region was deleted (Fig. 4B, C, and D). These findings

support the possibilities that several residues of this region act functionally together or that this region is important in distancing other motifs in the NiV F CT from the membrane.

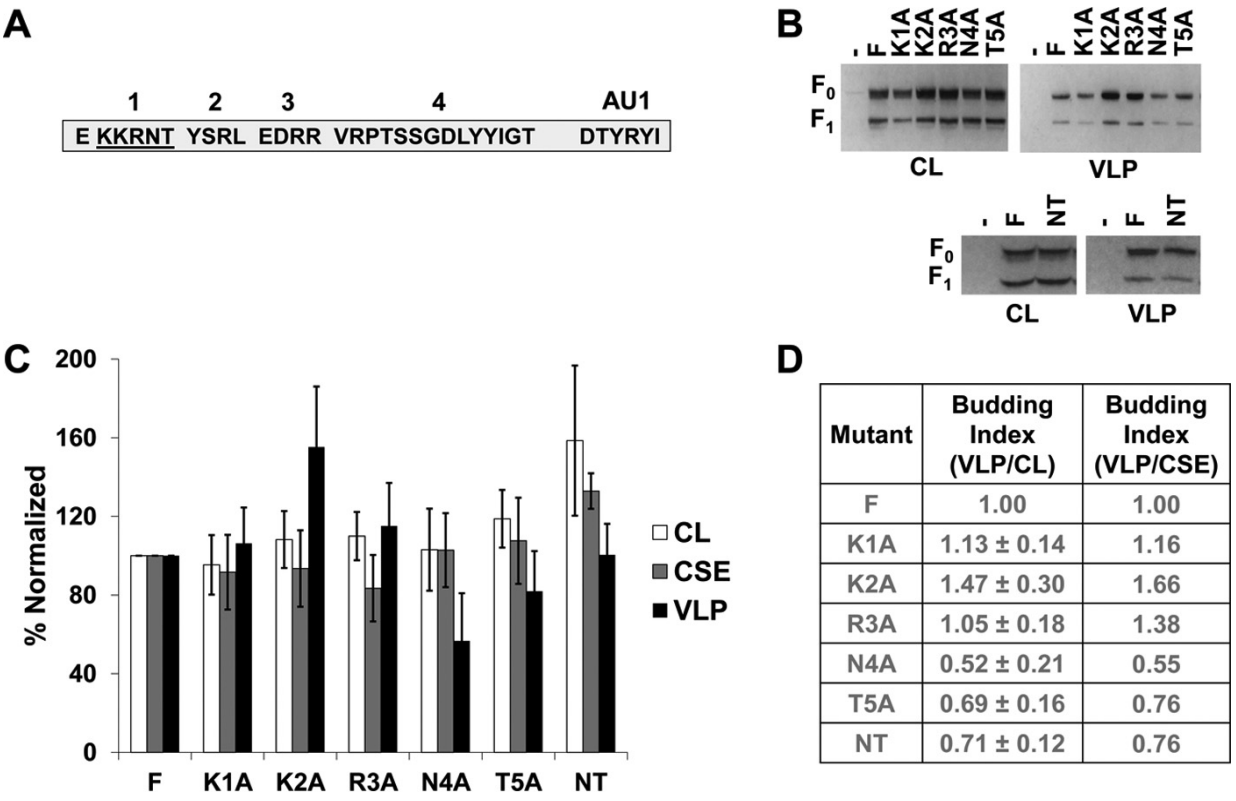

Mutant	Budding Index (VLP/CL)	Budding Index (VLP/CSE)
F	1.00	1.00
K1A	1.13 ± 0.14	1.16
K2A	1.47 ± 0.30	1.66
R3A	1.05 ± 0.18	1.38
N4A	0.52 ± 0.21	0.55
T5A	0.69 ± 0.16	0.76
NT	0.71 ± 0.12	0.76

FIG 2.4 A region including a membrane-proximal polybasic cluster mildly modulates budding of F. (A) Schematic for the cytoplasmic tail of NiV F designating the region being alanine screened. (B) HEK293T cells were transfected for 24 h with an empty vector, wild-type NiV F, one of the five alanine mutants of region T1, or the NT double mutant. Both cell lysates and VLPs were harvested and run in SDS-PAGE followed by Western blot analysis. (C) Densitometry was used to quantify band intensity for cell lysates and VLPs. In addition, flow cytometric analyses were used to evaluate the levels of CSE for each of the mutants relative to the wild-type F. (D) The cell lysate and VLP band intensities were used to calculate budding indices and all were normalized to wild-type F. A similar index is also shown using values for VLP intensity and corresponding CSE values. Error bars designate values for standard errors of the mean. Three or more independent experiments were used for each ratio, and the statistical significance was evaluated with one-sample t tests.

A tyrosine motif in the NiV F cytoplasmic tail modulates NiV F budding. In other viruses such as HIV-1 and HIV-2, YXXØ motifs such as the T2 region have been linked to viral protein sorting as well as particle assembly in some cases (40–43). Interestingly, a YXXØ motif in the NiV M protein has been suggested to influence M trafficking and budding (22). In addition, studies have identified this motif as contributing to the endocytosis event leading to NiV F maturation into a cleaved, fusogenic form (34, 44). Despite the role of this motif in supporting endocytosis of F, several studies have suggested that mutation of this region is not necessary for cleavage to occur for NiV F (35, 36). Other motifs such as the polybasic cluster may also be important for endocytosis (36). Also, one such study demonstrated a much more significant reduction of processing when the YXXØ motif was deleted in Hendra virus F than seen for NiV F (36). Region T2 (YSRL) has also been shown to be involved in sorting of NiV F based on identified interactions with clathrin adaptor AP proteins (21). Since deletion of T2 also led to a marked drop in budding, single residue analysis was conducted to understand the importance of each for appearance of this phenotype (Fig. 5A). Alanine scanning yielded that mutation of the tyrosine (73% decrease; $P < 0.05$) and leucine (67% decrease; $P < 0.001$) residues, but not the serine and arginine residues, led to significant decreases in budding (Fig. 5D). These findings strongly support the importance of the YXXØ motif itself as a driving factor for budding. Further, based on values for cell surface expression, the budding defects were not caused by a failure to transport F to the plasma membrane. While the mechanism for the YXXØ motif to modulate budding is unknown, it is likely related to interactions with host cellular machinery that either support trafficking to

specific sites of assembly or drive the process of viral budding directly.

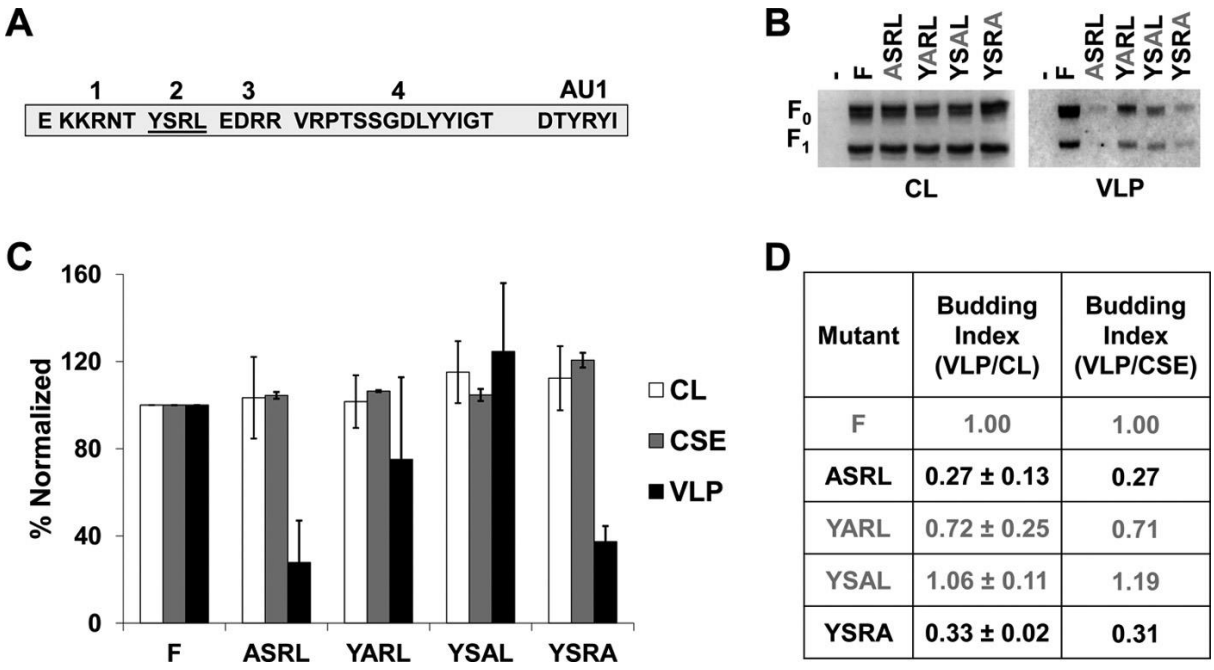

Mutant	Budding Index (VLP/CL)	Budding Index (VLP/CSE)
F	1.00	1.00
ASRL	0.27 ± 0.13	0.27
YARL	0.72 ± 0.25	0.71
YSAL	1.06 ± 0.11	1.19
YSRA	0.33 ± 0.02	0.31

FIG 2.5 A tyrosine motif in the NiV F cytoplasmic tail modulates NiV F budding. (A) Schematic for the cytoplasmic tail of NiV F designating the region being alanine screened. (B) HEK293T cells were transfected for 24 h with an empty vector, wild-type NiV F, or one of the four alanine mutants of region T2. Both cell lysates and VLPs were harvested and run in SDS-PAGE followed by Western blot analysis. (C) Densitometry was used to quantify band intensity for cell lysates and VLPs. In addition, flow cytometric analyses were used to evaluate the levels of CSE for each of the mutants relative to the WT. (D) The cell lysate and VLP band intensities were used to calculate budding indices and all were normalized to wild-type F. A similar index is also shown using values for VLP intensity and corresponding CSE values. Mutants exhibiting budding at levels significantly below WT have their values in black. Error bars designate values for standards error of the mean. Three or more independent experiments were used for each ratio, and the statistical significance was evaluated with one-sample t tests.

A dityrosine trafficking motif drives NiV F budding and likely the T4 deletion phenotype. We hypothesized that the budding phenotype observed for the largest NiV F CT deletion mutant, T4, would be most likely dependent on a couple of motifs. Considering our mass spectrometric data indicating phosphorylation of two adjacent serine residues in T4 (SS), and a dityrosine (YY) motif known to be important in NiV F trafficking in some cell types (20, 21), double-alanine mutants were generated for each of these motifs (Fig. 6A). While the SS mutant exhibited roughly WT levels of total and surface expression in addition to efficient formation of VLPs, mutation of both tyrosine residues nearly abrogated budding completely (95% reduction; $P < 0.0001$; Fig. 6A, B, and C). This effect was not due to failure to express on the cellular surface, as levels of CSE were close to wild-type CSE levels. Interestingly, a mild increase in the total expression level was observed for this mutant ($P < 0.05$; Fig. 6B and C).

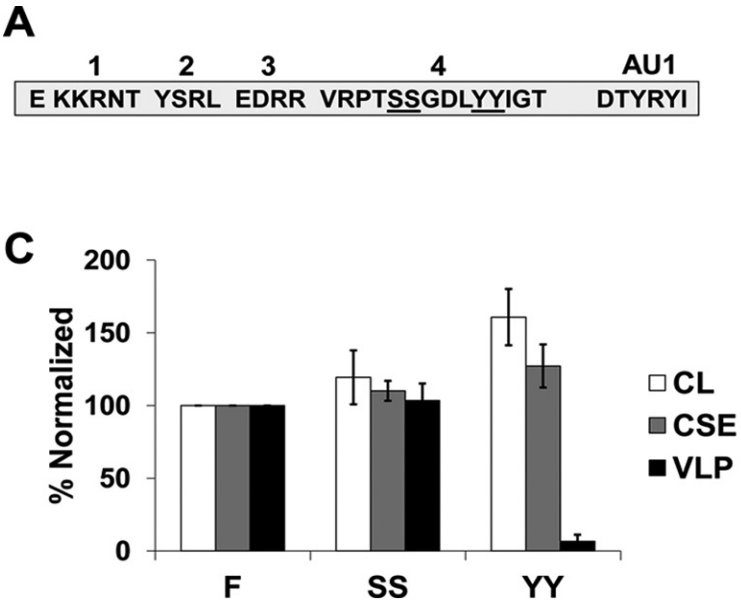

D

Mutant	Budding Index (VLP/CL)	Budding Index (VLP/CSE)
F	1.00	1.00
SS	0.89 ± 0.08	0.94
YY	0.05 ± 0.04	0.05

FIG 2.6 A dityrosine trafficking motif drives NiV F budding and likely the T4 deletion phenotype. (A) Schematic for the cytoplasmic tail of NiV F designating both double-alanine mutations. (B) HEK293T cells were transfected for 24 h with an empty vector, wild-type NiV F, or one of the two double-alanine mutants. Both cell lysates and VLPs were harvested and run in SDS-PAGE followed by Western blot analysis. (C) Densitometry was used to quantify band intensity for cell lysates and VLPs. In addition, flow cytometric analyses were used to evaluate the levels of CSE for each of the mutants relative to the WT.
(D) The cell lysate and VLP band intensities were used to calculate budding indices and all were normalized to WT F. A similar index is also shown using values for VLP intensity and corresponding CSE values. Mutants exhibiting budding at levels significantly below wild-type F have their values in black. Error bars designate values for standard errors of the mean. Three or more independent experiments were used for each ratio, and the statistical significance was evaluated with Student t tests.

The budding capabilities of NiV F are important for G incorporation into VLPs. To verify the importance of autonomous NiV F budding in the context of F, G, and M incorporation into viral particles, we cotransfected the T2 deletion mutant of F with combinations of the other structural proteins, as shown for Fig. 1. Based on better

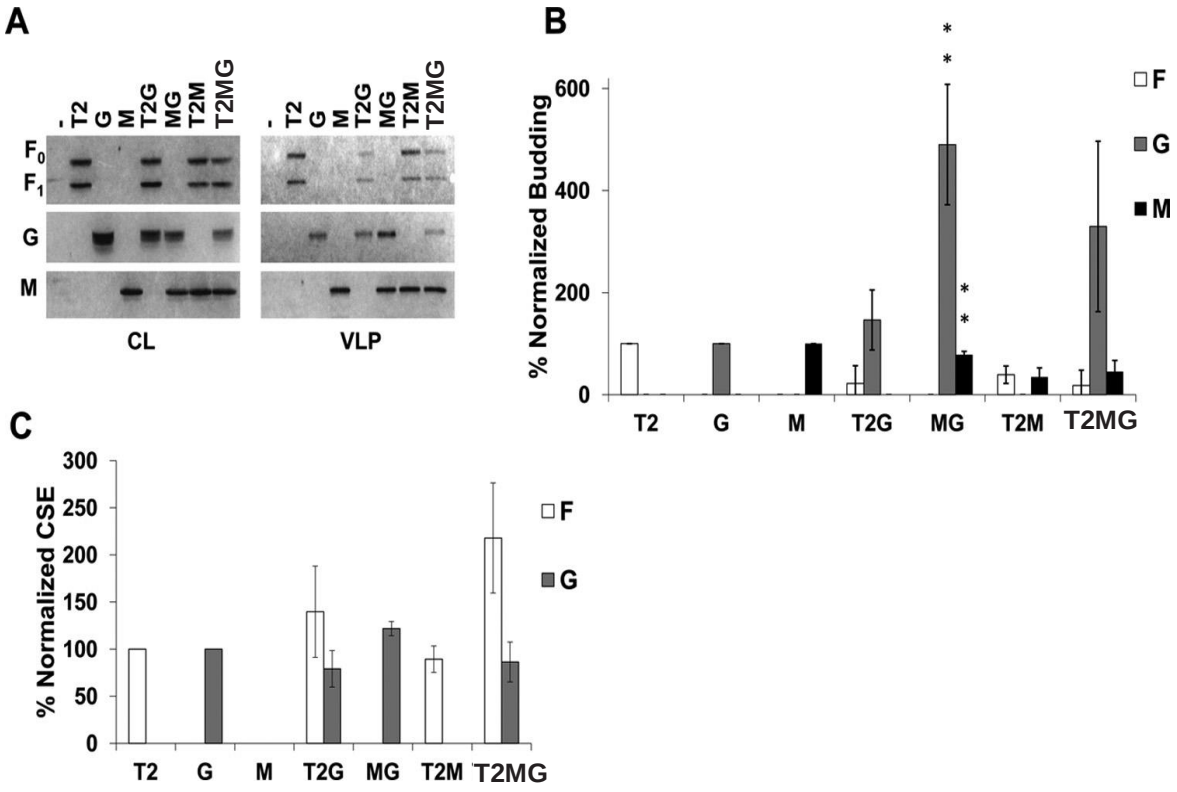

FIG 2.7 The budding capabilities of NiV F are important for G incorporation into VLPs. The same experiments and analyses were completed as in Fig. 1 except the T2 mutant was used in place of the wild type. Error bars designate values for standard errors of the mean. Three or more independent experiments were used for each ratio, and the statistical significance was evaluated with one-sample t tests. Statistical significance is designated by asterisks: *, P < 0.05; and **, P < 0.01.

incorporation of each protein, the 4:1:1 DNA expression plasmid ratio was selected. As would be expected if F drove G incorporation into VLPs, the T2G combination did not show statistically significant increases in G levels beyond that of single G expression (Fig. 7A and B). Analysis with coimmunoprecipitation of G with T2 supports that this behavior is not due to any change in F:G avidities caused by the T2 deletion (Fig. 8A and B). Further, we observed that while G appears to be incorporated about three times more in the T2MG combination than for G alone (Fig. 7A and B), the difference is not statistically significant (*P* > 0.2). None of these effects appeared to be caused by changes in cell surface expression (Fig. 7C). Together, these and the above findings highlight a crucial role of NiV F, driven by regions and residues of its CT, in the presence or absence of M expression during the incorporation of G into viral particles.

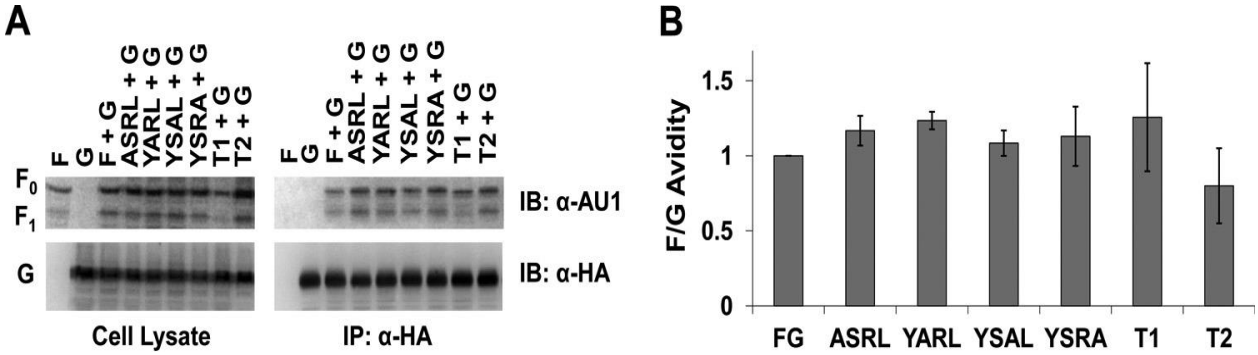

FIG 2.8 Mutation of the NiV F CT does not alter F-G avidity. HEK293T cells were transfected for G and different mutants of NiV F at an F:G ratio of 4:1. Cells were harvested and lysed. Part of the lysate was immunoprecipitated for NiV G. (A) Both the cell lysates and eluates were run through SDS-PAGE and Western blotted for F and G. (B) bands were quantified with blot densitometry, and the results for two experiments were averaged. Avidity was determined from the levels of (IP F)/(IP G * CL F). The standard error for each set is shown.

DISCUSSION

Previous work has suggested that NiV M, as for many of the paramyxoviruses, is the key player in viral assembly and budding (12, 23, 24, 26, 27, 29). As with other paramyxoviruses, studies for NiV have so far suggested that NiV M does not require F or G to form VLPs (22, 25). While our findings support this conclusion, prior studies have focused primarily on M as the indicator for VLP formation, whereas we have increased the scope to the incorporation of F, G, and M in all possible combinations. In doing so, we have increased the knowledge on the functional roles for these three structural proteins and advanced toward the understanding of viral particle formation. Our results show that both F and M can drive incorporation of G into viral particles several times more effectively than G alone (Fig. 1). While F and M significantly affected G incorporation, we report that F and M did not appear to significantly affect incorporation of each other (Fig. 1 and 2). Interestingly, coexpression of the F T2 deletion mutant with M did not result in any significant recovery of F budding (Fig. 7). This may suggest that F-M interactions are limited and/or that the mechanisms of particle egress driven by F or M differ significantly. For several paramyxoviruses, including parainfluenza virus 5 and mumps virus, viral budding is driven by proteins of the endosomal sorting complex required for transport (ESCRT) system (30, 31). ESCRT proteins have also been shown to be important in viral particle formation for many enveloped viruses (45). Still, in cases such as influenza virus and vesicular stomatitis virus, viral assembly and budding are thought to follow ESCRT-independent pathways (46–49). Importantly, initial experiments with NiV supported that this virus also utilized ESCRT-independent methods of budding. Specifically, when NiV M was previously coexpressed with dominant negative Vps4, the ATPase responsible for driving

ESCRT function, no significant decrease in budding was found (50). Such findings are not unprecedented for viruses somewhat related to NiV. Specifically, human respiratory syncytial virus can bud independently of the ESCRT system in a mechanism driven by Rab11 family interacting protein 2 (51). Importantly, a recent study revealed interactions between the NiV C protein and Tsg101, an ESCRT factor. These interactions increase M budding efficiency. The same study also demonstrated that live NiV titers decreased when the ESCRT machinery was inhibited (52). While the exact mechanism of NiV F budding is not known, one possibility is that regions of the cytoplasmic tail interact with ESCRT proteins to drive viral particle assembly and/or egress from the cell. A likely binding partner of NiV F is the ESCRTassociated protein, AIP-1/Alix. Several viruses, including some poxviruses, arenaviruses, and lentiviruses utilize YXXL motifs similar to that in the NiV F CT to interact with Alix/AIP1 and recruit ESCRT machinery during egress (53–55). Further experiments would be needed to explore this possibility.

The ability for a paramyxovirus protein other than M to bud autonomously has been seen in the cases of Sendai and measles virus F proteins but is rather rare among paramyxoviruses (26, 28, 29). We have also shown that autonomous budding behaviors of F are at least partially dependent on regions of its cytoplasmic tail (Fig. 3). These regions include a polybasic motif, an YXXL motif, and a dityrosine motif (Fig. 4, 5, and 6). All of these regions have been previously implicated in modulating biological functions of NiV F such as trafficking, endocytosis, and/or fusogenicity (21, 34, 35, 56). The envelope glycoproteins of both HIV-1 and -2 have cytoplasmic tails that contain YXXØ motifs important for proper trafficking (40–43). For HiV-2, proper trafficking has been shown to be dependent on interactions between the YXXØ motif and AP-2 (42). Further, this

tyrosine motif has also been shown to be a significant factor driving HIV-2 viral particle formation (42, 43). Although we report that T2 and T4 contain specific motifs that may be responsible for modulation of budding by those regions, we failed to identify a residue in the T1 region that confers a strong budding phenotype (Fig. 4). One possibility, supported by decreased budding after deletion of the whole region, is that T1 is important for spacing of the YXXØ motif directly following it. Other studies with transmembrane proteins have shown that specific trafficking patterns can depend not only on the presence of a YXXØ motif in the CT but also by the distance of the motif from the membrane. Lysosomal targeting, in particular, is characterized by a YXXØ motif six to nine residues from the membrane, which is interesting as the YXXØ motif in the NiV F CT starts at seven residues after the end of the transmembrane domain (57, 58).

The ties between the motifs we have identified as modulators of budding and lysosomal signaling are strengthened by the identification of the dityrosine motif in region T4 as basically necessary for F budding. We found that mutation of the dityrosine motif to alanines led to the nearly complete loss of VLP production. Importantly, diaromatic motifs similar to YY have been shown to be signals for lysosomal avoidance (58). While the underlying mechanism of budding remains unknown for NiV F, it may be that the interactions between this protein and trafficking factors, such as AP complexes (21, 34), indirectly or directly drive particle formation.

The observations concerning incorporation of NiV F, G, and M are most similar to the patterns of budding that have been reported for Sendai virus. Specifically, the fusion, but not the attachment glycoprotein, assists in budding (28, 29). Our findings that the substantial increase of G incorporation when G is coexpressed with F and/or

M is lost when the T2 mutant is used in place of WT F, supports the role of F as significantly supportive during viral particle formation. While we have shown the importance of the ability for F to drive budding during incorporation of itself and of G, it remains clear from previous studies that M is essential for the efficient production of infectious virions (59).

Importantly, we must keep in mind that in the context of simultaneous expression of the M, F, and G proteins, VLPs assembled and budded will include M-only, F-only, G-only, MF, MG, FG, and MFG VLPs. In this mixture of VLP populations, it remains to be seen what proportions of VLPs incorporate each of these proteins best. Although studies concerning the analysis of multiple populations are technically complicated, continually advancing techniques such as flow virometry may make these analyses more feasible, and we are currently enhancing this technique to accomplish these studies (33).

Although we have made strides in understanding the interactions between NiV F, G, and M in the process of particle formation, several questions remain. The importance of the F CT regions and residues we have identified as crucial for F budding should be tested in the context of the live virus under BSL-4 conditions. Our findings also support the importance of cellular factors in F budding and highlight several possible interactions of interest. Further studies could be conducted to identify which cellular factors are responsible for these assembly/budding phenotypes and help identify possible targets for treatments. While the mechanisms of NiV and closely related viruses remain to be completely understood, our identification of NiV F as a viral factor with importance not only in entry but also in egress may support future studies of assembly and VLP-based vaccine development.

MATERIALS AND METHODS

Antibodies. Mouse AU1 and HA monoclonal antibodies were purchased from BioLegend. For flow cytometric analyses, rabbit antiserum 835 was used to detect NiV F (60). Rabbit AU1 and HA antibodies were obtained from Bethyl Laboratories and used to detect NiV F and G, respectively, during Western blot analysis. Mouse antibodies against the FLAG epitope on NiV M were purchased from Thermo Scientific Pierce.

Cell culture. HEK293T (ATCC) cells were cultured in Dulbecco modified Eagle medium (Life Technologies) supplemented with 10% fetal bovine serum (FBS) and 1% PenStrep (Life Technologies). All experiments were conducted using HEK293T cells.

Plasmids. Codon-optimized sequences for NiV F and G were inserted into pcDNA3.1 expression vectors and tagged with AU1 (C terminal) and hemagglutinin (HA; C terminal), respectively, as published previously (61). Codon-optimized NiV M was inserted into a pCMV-3×-FLAG vector with an N-terminal FLAG tags as described previously (62). NiV F and all mutants were produced as described previously (35).

Cell surface expression. HEK293T cells were transfected in six-well plates with 3 µg of total DNA per well between 65 and 85% confluence using TurboFect (Thermo Fisher). After 24 h, cells were harvested with 10 mM EDTA and then collected by centrifugation at 350 × *g* for 30 s at 4°C. The pellet was resuspended with Dulbecco phosphate-buffered saline supplemented with 1% FBS. After staining of NiV F with rabbit polyclonal antibody 835 (1:250 dilution) and NiV G with mouse monoclonal antibody against HA

(BioLegend; 1:200 dilution) for 1 h, three washes were completed at 4°C and 800 × *g* for 5 min each. Afterward, goat anti-mouse and goat anti-rabbit secondary antibodies (Life Technologies) wereapplied at 1:2,000 dilution for 30 min, followed by two more washes and a fixation in 0.5% paraformaldehyde. After fixation, the cells were processed using a Millipore Guavasoft flow cytometer 8HT; 10,000 live cells were analyzed per sample.

Western blot analysis. SDS–10% polyacrylamide gels were run and transferred onto polyvinylidene difluoride (PVDF) membranes. Odyssey blocking buffer (LiCor Biosciences) was used to block membranes overnight. Primary and secondary antibodies were incubated for 1 h and 45 min, respectively. Washing with 0.2% Tween 20 in PBS was completed after each antibody incubation. After membrane blotting, imaging and densitometric analyses were completed on a Bio-Rad ChemiDoc MP imaging system. When necessary, blot stripping was done with NewBlot PVDF stripping buffer according to manufacturer suggestions.

Coimmunoprecipitation of F and G. HEK293T cells were seeded into six-well plates, and each well was transfected with F and/or G at a 4:1 ratio (a total of 2 µg of DNA per well) with Lipofectamine 2000 for 24 h. To ensure plenty of protein, three wells were combined for each sample. After transfection, the cells were lysed in lysis buffer (Miltenyi Biotec). Immunoprecipitations were completed according to manufacturer specification (Miltenyi Biotec) with the exception that all washes were completed with lysis buffer containing 150 mM NaCl, 1% Triton X-100, and 50 mM Tris HCl (pH 8.0) provided containing added the 1× protease inhibitor cOmplete ULTRA (Roche).

Coimmunoprecipitation eluates and cell lysates were subjected to SDS–10% PAGE and analyzed as described above.

Virus-like particle detection. Cells were transfected with TurboFect (Thermo Fisher) at 65 to 85% confluence in six-well plates. Then, 3 μg of total DNA was used per well as described for cell surface expression. After 24 h, the medium was collected and spun down at 376 × *g* for 10 min to pellet cellular debris. The supernatant medium was then loaded over 2 ml of 20% sucrose in NTE buffer and spun at 110,000 × *g* for 90 min at 4°C. After sucrose cushion ultracentrifugation, the pellets were resuspended in loading dye with 2% þ-mercaptoethanol and stored until loaded into a gel for SDS-PAGE.

ACKNOWLEDGMENTS

This study was supported by NIH/NIAID grant AI109022 to H.C.A. Graduate students G.P.J., E.M.C., and V.O. were supported by NIH/NIGMS training grant T32GM008336.

REFERENCES

1. Luby SP, Hossain MJ, Gurley ES, Ahmed B-N, Banu S, Khan SU, Homaira N, Rota PA, Rollin PE, Comer JA, Kenah E, Ksiazek TG, Rahman M. 2009. Recurrent zoonotic transmission of Nipah virus into humans, Bangladesh, 2001-2007. Emerg Infect Dis 15:1229–1235. https://doi.org/10 .3201/eid1508.081237.
2. Wu Z, Yang L, Yang F, Ren X, Jiang J, Dong J, Sun L, Zhu Y, Zhou H, Jin Q. 2014. Novel henipa-like virus, Mojiang paramyxovirus, in rats, China, 2012. Emerg Infect Dis 20:1064–1066. https://doi.org/10.3201/eid2006 .131022.
3. Drexler JF, Corman VM, Müller MA, Maganga GD, Vallo P, Binger T, Gloza-Rausch F, Rasche A, Yordanov S, Seebens A, Oppong S, Sarkodie YA, Pongombo C, Lukashev AN, Schmidt-Chanasit J, Stöcker A, Carneiro AJB, Erbar S, Maisner A, Fronhoffs F, Buettner R, Kalko EKV, Kruppa T, Franke CR, Kallies R, Yandoko ERN, Herrler G, Reusken C, Hassanin A, Krüger DH, Matthee S, Ulrich RG, Leroy EM, Drosten C. 2012. Bats host major mammalian paramyxoviruses. Nat Commun 3:796. https://doi.org/ 10.1038/ncomms1796.
4. Chua KB. 2000. Nipah virus: a recently emergent deadly paramyxovirus. Science 288:1432–1435. https://doi.org/10.1126/science.288 .5470.1432.
5. Enserink M. 1999. Epidemiology: new virus fingered in Malaysian epidemic. Science 284:407–410. https://doi.org/10.1126/science.284.5413 .407.
6. Parashar UD, Sunn LM, Ong F, Mounts AW, Arif MT, Ksiazek TG, Kamaluddin MA, Mustafa AN, Kaur H, Ding LM, Othman G, Radzi HM, Kitsutani PT, Stockton PC, Arokiasamy J, Gary HE Jr, Anderson LJ. 2000. Casecontrol study of risk factors for human infection with a new zoonotic paramyxovirus, Nipah virus, during a 1998-1999 outbreak of severe encephalitis in Malaysia. J Infect Dis 181:1755–1759. https://doi.org/10 .1086/315457.
7. Aguilar HC, Lee B. 2011. Emerging paramyxoviruses: molecular mechanisms and antiviral strategies. Expert Rev Mol Med 13:e6. https://doi.org/ 10.1017/S1462399410001754.
8. World Health Organization. 2015. Blueprint for R&D preparedness and response to public health emergencies due to highly infectious pathogens. World Health Organization, Geneva, Switzerland.
9. Samal SK (ed). 2011. The biology of paramyxoviruses. Caister Academic Press, Norfolk, United Kingdom.
10. Wong KT, Shieh W-J, Kumar S, Norain K, Abdullah W, Guarner J, Goldsmith CS, Chua KB, Lam SK, Tan CT, Goh KJ, Chong HT, Jusoh R, Rollin PE, Ksiazek TG, Zaki SR; Nipah Virus Pathology Working Group. 2002. Nipah virus infection: pathology and pathogenesis of an emerging paramyxoviral zoonosis. Am J Pathol 161:2153–2167. https://doi.org/10.1016/ S0002-9440(10)64493-8.
11. Aguilar HC, Iorio RM. 2012. Henipavirus membrane fusion and viral entry, p 79–94. In Lee B, Rota PA (ed), Henipavirus. Springer, Berlin, Germany.
12. Harrison MS, Sakaguchi T, Schmitt AP. 2010. Paramyxovirus assembly and

budding: building particles that transmit infections. Int J Biochem Cell Biol 42:1416–1429. https://doi.org/10.1016/j.biocel .2010.04.005.

13. Aguilar HC, Henderson BA, Zamora JL, Johnston GP. 2016. Paramyxovirus glycoproteins and the membrane fusion process. Curr Clin Microbiol Rep 3:142–154. https://doi.org/10.1007/s40588-016-0040-8.

14. Negrete OA, Wolf MC, Aguilar HC, Enterlein S, Wang W, Mühlberger E, Su SV, Bertolotti-Ciarlet A, Flick R, Lee B. 2006. Two key residues in EphrinB3 are critical for its use as an alternative receptor for Nipah virus. PLoS Pathog 2:e7. https://doi.org/10.1371/journal.ppat.0020007.

15. Negrete OA, Levroney EL, Aguilar HC, Bertolotti-Ciarlet A, Nazarian R, Tajyar S, Lee B. 2005. EphrinB2 is the entry receptor for Nipah virus, an emergent deadly paramyxovirus. Nature 436:401–405.

16. Aguilar HC, Aspericueta V, Robinson LR, Aanensen KE, Lee B. 2010. A quantitative and kinetic fusion protein-triggering assay can discern distinct steps in the Nipah virus membrane fusion cascade. J Virol 84:8033–8041. https://doi.org/10.1128/JVI.00469-10.

17. Liu Q, Stone JA, Bradel-Tretheway B, Dabundo J, Benavides Montano JA, Santos-Montanez J, Biering SB, Nicola AV, Iorio RM, Lu X, Aguilar HC. 2013. Unraveling a three-step spatiotemporal mechanism of triggering of receptor-induced Nipah virus fusion and cell entry. PLoS Pathog 9:e1003770. https://doi.org/10.1371/journal.ppat.1003770.

18. Bonaparte MI, Dimitrov AS, Bossart KN, Crameri G, Mungall BA, Bishop KA, Choudhry V, Dimitrov DS, Wang L-F, Eaton BT, Broder CC. 2005. Ephrin-B2 ligand is a functional receptor for Hendra virus and Nipah virus. Proc Natl Acad SciUSA102:10652–10657. https://doi.org/10 .1073/pnas.0504887102.

19. Lamp B, Dietzel E, Kolesnikova L, Sauerhering L, Erbar S, Weingartl H, Maisner A. 2013. Nipah virus entry and egress from polarized epithelial cells. J Virol 87:3143–3154. https://doi.org/10.1128/JVI.02696-12.

20. Erbar S, Maisner A. 2010. Nipah virus infection and glycoprotein targeting in endothelial cells. Virol J 7:305. https://doi.org/10.1186/1743-422X -7-305.

21. Mattera R, Farías GG, Mardones GA, Bonifacino JS. 2014. Co-assembly of viral envelope glycoproteins regulates their polarized sorting in neurons. PLoS Pathog 10:e1004107. https://doi.org/10.1371/journal .ppat.1004107.

22. Ciancanelli MJ, Basler CF. 2006. Mutation of YMYL in the Nipah virus matrix protein abrogates budding and alters subcellular localization. J Virol 80:12070–12078. https://doi.org/10.1128/JVI.01743-06.

23. Coronel EC, Murti KG, Takimoto T, Portner A. 1999. Human parainfluenza virus type 1 matrix and nucleoprotein genes transiently expressed in mammalian cells induce the release of virus-like particles containing nucleocapsid-like structures. J Virol 73:7035–7038.

24. Pantua HD, McGinnes LW, Peeples ME, Morrison TG. 2006. Requirements for the

assembly and release of Newcastle disease virus-like particles. J Virol 80:11062–11073. https://doi.org/10.1128/JVI.00726-06.

25. Patch JR, Crameri G, Wang L-F, Eaton BT, Broder CC. 2007. Quantitative analysis of Nipah virus proteins released as virus-like particles reveals central role for the matrix protein. Virol J 4:1. https://doi.org/10.1186/ 1743-422X-4-1.

26. Pohl C, Duprex WP, Krohne G, Rima BK, Schneider-Schaulies S. 2007. Measles virus M and F proteins associate with detergent-resistant membrane fractions and promote formation of virus-like particles. J Gen Virol 88:1243–1250. https://doi.org/10.1099/vir.0.82578-0.

27. Runkler N, Pohl C, Schneider-Schaulies S, Klenk H-D, Maisner A. 2007. Measles virus nucleocapsid transport to the plasma membrane requires stable expression and surface accumulation of the viral matrix protein. Cell Microbiol 9:1203–1214. https://doi.org/10.1111/j.1462-5822.2006 .00860.x.

28. Sugahara F, Uchiyama T, Watanabe H, Shimazu Y, Kuwayama M, Fujii Y, Kiyotani K, Adachi A, Kohno N, Yoshida T, Sakaguchi T. 2004. Paramyxovirus Sendai virus-like particle formation by expression of multiple viral proteins and acceleration of its release by C protein. Virology 325:1–10. https://doi.org/10.1016/j.virol.2004.04.019.

29. Takimoto T, Murti KG, Bousse T, Scroggs RA, Portner A. 2001. Role of matrix and fusion proteins in budding of Sendai virus. J Virol 75: 11384–11391. https://doi.org/10.1128/JVI.75.23.11384-11391.2001.

30. Li M, Schmitt PT, Li Z, McCrory TS, He B, Schmitt AP. 2009. Mumps virus matrix, fusion, and nucleocapsid proteins cooperate for efficient production of virus-like particles. J Virol 83:7261–7272. https://doi.org/10.1128/ JVI.00421-09.

31. Schmitt AP, Leser GP, Waning DL, Lamb RA. 2002. Requirements for budding of paramyxovirus simian virus 5 virus-like particles. J Virol 76:3952–3964. https://doi.org/10.1128/JVI.76.8.3952-3964.2002.

32. Walpita P, Barr J, Sherman M, Basler CF, Wang L. 2011. Vaccine potential of Nipah virus-like particles. PLoS One 6:e18437. https://doi.org/10.1371/ journal.pone.0018437.

33. Landowski M, Dabundo J, Liu Q, Nicola AV, Aguilar HC. 2014. Nipah virion entry kinetics, composition, and conformational changes determined by enzymatic virus-like particles and new flow virometry tools. J Virol 88:14197–14206. https://doi.org/10.1128/JVI.01632-14.

34. Vogt C, Eickmann M, Diederich S, Moll M, Maisner A. 2005. Endocytosis of the Nipah virus glycoproteins. J Virol 79:3865–3872. https://doi.org/ 10.1128/JVI.79.6.3865-3872.2005.

35. Aguilar HC, Matreyek KA, Choi DY, Filone CM, Young S, Lee B. 2007. Polybasic KKR motif in the cytoplasmic tail of Nipah virus fusion protein modulates membrane fusion by inside-out signaling. J Virol 81: 4520–4532. https://doi.org/10.1128/JVI.02205-06.

36. Khetawat D, Broder CC. 2010. A functional henipavirus envelope glycoprotein pseudotyped lentivirus assay system. Virol J 7:312. https://doi .org/10.1186/1743-422X-7-312.

37. Weise C, Erbar S, Lamp B, Vogt C, Diederich S, Maisner A. 2010. Tyrosine residues in the cytoplasmic domains affect sorting and fusion activity of the Nipah virus glycoproteins in polarized epithelial cells. J Virol 84: 7634–7641. https://doi.org/10.1128/JVI.02576-09.

38. El Najjar F, Schmitt A, Dutch R. 2014. Paramyxovirus glycoprotein incorporation, assembly and budding: a three-way dance for infectious particle production. Viruses 6:3019–3054. https://doi.org/10 .3390/v6083019.

39. Yonemura S, Hirao M, Doi Y, Takahashi N, Kondo T, Tsukita S, Tsukita S. 1998. Ezrin/radixin/moesin (ERM) proteins bind to a positively charged amino acid cluster in the juxta-membrane cytoplasmic domain of CD44, CD43, and ICAM-2. J Cell Biol 140:885–895. https://doi.org/10.1083/jcb .140.4.885.

40. Deschambeault J, Lalonde JP, Cervantes-Acosta G, Lodge R, Cohen EA, Lemay G. 1999. Polarized human immunodeficiency virus budding in lymphocytes involves a tyrosine-based signal and favors cell-to-cell viral transmission. J Virol 73:5010–5017.

41. Lodge R. 1997. The membrane-proximal intracytoplasmic tyrosine residue of HIV-1 envelope glycoprotein is critical for basolateral targeting of viral budding in MDCK cells. EMBO J 16:695–705. https://doi.org/10 .1093/emboj/16.4.695.

42. NobleB,AbadaP,Nunez-IglesiasJ,CannonPM.2006.Recruitmentofthe adaptor protein 2 complex by the human immunodeficiency virus type 2 envelope protein is necessary for high levels of virus release. J Virol 80:2924–2932. https://doi.org/10.1128/JVI.80.6.2924-2932.2006.

43. Abada P, Noble B, Cannon PM. 2005. Functional domains within the human immunodeficiency virus type 2 envelope protein required to enhance virus production. J Virol 79:3627–3638. https://doi.org/10.1128/ JVI.79.6.3627-3638.2005.

44. Diederich S, Sauerhering L, Weis M, Altmeppen H, Schaschke N, Reinheckel T, Erbar S, Maisner A. 2012. Activation of the Nipah virus fusion protein in MDCK cells is mediated by cathepsin B within the endosomerecycling compartment. J Virol 86:3736–3745. https://doi.org/10.1128/ JVI.06628-11.

45. Votteler J, Sundquist WI. 2013. Virus budding and the ESCRT pathway. Cell Host Microbe 14:232–241. https://doi.org/10.1016/j.chom.2013.08 .012.

46. Rossman JS, Jing X, Leser GP, Lamb RA. 2010. Influenza virus M2 protein mediates ESCRT-independent membrane scission. Cell 142:902–913. https://doi.org/10.1016/j.cell.2010.08.029.

47. Chen BJ, Leser GP, Morita E, Lamb RA. 2007. Influenza virus hemagglutinin and neuraminidase, but not the matrix protein, are required for assembly and budding of plasmid-derived virus-like particles. J Virol 81:7111–7123. https://doi.org/10.1128/JVI.00361-07.

48. Chen BJ, Lamb RA. 2008. Mechanisms for enveloped virus budding: can some viruses do without an ESCRT? Virology 372:221–232. https://doi .org/10.1016/j.virol.2007.11.008.

49. Irie T, Licata JM, McGettigan JP, Schnell MJ, Harty RN. 2004. Budding of PPxY-containing rhabdoviruses is not dependent on host proteins TGS101 and VPS4A. J Virol 78:2657–2665. https://doi.org/10.1128/JVI.78 .6.2657-2665.2004.

50. Patch JR, Han Z, McCarthy SE, Yan L, Wang L-F, Harty RN, Broder CC. 2008. The YPLGVG sequence of the Nipah virus matrix protein is required for budding. Virol J 5:137. https://doi.org/10.1186/1743-422X-5-137.

51. Utley TJ, Ducharme NA, Varthakavi V, Shepherd BE, Santangelo PJ, Lindquist ME, Goldenring JR, Crowe JE. 2008. Respiratory syncytial virus uses a Vps4-independent budding mechanism controlled by Rab11FIP2. Proc Natl Acad SciUSA105:10209–10214. https://doi.org/10 .1073/pnas.0712144105.

52. Park A, Yun T, Vigant F, Pernet O, Won ST, Dawes BE, Bartkowski W, Freiberg AN, Lee B. 2016. Nipah virus C protein recruits Tsg101 to promote the efficient release of virus in an ESCRT-dependent pathway. PLoS Pathog 12:e1005659. https://doi.org/10.1371/journal.ppat.1005659.

53. Honeychurch KM, Yang G, Jordan R, Hruby DE. 2007. The vaccinia virus F13L YPPL motif is required for efficient release of extracellular enveloped virus. J Virol 81:7310–7315. https://doi.org/10.1128/JVI .00034-07.

54. Shtanko O, Watanabe S, Jasenosky LD, Watanabe T, Kawaoka Y. 2011. ALIX/AIP1 is required for NP incorporation into Mopeia virus Z-induced virus-like particles. J Virol 85:3631–3641. https://doi.org/10.1128/JVI .01984-10.

55. Bieniasz PD. 2006. Late budding domains and host proteins in enveloped virus release. Virology 344:55–63. https://doi.org/10.1016/j.virol .2005.09.044.

56. Weis M, Maisner A. 2015. Nipah virus fusion protein: Importance of the cytoplasmic tail for endosomal trafficking and bioactivity. Eur J Cell Biol 94:316–322. https://doi.org/10.1016/j.ejcb.2015.05.005.

57. Rohrer J. 1996. The targeting of Lamp1 to lysosomes is dependent on the spacing of its cytoplasmic tail tyrosine sorting motif relative to the membrane. J Cell Biol 132:565–576. https://doi.org/10.1083/jcb.132.4 .565.

58. Bonifacino JS, Traub LM. 2003. Signals for sorting of transmembrane proteins to endosomes and lysosomes. Annu Rev Biochem 72:395–447. https://doi.org/10.1146/annurev.biochem.72.121801.161800.

59. Dietzel E, Kolesnikova L, Sawatsky B, Heiner A, Weis M, Kobinger GP, Becker S, von Messling V, Maisner A. 2016. Nipah virus matrix protein influences fusogenicity and is essential for particle infectivity and stability. J Virol 90:2514–2522. https://doi.org/10.1128/JVI.029 20-15.

60. DeBuysscher BL, Scott D, Marzi A, Prescott J, Feldmann H. 2014. Singledoselive-attenuatedNipahvirusvaccinesconfercompleteprotectionby eliciting antibodies directed against surface glycoproteins. Vaccine 32: 2637–2644.

https://doi.org/10.1016/j.vaccine.2014.02.087.

61. Aguilar HC, Matreyek KA, Filone CM, Hashimi ST, Levroney EL, Negrete OA, Bertolotti-Ciarlet A, Choi DY, McHardy I, Fulcher JA, Su SV, Wolf MC, Kohatsu L, Baum LG, Lee B. 2006. N-glycans on Nipah virus fusion protein protect against neutralization but reduce membrane fusion and viral entry. J Virol 80:4878–4889. https://doi.org/10.1128/JVI.80.10.4878 -4889.2006.

62. Wang YE, Park A, Lake M, Pentecost M, Torres B, Yun TE, Wolf MC, Holbrook MR, Freiberg AN, Lee B. 2010. Ubiquitin-regulated nuclearcytoplasmic trafficking of the Nipah virus matrix protein is important for viral budding. PLoS Pathog 6:e1001186. https://doi.org/10.1371/journal .ppat.1001186.

CHAPTER 3

Nipah Virus-Like Particle Egress is Modulated by Cytoskeletal and Vesicular Trafficking Pathways: a Proteomics Analysis

Gunner P. Johnston[1], Birgit Bradel-Tretheway[2], Paul D. Piehowski[3], Heather M. Brewer[3], J. Lizbeth Zamora[1], Victoria Ortega[1], Erik M. Contreras[1], Jeremy R. Teuton[3], Jason P. Wendler[3], Keesha M. Matz[2], Nicholas T. Usher[1], Joshua N. Adkins[3#], Hector C. Aguilar[1#]

[1]Department of Microbiology and Immunology, College of Veterinary Medicine, Cornell University, Ithaca, New York

[2]Paul G. Allen Center for Global Animal Health, Washington State University, Pullman, Washington

[3]Pacific Northwest National Laboratories, Richland, Washington

[#]Corresponding Authors

Please send correspondence to: Hector C. Aguilar (ha363@cornell.edu) or Joshua Adkins (Joshua.Adkins@pnnl.gov).

Key Words: Nipah virus, Paramyxovirus, Proteomics, Vesicular trafficking, Endocytosis, Cytoskeleton, Host-Pathogen Interaction

Running Title: Host Cellular Modulation of Nipah Virus Egress

*This manuscript was submitted to *mSystems* in March of 2019.

Abstract

Classified as a biosafety level 4 select agent, Nipah virus (NiV) is a deadly paramyxovirus with significant potential to cause substantial damage to global human and animal health. The recent findings of over twenty related viruses in the Henipavirus genus likely carried by bat and rodent reservoirs underscore the urgency of Henipaviral research. Elucidating the process of viral particle production in host cells is imperative both for targeted drug design and viral particle-based vaccine development. However, relatively little is understood concerning the functions of cellular machinery in paramyxoviral and henipaviral assembly and budding from host cells. Recent studies showed evidence for the involvement of multiple NiV proteins in viral particle formation, in contrast to the mechanisms understood for several paramyxoviruses as reliant on the matrix (M) protein alone. Further, the levels and purposes of cellular factor incorporation into viral particles are largely unexplored for the paramyxoviruses. To better understand the involvement of cellular machinery and the major structural viral fusion (F), attachment (G), and matrix (M) proteins during NiV assembly and budding, we performed proteomics analyses on virus-like particles (VLPs) produced from several combinations of these NiV proteins. Our findings indicate NiV VLPs incorporate vesicular trafficking and actin cytoskeletal factors. The involvement of these biological processes was validated by experiments indicating that perturbation of key factors in these cellular processes substantially modulated viral particle formation. These viral budding effects were most impacted when NiV-F was expressed alone or in combination with other NiV proteins, indicating that NiV-F relies heavily on these cellular processes during its role(s) in budding. These findings indicate a significant involvement

of the NiV fusion protein, vesicular trafficking, and actin cytoskeletal processes in efficient viral assembly and budding.

Importance

Nipah virus is a zoonotic bio-safety level 4 agent with high mortality outcomes in humans. The genus to which Nipah virus belongs, *Henipavirus,* includes five officially recognized pathogens; however, over twenty species have been identified in multiple continents within the last several years. As there are still no vaccines or treatments for NiV infection, elucidating its process of viral particle production is imperative both for targeted drug design as well as for particle-based vaccine development. Developments in high-throughput technologies makes proteomic analysis of isolated viral particles a highly insightful approach to understanding the life cycle of pathogens such as Nipah virus.

Introduction

Nipah virus (NiV) is a pathogen in the family *Paramyxoviridae* which includes measles and mumps viruses. It is highly virulent and capable of infecting numerous species of mammals. NiV particles are enveloped and transmissible to humans from fruit bat reservoirs as well as from livestock and other humans. Infection in humans leads to respiratory disease, severe encephalitis, and a case mortality rate between 40%-100% (1). Based on the absence of approved vaccines or treatments with the emerging threat that these viruses pose to human health, NiV and the closely related Hendra virus (HeV) are classified as Biosafety Level 4 (BSL4) agents and are included within the genus *Henipavirus*. Moreover, the World Health Organization recently listed NiV among the most likely pathogens to cause a major pandemic (2). Importantly, at least 20 new henipa-like viruses have been discovered in the last decade, underscoring the potential threat of NiV and related pathogens (3–5). The identification of pathogen-host interactions and elucidation of how these pathogens produce viral particles may yield novel anti-viral therapeutics or support development of particle-based vaccines such as those approved by the FDA for hepatitis B virus and human papillomavirus (6–8). Formation of infectious paramyxovirus particles must include incorporation of two kinds of transmembrane proteins, the fusion (F) and attachment (termed G for NiV and other henipaviruses) glycoproteins, which co-operate for viral entry in addition to the viral ribonucleoprotein complex, which includes the single-stranded, negative-sense viral genome and several viral proteins needed for transcription and replication (9). All paramyxoviruses additionally produce a matrix (M) protein which is generally thought to be central to the assembly and budding of viral components into new particles (10).

Specifically, several paramyxovirus M proteins drive budding largely through oligomerization into a scaffolding array capable of inducing membrane curvature (11). While for some paramyxoviruses, the matrix protein is solely required to produce particles (12, 13), for Sendai virus, mumps virus, and simian virus 5, one or both glycoproteins are supportive or essential for particle formation (14–17). Interestingly, live NiV containing a deletion of the M gene yielded a dramatic reduction in, but not complete loss of infectivity (18). Further, potential roles for NiV proteins other than M in viral production have begun to be identified (19–22).

Unlike paramyxovirus matrix proteins, which appear to primarily use electrostatic interactions between M monomers to drive budding (11, 23, 24), other paramyxovirus proteins appear to instead re-appropriate cellular machinery to accomplish budding (16, 20–22, 25). For example, proteins of the Endosomal Sorting Complexes Required for Transport (ESCRTs) and associated factors are specifically targeted for recruitment to budding sites by numerous enveloped viruses which include conserved motifs, termed late domains, within their viral proteins (26–32, 20, 33). Generally, removal or mutation of these late domains drastically reduces particle formation efficiency. Viral utilization of cellular factors other than ESCRTs for viral budding have also been reported including Rab11 GTPase, involved in recycling endosome function, and known Rab11-interacting factors (34–36). Another cellular machinery known to be involved in several mechanisms of assembly and/or egress is the actin cytoskeleton; however, its roles vary greatly and, for many viruses, are poorly understood (25, 37–40). highlighting the many strategies viruses have adopted to ensure their replication and spread.

An approach to the identification and elucidation of roles for cellular machinery in

enveloped particle formation is the use of proteomics to identify the host proteins enriched in viral particles and the cellular processes involved (41–43). A recent study by Vera-Velasco *et al.* focused on the identification of host cellular proteins in NiV virus-like particles (VLPs) produced from co-transfection of the NiV F, G, and M proteins (44). Among the insights gained in this study, 67 human proteins were identified, primarily associated with vesicular transport and sorting. However, the importance of these cellular factors during viral particle formation and the involvement of each F, G, and M viral proteins in the recruitment or incorporation of such cellular factors into VLPs remains elusive.

Based on two studies indicating roles of the NiV and HeV F proteins in particle formation (19, 45), we expanded this VLP proteomics approach to include several combinations of particles produced from co-expression of F, G, and M. Our subsequent finding that F- but not M-derived VLPs incorporate numerous cellular factors adds support to the notion that henipaviral F proteins are involved in viral assembly and budding with a heavy reliance on cellular factors. Our results validate the importance of the most enriched processes, vesicular trafficking and the cytoskeleton, as modulatory of NiV particle release primarily through F-driven budding.

Methods

Cells, DNA Plasmids, and Antibodies

HEK293T cells were obtained from ATCC and used for all experiments. These cells were grown in Dulbecco's Modified Eagle Medium (DMEM, Corning) supplemented with 10% Fetal Bovine Serum (FBS) and 1% Penicillin/Streptomycin (Gibco) at 37ºC with 5% CO_2. Previously published DNA constructs for NiV proteins: pcDNA3.1-F-AU1, pcDNA3.1-G-HA, and pCMV-3XFLAG-M were used (19). These constructs were also used to make pCAGGS-NiV-F-AU1 and pCAGGS-NiV-M-3XFLAG. A dominant-negative (DN; S25N) mutant of Rab11 (46) inserted into a pGL vector was generously provided by Dr. Ruth Collins (Cornell University). PEGFP constructs containing previously described dominant-negative mutants of dynamin-2 (DN-Dynamin; K44A) and eps15 (DN-Eps15; Δ95/295) were used (47–49). pcDNA3.1 constructs containing constitutively-active (CA) and dominant-negative RhoA, Rac1, and Cdc42 were used (50). The dominant-negative Vps4A (DN-Vps4A) mutant (51) was synthesized and inserted into a pcDNA3.1 vector (Biomatik). Antibodies used against NiV F were: rabbit polyclonal 835term for flow cytometry (52) and mouse monoclonal anti-AU1 for western blots (Biolegend). Also used were primary antibodies against G: mouse monoclonal anti-HA for flow cytometry (Biolegend) and rabbit polyclonal anti-HA for western blots (Bethyl). Mouse monoclonal M2 anti-FLAG was used to detect NiV M for western blots (Sigma-Aldrich). Mouse monoclonal anti-sequestosome-1 antibodies were used to validate VLP proteomics (Abcam, ab56416). Goat anti-mouse and anti-rabbit 647 and 488 secondaries (ThermoFisher Scientific) were used for western blotting and flow cytometry as described previously (19).

NiV VLP production and Sample Preparation for Proteomic Analyses

Five 15-cm^2 dishes confluent with HEK293T cells were transfected using polyethylimine (PEI, Polysciences inc.) at 1mg/mL for each of the following combinations of plasmid constructs: pcDNA3.1, F, M, MG, FM, and FMG at an FMG DNA ratio of 24:1:5 (F:G:M; Table in Fig. 1A shows this as well). For each dish, 30µg of total DNA was transfected at a 4:1 ratio of PEI to DNA as described previously (53). For these experiments, pCAGGS versions of NiV-F and NiV-M constructs were used for optimal expression. After 48 hours, the media was collected and cleared of cellular debris by centrifugation at 376 x g for 10 minutes, as previously described (19). The resulting supernatant was collected and layered over 20% sucrose in NTE buffer and spun at 110,000 x g for 90 minutes. After this VLP purification spin, VLPs were resuspended with 5% sucrose in NTE buffer and shipped to Pacific Northwest National Laboratories for VLP proteomics analyses, described next.

Sample Preparation for VLP Proteomics

Purified viral-like particle samples were lysed and extracted by adding 1.0mL of 2:1 (v:v) chloroform:methanol and vortexing before storing on ice. The samples were then placed in a centrifugal concentrator and dried completely overnight. Proteins were solubilized with the addition of 10uL of homogenization buffer (8M urea, 10mM dithiothreitol, 50mM Tris pH 8) followed by 30s in a bath sonicator. The lysate was then incubated at 60 °C for 30min to denature and reduce the proteins. Protein solution was quantitatively transferred to a low retention LC vial (Waters) using 25µL of 50mM Tris pH 8. SNaPP

analysis was carried out as described previously (54, 55). Briefly, 25uL of sample was injected onto a 150µm x 2cm immobilized enzyme reactor for digestion. The digestion column was syringe packed using Poroszyme immobilized trypsin (Applied Biosystems). Following digestion, peptides were separated using a 100min gradient on an in-house packed 50µm x 75cm C18 (Phenomenex) analytical column. The SNaPP system was coupled to a QExactive Plus mass spectrometer (Thermo Scientific) operated at a mass resolution of 70K for MS1 and 17.5 for MS2 collection. Data was collected in DDA mode with a top 12 method and a dynamic exclusion window of 30s. The maximum IT was increased to 200ms for MS2 to maximize identifications from low sample loadings.

Proteomics

Peptide samples (5uL) were analyzed by LC-MS/MS using a Waters nano-Acquity M-Class dual pumping UPLC system (Milford, MA) configured for on-line trapping at 5µL/min for 8min followed by gradient elution through a reversed-phase analytical column at 300nL/min. Columns were packed in-house using 360µm o.d. fused silica (Polymicro Technologies Inc.) and contained Jupiter C18 media (Phenomenex) in 5µm particle size for the trapping column (100µm i.d. x 4cm long) and 3µm particle size for the analytical column (75µm i.d. x 70 cm long). Mobile phases consisted of (MP-A) 0.1% formic acid in water; and (MP-B) 0.1% formic acid in acetonitrile with the following gradient profile (min, % MP-B): 0, 1; 2, 8; 20, 12; 75, 30; 97, 45; 100, 95; 110, 95.

MS analysis was performed using a Q-Exactive HF mass spectrometer (Thermo Scientific, San Jose, CA). Electrospray emitters were prepared in-house using 150µm o.d. x 20µm i.d. chemically etched fused silica (Kelly et al., 2006) and subsequently

attached to the column using a metal union and coupled to the mass spec via a custom built nanospray source . Electrospray voltage (2.2 kV) was applied at the metal union providing ions to the heated (325ºC) ion transfer tube entrance of the MS. Data was started 20 min after the gradient began and continued for a total acquisition time of 100 min. Precursor MS spectrum were acquired from 400–2000 *m/z* at resolution 60k (AGC target 3e6, max IT 20 ms) followed by data-dependent MS/MS spectra of the top 12 most abundant ions from the precursor spectrum with an isolation window of 2.0 *m/z* and at a resolution of 15k (AGC target 1e5, max IT 200 ms) using a normalized collision energy of 30 and a 45 sec exclusion time.

VLP Proteomics Analyses

Modern mass spectrometers can observe very low abundance contaminants in low complexity samples, such as VLPs. Further, the experimental enrichment of very small particle with subsequent sample preparation by SNaPP result in approximation of loading protein quantity. Hence, samples are batched as sets and then randomized within sets to allow for interpretation of potential carry-over from abundant proteins from one VLP composition measurement to another. Relative quantification was performed via a spectral counting approach where the number of tandem mass spectra identified as matching a protein is used as a proxy for abundance that can be compared across datasets.

Further, the identification of peptides corresponding the three NiV proteins: F, G, and M was used to evaluate the quality of measurements. LC-MS/MS analyses considered for further analysis were included or excluded based on expected viral

protein compositions. Specifically, we set the requirement that a replicate would only be included in the next stages of analysis if it contained no more than 2 observed peptides corresponding to unexpected viral protein carry-over (e.g. M peptides in an F sample replicate). Similarly, we also set the requirement that each included replicate would require at least two observed peptides for each expected viral protein. Potential limitations of this were that the viral proteins did have different observation rates due to different lengths and expression levels, however, levels of peptides for viral proteins within samples they were expected were almost always much greater than in samples in which they were unexpected, regardless of the viral protein.

To identify host-derived proteins considered incorporated into VLPs of each combination, an approach based on averaged observed peptides was used. All proteins considered incorporated in any type of VLP were not allowed to have any more than an average observed peptide count of 2 in the control samples (VLPs isolated from cells transfected with an empty vector) and were required to have at least an average of 4.33 observed peptides in the VLP type of interest. By setting a low maximum threshold for observed peptides in the empty vector control, we sought to remove cellular factors highly enriched in background exosomes and microvesicles. An average observed peptide count of 4.33 in VLPs was set as the threshold as this corresponded to the lowest level of average peptide incorporation for any expected viral protein in any of the VLP combination types.

After incorporated host-protein protein lists were determined for each VLP combination, comparisons were done using InteractiVenn (56). Further, protein-protein interaction mapping were completed using STRING and Cytoscape softwares (57, 58).

Gene ontological designations used for Table 1 and the protein interaction map were conducted using GOTermFinder (59).

VLP Budding Assay

HEK293T cells were transfected between 65% and 85% confluency using 1mg/mL PEI. After 24 hours, media was collected and pre-cleared by centrifugation as above, while the transfected cells were harvested with 10mM EDTA (from 0.5M stock, VWR) in Dulbecco's Phosphate Buffered Saline (DPBS, Corning) and split into two groups: cell lysate and cell surface expression. For both groups, cells were pelleted by centrifugation at 376 x g for 10 minutes and the supernatant removed. For the cell lysate fraction, 1X RIPA buffer (Sigma-Aldrich) was prepared in tissue culture grade water (Corning) with cOmplete^{TM} ULTRA protease inhibitor (Roche) and added to the pellet prior to 30 minutes of vortexing and rotating at 4ºC. Lysate supernatant was collected and prepared for 10% SDS-PAGE (Protogel), transfer to activated PVDF membrane (ThermoFisher Scientific), and blotting with antibodies against AU1, HA, and FLAG tags, as described previously (19). For the group to be assessed for cell surface expression, the pellet was resuspended with FACS buffer (1% FBS in DPBS) and stained with rabbit polyclonal 835term (for F) and mouse monoclonal anti-HA (for G) for one hour prior to three washes with FACS buffer, secondary antibody staining for 30 minutes, two final FACS washes and analysis with a Millipore Guava easyCyte flow cytometer 8HT; 10,000 or more cells were analyzed per sample, as described (19).

Transmission Electron Microscopy Sample Preparation and Imaging

One 15-cm dish of HEK293T cells was transfected using PEI as discussed above for each combination of F, G, and M. VLPs were harvested and negatively stained with 1% Uranyl Acetate and visualized using a Tecnai T12 Spirit (FEI) at 120kV located in the Cornell University Center for Materials Research.

Cell-cell Fusion Assay

HEK293T cells were transfected at 80-95% confluency with NiV F, G, and either pcDNA3.1 or one of the mutant cellular factors described in previous figures at a DNA:PEI ratio of 1:3 with a total transfection of 2.1µg of DNA (F:G:pcDNA or cell factor ratio of 3:1:3). After 12 hours, the cells were fixed in 1% paraformaldehyde at 37ºC for one hour and imaged on a Leica brightfield scope. Five fields of view at 200x magnification were used to quantify levels of cell-cell fusion, where each nucleus associated with a syncytium of four or more nuclei was counted. For each transfected sample, the fields of view were averaged, reduced by background syncytia levels (empty vector control), and normalized to the positive control (set at 100%) (60–63)

Results

Overview of workflow and results from VLP and cellular proteomics. To help identify specific cellular factors and machinery incorporated during NiV budding, we transfected human embryonic kidney (HEK293T) cells with plasmid constructs coding for individual structural NiV proteins: F, G, and M. To best elucidate the relative importance of the F and M proteins for incorporation of cellular factors, five combinations (F-alone, M-alone, FM, MG, and FMG) of transfections were completed in addition to an empty vector control, a background for naturally expressed extracellular vesicles (e.g. exosomes and microvesicles) (Fig. 1A). Forty-eight hours after transfection, VLPs and their corresponding transfected cells were separately isolated and prepared for proteomic analyses (Fig. 1A). As described in the methods, observed peptide counts were used to remove replicates indicating contamination from overflow, resulting in 3-5 biological replicates per transfection type being used for further analyses. Average peptide counts were used to identify which cellular factors were incorporated into VLPs using two thresholds: a minimum average peptide count of 4.33 for the replicates of a given transfection type (e.g. F-only), based on the average observed peptide counts of the viral proteins themselves, as well as a maximum average count of 2 in empty vector controls to remove proteins highly expressed in background extracellular vesicles. To verify that this approach produces vesicles and to visualize vesicles for each combination, negative staining and transmission electron microscopy was used (Fig. 1B). Importantly, spikes were most apparent in combinations containing F and/or G supporting the incorporation of these proteins, whereas M-only VLPs lacked spikes and tended to include high-contrast structures internally (Fig. 1B).

From the VLP proteomics, the following number of cellular proteins was identified for each VLP sample type: 8 (M), 83 (F), 41 (FM), 7 (MG), and 97 (FMG) (Fig. 1C). A Venn diagram was constructed to help identify cellular proteins that were common to all, some, or only one VLP combination.

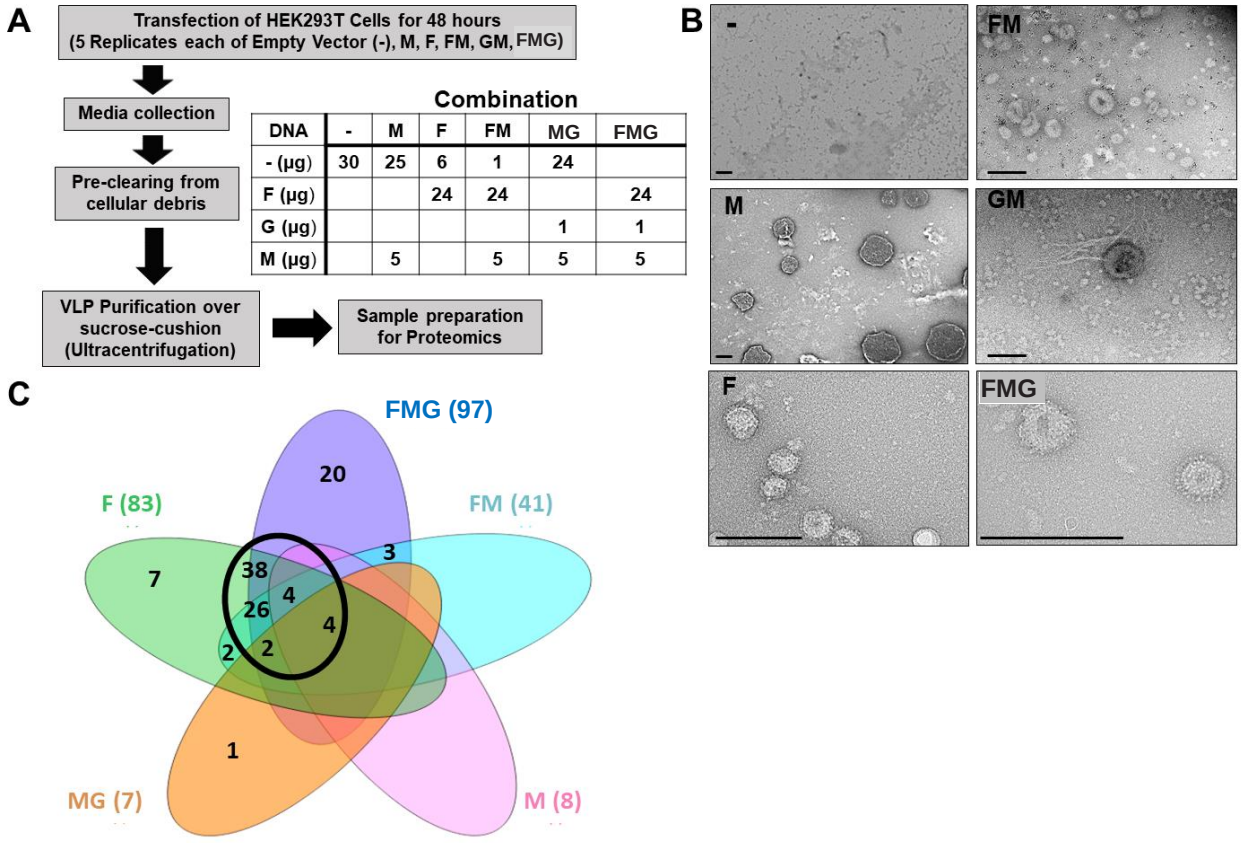

Fig. 3.1: Overview of workflow and results from VLP and cellular omics. Human embryonic kidney (HEK293T) cells were transfected with combinations of constructs coding for the Nipah virus fusion (F), attachment (G), and matrix (M) proteins. Media and cells were collected after 48 hours. Media supernatant was used to isolate virus-like particles (VLPs) then both VLPs and cells were prepared for proteomics analysis. (B) VLPs produced from the listed combinations of viral protein transfection were isolated and negatively stained with 1.5% uranyl acetate. Scale bars indicate 250nm. (C) Venn diagram summarizing the number of proteins identified as enriched in each VLP combination and their distribution of overlap. The black circle highlights the significant overlap between combinations including F.

VLP proteomics highlighted by enrichment of cytoskeletal and endosomal trafficking machinery. We next created a protein interaction map by combining our FMG VLP proteomics data with the data from a recent proteomics composition study on NiV FMG VLPs (41), to help us identify protein clusters consistently incorporated into VLPs. Overall, the enriched processes and protein-protein interaction sets have a high degree of overlap; however, specific proteins identified in common are relatively few. Small differences in specific protein compositions for VLPs are likely influenced by differences in methodologies; however, the consistent enrichment of several processes suggests their underlying involvement. Namely, two of the most enriched functional groups of proteins were vesicle-mediated transport and the actin cytoskeleton (Fig. 2A). Sequestosome-1 (SQSTM1), an adapter protein involved in vesicle-mediated transport , namely macroautophagy (64) was found to be among the most enriched proteins, particularly in VLPs produced from cells expressing F (Table 1). To support the validity of our VLP proteomics platform, the VLP samples used in proteomics were also analyzed by Western blot analysis and the pattern of SQSTM1 incorporation primarily into VLPs containing NiV-F was confirmed (Fig. 2B). A full list of VLP incorporated proteins is shown in Table 1, comparing the proteins identified in different types of VLPs (F, M, etc) with those in FMG VLPs in Vera-Velasco *et al.*, and further identifying whether each protein is associated with vesicle-mediated transport or the cytoskeleton.

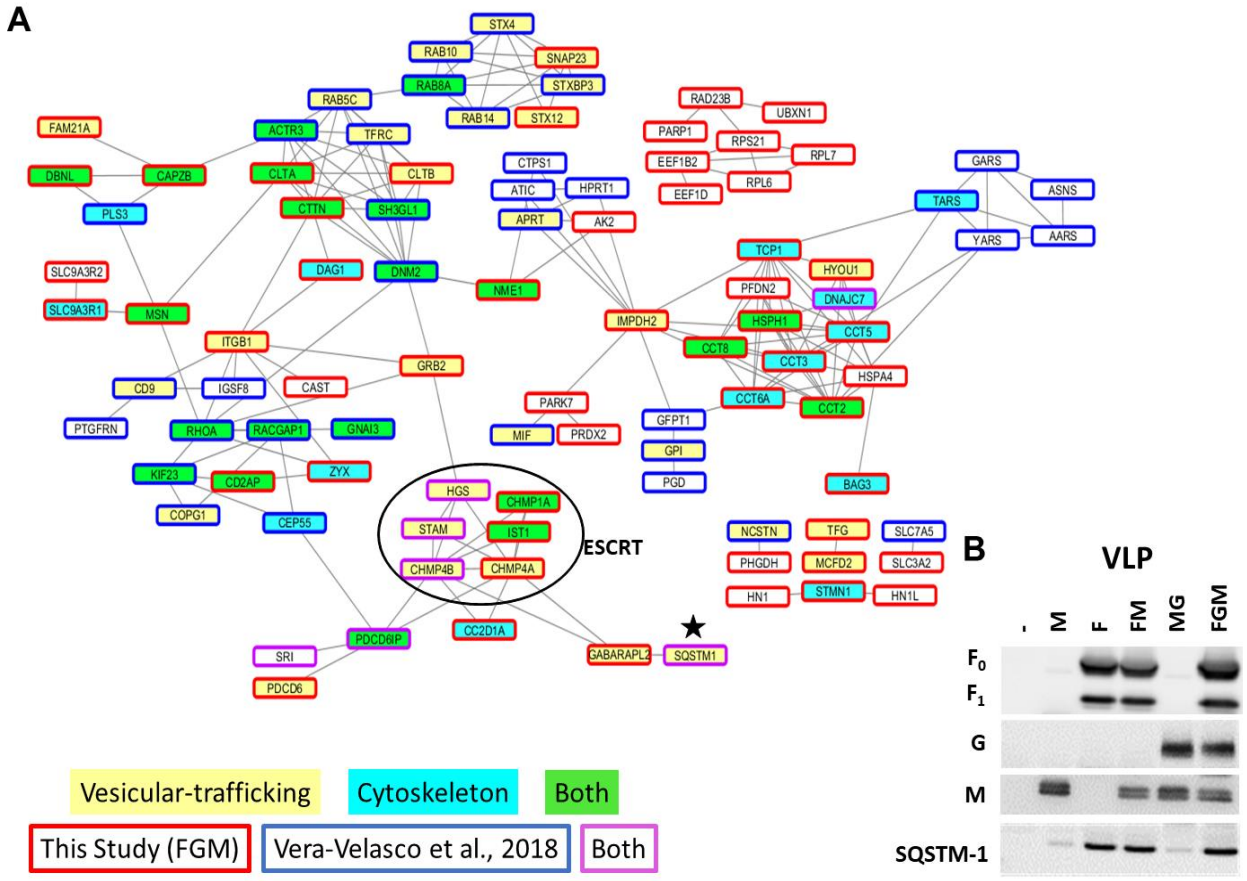

Fig. 3.2: VLP proteomics highlighted by enrichment of cytoskeletal and endosomal trafficking machinery. (A) A STRING protein interaction map comparing between proteins identified in the FMG VLPs described in Vera-Velasco et al. (blue border) and this study (red border). This map identifies which protein clusters have associated factors included in one or both (purple border) studies. Among the most enriched groups based on gene ontological analyses of the combined dataset are vesicular trafficking (yellow) and the cytoskeleton (light blue) with proteins that belong to both also designated (green). ESCRTs which overlap somewhat with both processes were observed in both studies and are in a black circle. Note that the clusters associated with these processes tend to have included proteins identified in both studies analyzed. Importantly, only proteins with at least one interaction were shown on this map, a full list can be found in Table 1. One of the most clearly enriched proteins in VLP proteomics for this study and Vera-Velasco et al. was the autophagy adapter protein, sequestosome-1 (SQSTM1, designated by small black star). (B) Using western blot analysis of VLPs for each combination, Sequestosome-1 was used to validate the accuracy of our VLP proteomics, since it exhibited highly similar expression patterns as peptide counts. Western blot is representative of at least three replicates.

Table 3.1: All VLP incorporated proteins. Proteins identified in VLPs from at least one type of transfection and/or Vera-Velasco et al., are listed along with their uniprot identifier totaling 166 proteins. The inclusion of any given protein in any of these sample sets or in the gene ontological (GO) groups of vesicle-mediated transport (VMT) or cytoskeleton are indicated by grey shading. White shading indicates that the protein of interest was not identified in that group. The number of proteins identified in each transfection or GO set from the full list of 166 proteins is indicated next to the header for the transfection or GO group.

SYMBOL	FULL NAME	ACCESSION	VMT (65/166)	Cytoskeleton (54/166)	M (8/166)	F (83/166)	FM (41/166)	MG (7/166)	FGM (97/166)	Vera-Velasco (67/166)
CAST	calpastatin	E7ES10							■	
DYNC1LI1	dynein cytoplasmic 1 light intermediate chain 1	Q9Y6G9	■	■						■
CHMP4B	charged multivesicular body protein 4B	Q9H444	■			■	■		■	■
TSPAN3	tetraspanin 3	L8E893								■
CHMP4A	charged multivesicular body protein 4A	Q9BY43	■			■			■	
RPL15	ribosomal protein L15	E7ERA2				■				
CAPZA1	capping actin protein of muscle Z-line alpha subunit 1	P52907	■	■		■				
PGD	phosphogluconate dehydrogenase	K7EMN2								■
TSPAN6	tetraspanin 6	A0A024RCI0								■
CCT2	chaperonin containing TCP1 subunit 2	F8VQ14	■	■		■	■		■	
CCT3	chaperonin containing TCP1 subunit 3	P49368		■		■	■		■	
PRKCSH	protein kinase C substrate 80K-H	A0A0S2Z4D8				■			■	
SLC7A5	solute carrier family 7 member 5	Q01650								■
CD2AP	CD2 associated protein	Q9Y5K6	■	■		■			■	
SLC16A1	solute carrier family 16 member 1	A0A024R0H1		■						■
DNAJC7	DnaJ heat shock protein family	K7EQ73		■		■			■	■
STAM	signal transducing adaptor molecule	B4DZT2	■						■	■
PLS3	plastin 3	H7C4N2		■						■
PLD3	phospholipase D family member 3	Q8IV08								■
DBNL	drebrin like	H7C111	■	■		■			■	
YARS	tyrosyl-tRNA synthetase	A0A0S2Z4R1								■
gnai3	G protein subunit alpha i3	P08754	■	■						■
ERP29	endoplasmic reticulum protein 29	F8W1G0				■	■		■	
AARS	alanyl-tRNA synthetase	P49588								■
OLA1	Obg like ATPase 1	J3KQ32	■	■						■
RPS18	ribosomal protein S18	J3JS69				■	■			
IGSF8	immunoglobulin superfamily member 8	Q969P0								■
COPG1	coatomer protein complex subunit gamma 1	D6RG17	■							■
NME1	NME/NM23 nucleoside diphosphate kinase 1	E7ERL0	■	■		■			■	
RAB14	RAB14, member RAS oncogene family	P61106	■							■
SDCBP	syndecan binding protein	E9PBU7	■	■						■
STMN1	stathmin 1	A2A2D0		■	■	■	■	■	■	
PDCD6IP	programmed cell death 6 interacting protein	F8WBR8	■	■		■	■	■	■	
PTGFRN	prostaglandin F2 receptor inhibitor	A4QPA1								■
RAB10	RAB10, member RAS oncogene family	Q9UL28	■							■
DBN1	drebrin 1	D6RCR4		■					■	
SH3GL1	SH3 domain containing GRB2 like 1, endophilin A2	Q9BVL7	■	■						■
SRI	sorcin	C9J0K6				■	■		■	■
RAD23B	RAD23 homolog B, nucleotide excision repair protein	Q5W0S5			■	■	■		■	
CDV3	CDV3 homolog	D6R973				■	■		■	
EEF1B2	eukaryotic translation elongation factor 1 beta 2	F8WFC9			■	■	■	■	■	
LMNB1	lamin B1	B4DZT3		■					■	
GRB2	growth factor receptor bound protein 2	J3QRL5	■			■			■	
DAG1	dystroglycan 1	C9JQL4		■		■			■	
CTPS1	CTP synthase 1	P17812								■
GIPC1	GIPC PDZ domain containing family member 1	K7EJ33	■						■	
CAPZB	capping actin protein of muscle Z-line beta subunit	B1AK87	■	■		■			■	
ITGB1	integrin subunit beta 1	P05556	■				■		■	
CDC37	cell division cycle 37	Q16543							■	
CALU	calumenin	A0A024R755				■			■	
ALCAM	activated leukocyte cell adhesion molecule	F5GXJ9				■				
STX12	syntaxin 12	Q86Y82	■			■			■	
PSMB6	proteasome subunit beta 6	Q6IAT9								■
RPL7	ribosomal protein L7	P18124				■	■		■	
RPL6	ribosomal protein L6	F8VU16				■	■	■	■	
NDRG1	N-myc downstream regulated 1	Q8N959		■		■			■	■
RPS21	ribosomal protein S21	Q6FGH5							■	
SDF4	stromal cell derived factor 4	Q9BRK5	■			■			■	
GABARAPL2	GABA type A receptor associated protein like 2	H3BU36	■			■			■	
RAB8A	RAB8A, member RAS oncogene family	P61006	■	■						■
EPB41	erythrocyte membrane protein band 4.1	Q4VB87		■						■
CD276	CD276 molecule	H0YN85								■
GARS	glycyl-tRNA synthetase	A0A090N8G0								■
AK2	adenylate kinase 2	F8VZG5				■	■		■	
TPD52L2	tumor protein D52 like 2	O43399				■			■	
TAX1BP1	Tax1 binding protein 1	C9JBZ7				■			■	
PPA1	pyrophosphatase	Q5SQT6							■	■
HN1L	hematological and neurological expressed 1 like	Q9H910				■			■	
HYOU1	hypoxia up-regulated 1	A0A087WW13	■						■	
TXNDC12	thioredoxin domain containing 12	V9GY50				■			■	
CCT5	chaperonin containing TCP1 subunit 5	E7ENZ3		■		■	■		■	
PPIB	peptidylprolyl isomerase B	P23284				■			■	
DSG2	desmoglein 2	J3KSI6			■	■	■	■	■	
CCT8	chaperonin containing TCP1 subunit 8	H7C2U0	■	■		■	■		■	
CPNE1	copine 1	Q99829	■							■
HGS	hepatocyte growth factor-regulated tyrosine kinase substrate	I3L1E3	■						■	■
CPNE3	copine 3	E5RFT7	■							■
PARP1	poly	Q5VX85			■	■	■		■	
PDCD6	programmed cell death 6	A0A024QZ42	■			■	■		■	
KIF23	kinesin family member 23	H7BYN4	■	■						■
CLTA	clathrin light chain A	C9J8P9	■	■		■			■	
CLTB	clathrin light chain B	D6RJD1	■						■	
RAB5C	RAB5C, member RAS oncogene family	F8VVK3	■							■
TOLLIP	toll interacting protein	Q6FIE9	■			■				
MARCKSL1	MARCKS like 1	P49006		■						■

HINT1	histidine triad nucleotide binding protein 1	H0YC49								
UCHL1	ubiquitin C-terminal hydrolase L1	P09936								
PRDX4	peroxiredoxin 4	A6NG45								
PRDX2	peroxiredoxin 2	A0A024R7F2								
slc9a3r2	SLC9A3 regulator 2	Q15599								
CXADR	coxsackie virus and adenovirus receptor	P78310								
ACTR3	ARP3 actin related protein 3 homolog	F8WEW2								
HSPH1	heat shock protein family H	A0A024RDS1								
CTTN	cortactin	H0YCD9								
BAG3	BCL2 associated athanogene 3	O95817								
RHOA	ras homolog family member A	C9JX21								
cc2d1a	coiled-coil and C2 domain containing 1A	K7EJY5								
ZYX	zyxin	H7C3R3								
MSN	moesin	V9HWC0								
IMPDH2	inosine monophosphate dehydrogenase 2	Q6QE17								
GOLM1	golgi membrane protein 1	C9J941								
ABCE1	ATP binding cassette subfamily E member 1	P61221								
STX4	syntaxin 4	Q12846								
FLOT2	flotillin 2	Q14254								
SLC3A2	solute carrier family 3 member 2	F5GZS6								
HN1	hematological and neurological expressed 1	J3KT51								
STXBP3	syntaxin binding protein 3	O00186								
CCT6A	chaperonin containing TCP1 subunit 6A	P40227								
SLC9A3R1	SLC9A3 regulator 1	O14745								
EPB41L2	erythrocyte membrane protein band 4.1 like 2	E9PMG5								
PFDN2	prefoldin subunit 2	Q9UHV9								
TARS	threonyl-tRNA synthetase	D6RCS6								
CHMP1A	charged multivesicular body protein 1A	F8VUA2								
CLIC4	chloride intracellular channel 4	Q9Y696								
TBCA	tubulin folding cofactor A	O75347								
IPO5	importin 5	C9J875								
NUCB2	nucleobindin 2	E9PLR0								
KHSRP	KH-type splicing regulatory protein	M0QYH3								
TOM1	target of myb1 membrane trafficking protein	H7BYN7								
GNAS	GNAS complex locus	Q5JWF2								
CA2	carbonic anhydrase 2	V9HW21								
MAPRE1	microtubule associated protein RP/EB family member 1	A2VCR0								
EEF1D	eukaryotic translation elongation factor 1 delta	Q9BW34								
TF	transferrin	C9JB55								
SLC39A14	solute carrier family 39 member 14	A0A0S2Z5C8								
USP5	ubiquitin specific peptidase 5	A0A140VJZ1								
CALCOCO2	calcium binding and coiled-coil domain 2	H0YBP4								
TFG	TRK-fused gene	Q92734								
ASNS	asparagine synthetase	C9J605								
CEP55	centrosomal protein 55	Q53EZ4								
HPRT1	hypoxanthine phosphoribosyltransferase 1	P00492								
MIF	macrophage migration inhibitory factor	I4AY87								
ANXA6	annexin A6	E5RFF0								
CD9	CD9 molecule	B4DK09								
CBR1	carbonyl reductase 1	E9PQ63								
ATIC	5-aminoimidazole-4-carboxamide ribonucleotide formyltransferase/IMP cyclohydrolase	V9HWH7								
SQSTM1	sequestosome 1	E7EMC7								
VPS35	VPS35, retromer complex component	Q96QK1								
HSPA4	heat shock protein family A	P34932								
SNAP23	synaptosome associated protein 23	O00161								
NENF	neudesin neurotrophic factor	Q9UMX5								
EHD4	EH domain containing 4	Q9H223								
UBXN1	UBX domain protein 1	Q04323								
fam21a	family with sequence similarity 21 member A	Q641Q2								
TCP1	t-complex 1	F5H7Y1								
SLC12A2	solute carrier family 12 member 2	B7ZM24								
VTA1	vesicle trafficking 1	Q9NP79								
NASP	nuclear autoantigenic sperm protein	E9PKR5								
NSFL1C	NSFL1 cofactor	R4GNE6								
RACGAP1	Rac GTPase activating protein 1	F8VZ66								
DBI	diazepam binding inhibitor, acyl-CoA binding protein	B8ZWD8								
PARK7	Parkinsonism associated deglycase	K7EN27								
APRT	adenine phosphoribosyltransferase	H3BQB1								
NCSTN	nicastrin	Q5T205								
GPI	glucose-6-phosphate isomerase	A0A0J9YXP8								
TFRC	transferrin receptor	A8K6Q8								
GFPT1	glutamine--fructose-6-phosphate transaminase 1	Q06210								
IST1	IST1, ESCRT-III associated factor	J3QQP8								
MCFD2	multiple coagulation factor deficiency 2	H7BZ18								
HSP90AB3P	heat shock protein 90 alpha family class B member 3, pseudogene	Q58FF7								
PHGDH	phosphoglycerate dehydrogenase	Q5SZU1								
AMOT	angiomotin	A2BDD9								
RCN1	reticulocalbin 1	E9PLM2								
DNM2	dynamin 2	K7EMR9								
CALM1	calmodulin 1	Q96HY3								
RCN2	reticulocalbin 2	L8E7F0								

Nipah virus F-driven budding is reduced upon inhibition of endocytic machinery.

Based on our proteomics analyses, F seemed more likely than M to utilize cellular machinery for its budding function. To further validate proteomics and determine whether NiV F-driven budding is dependent on machinery involved in vesicular trafficking, we measured F expression in cell lysates (CL), at the cell surface (CSE), and in viral particles (VLP) after co-transfection with an empty vector (positive control, set to 100%) or the following dominant negative (DN) constructs to inhibit several pathways of vesicular trafficking: DN-Dynamin (various endocytic pathways), DN-Eps15 (clathrin-mediated endocytosis), DN-Vps4A (function of ESCRT complexes involved in multivesicular body formation and several mechanisms of viral budding), and DN-Rab11 (primarily, recycling from endosomal system to the plasma membrane) (Fig. 3A). After quantification of these parameters with flow cytometry or densitometry, two budding indices, one based on each measurement of cellular expression, were calculated to assess actual budding efficiencies for each transfection condition: VLP/CL and VLP/CSE, with the positive control set to 100% for each budding index.

We report that F budding VLP/CL and/or VLP/CSE efficiencies were significantly reduced to a range of 4-49% as compared to the positive controls (assessed with one-sample T-tests) after co-expression with each of these constructs (Fig. 3B). The only index not meeting significance was VLP/CSE for DN-Rab11, which still appeared to trend towards a reduction (reduced to 66%, $P = 0.13$), with the VLP/CL reduction for DN-Rab11 being to 52.67%, $P = 0.0009$). F budding was most affected by DN-Vps4A, indicating the importance of ESCRT function in its budding mechanism, whether directly or indirectly. Since this study additionally focused on how these factors might affect G

and M budding efficiencies, they were similarly tested except that CSE cannot be

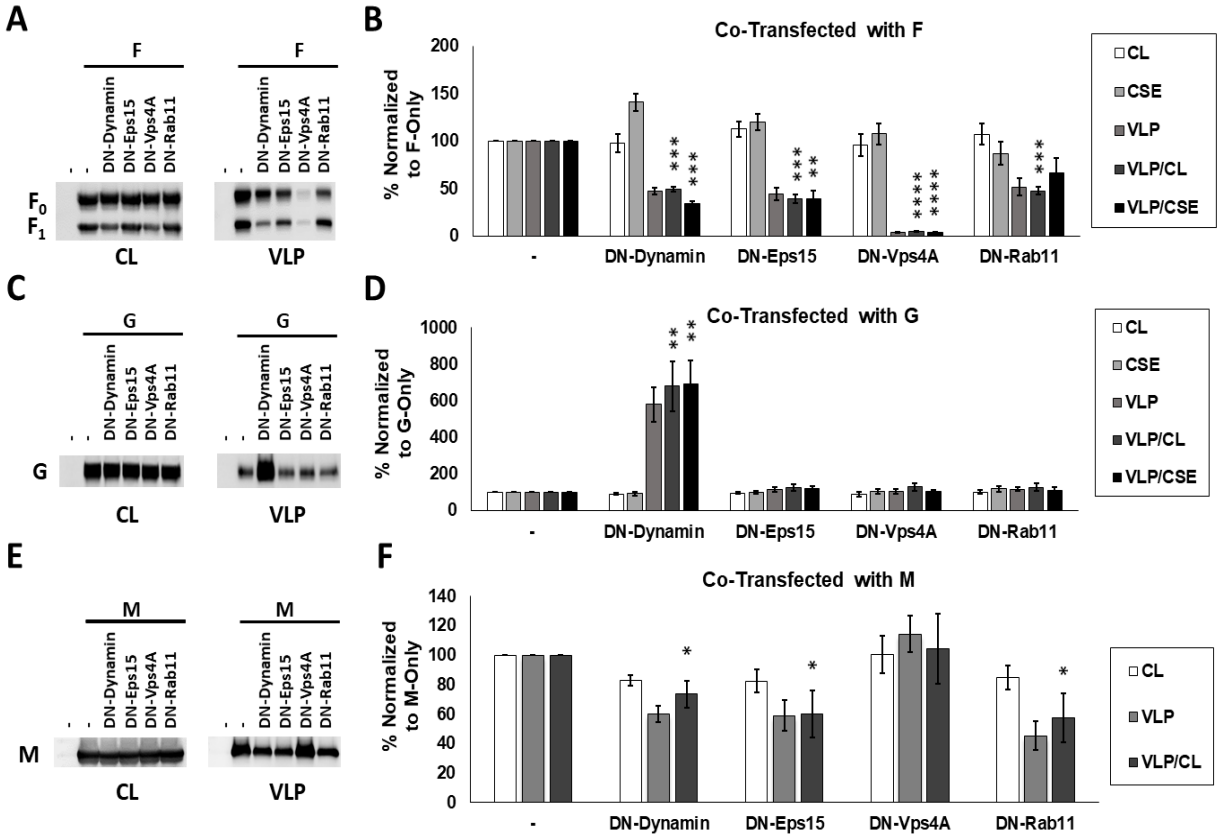

Fig. 3.3: Nipah virus budding is significantly modulated upon the inhibition of endocytosis, recycling, and ESCRT function. (A) HEK293T cells were transfected with NiV F alone or with dominant-negative (DN) mutants of key vesicular trafficking factors: Dynamin (endocytosis), Eps15 (clathrin-mediated endocytosis), VPS4A (ESCRT function), or Rab11 (recycling). Total cell lysates (CL) and virus-like particle fractions (VLP) were prepared 24 hours after transfection and used for SDS-PAGE and western blot analysis, whereas F cell surface expression (CSE) was measured using flow cytometry. (B) Using densitometry to assess the expression of the F protein in VLPs along with corresponding total cell lysate and CSE values, two indices were determined: VLP/CL and VLP/CSE. (C and D) As with (A) and (B), a construct encoding G was co-expressed with each DN factor and the following CL, CSE, VLP, and index values elucidated. Similarly, co-expression with these constructs were tested for effects on M expression in cell lysates and VLPs but not at the cell surface due to it being a cytoplasmic protein. Representative western blots (E) and quantification (F) are shown. Results are representative of at least three experiments with error bars indicating standard error of the mean. One-way student T-tests were used to assess significant differences in budding efficiency indices as compared to when they are co-transfected with pcDNA3.1, an empty vector (*, $P < 0.05$; **, $P < 0.01$; ***, $P < 0.001$; and ****, $P < 0.0001$).

measured for NiV M, which is not a transmembrane protein. Of significant interest, NiV G budding efficiency increased almost seven-fold based on both indices in the case of co-transfection with DN-Dynamin but did not change in any other condition (Fig. 3C and D). This result was entirely unexpected and suggests a novel function of dynamin, direct or indirect, in the unelucidated and normally relatively inefficient process of G-driven particle formation [Fig. 3C and (19, 65)]. As compared to F and G, the effects of these constructs on M budding were less dramatic, though DN-Dynamin, DN-Eps15, and DN-Rab11 co-expression led to significant ($P < 0.05$) M budding efficiency reductions by 27%, 40%, and 42%, respectively Fig. 3E and F). Importantly, the finding that DN-Vps4a does not affect NiV M budding efficiency is consistent with prior literature (66).

Nipah virus budding is significantly affected by actin cytoskeletal manipulation through mutant RhoGTPases. Actin cytoskeletal factor enrichment was largely specific to F-alone and FMG VLPs in our proteomics analysis, which suggests that these factors may be recruited specifically by the presence of F to sites of assembly and budding. The actin cytoskeleton is involved in many cellular processes (67, 68) as well as assembly and/or egress for some viruses; however, these roles vary greatly and, for many viruses, are poorly understood (25, 37–40). The actin cytoskeleton is comprised of monomeric globular (G-actin) and polymeric filamentous actin (F-actin), which are interconverted and organized by remodeling proteins including RhoGTPases (69–72). Major re-organization of the actin cytoskeleton into structures such as stress fibers, lamellipodia, and filopodia are regulated by the RhoGTPases RhoA, Rac1, and Cdc42, respectively (41). For an initial test of whether NiV F budding is modulated by the

activity of RhoGTPases, we assessed whether F budding efficiency indices (VLP/CL and VLP/CSE) are altered during co-expression of constitutively active (CA) and dominant negative (DN) mutants of RhoA, Rac1, or Cdc42. We found that CA-RhoA reduced the levels of F in VLPs [VLP/CL to 54% ($P < 0.01$) and VLP/CSE to 61% ($P < 0.05$)] (Fig. 4A and B). We also tested the effects of these constructs on G- and M-driven budding. After CA-RhoA and DN-Cdc42 co-expression G VLP/CL but not VLP/CSE to 140% and 122%, respectively (Fig. 4C and D). While the significance of inefficient G-driven budding is not understood, these findings may yield some insight into the processes involved. Interestingly, M budding was found to be increased by both CA-Rac1 and DN-Rac1, suggesting that perturbation of the function of this GTPase may support particle formation (Fig. 4E and F).

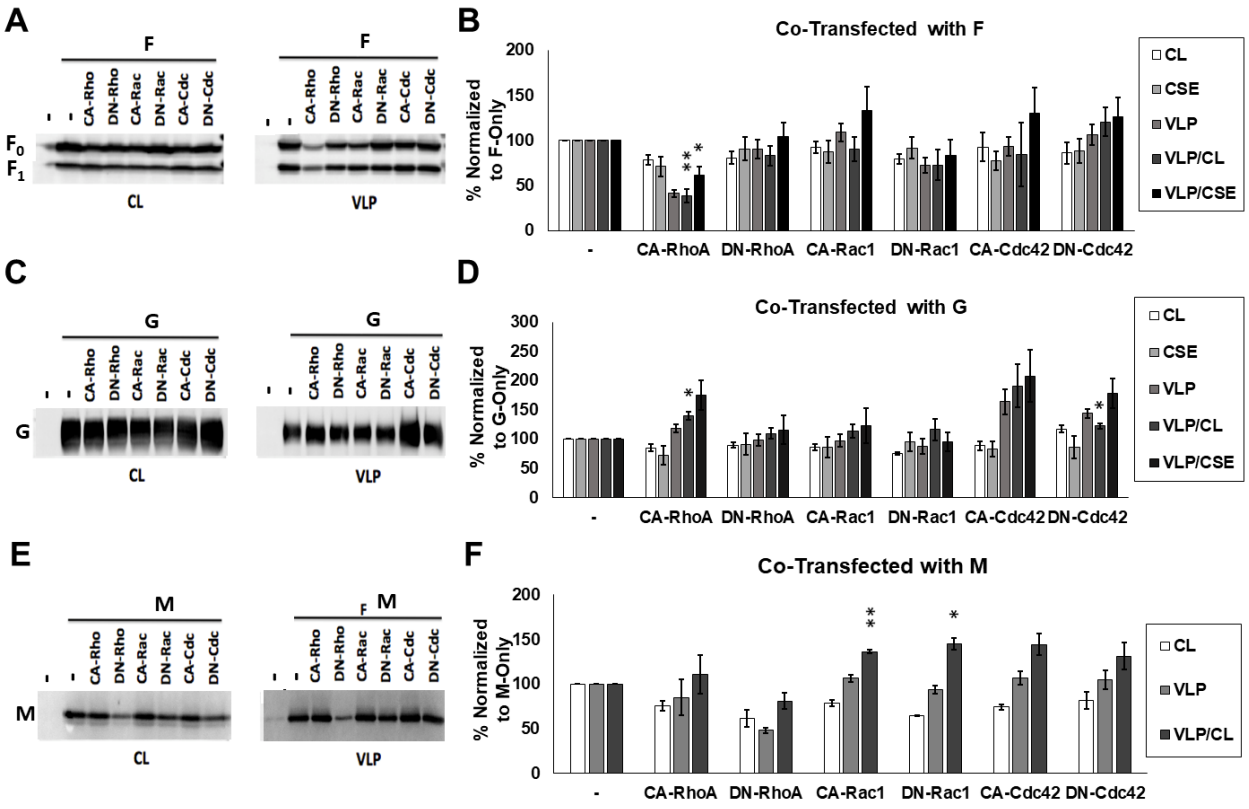

Fig. 3.4: Nipah virus budding is significantly affected by actin cytoskeletal manipulation through mutant RhoGTPases. (A and B) HEK293T cells were transfected with NiV F alone or with dominant-negative (DN) or constitutively active (CA) constructs for RhoA, Rac1, and Cdc42. As with Fig. 3: CL, CSE, and VLPs were quantified and the both budding indices assessed. SDS-PAGE and western blot analysis. Effects of co-expressing these mutants were assessed for G-driven (C and D) and M-driven (E and F) budding). Results are representative of at least three experiments with error bars indicating standard error of the mean. One-way student T-tests were used to assess significant differences in budding efficiency indices as compared to when they are co-transfected with pcDNA3.1, an empty vector (*, $P < 0.05$; **, $P < 0.01$).

Inhibition of Nipah virus fusion protein budding reduces attachment protein incorporation regardless of matrix protein expression. To better elucidate the importance of the mutant factors tested so far, several of the most interesting factors were also assessed in the context of F, G, and M co-expression, which should better compare to particles produced in live NiV infections (Fig. 5A). Despite the presence of the M protein, generally considered to be the most important viral protein in the process of paramyxovirus budding, we found that DN-Dynamin, DN-Vps4a, DN-Rab11, and CA-RhoA all significantly and consistently reduced both indices of F budding efficiency by 51%-88% (Fig. 5A and B). More strikingly still, we report that these reductions were also seen for NiV G in the context of F and M expression (FMG samples), which exhibited no less than a 77% reduction in budding efficiency in any tested combination (Fig. 5A and C). This was particularly interesting since only DN-Dynamin and CA-RhoA appeared to previously affect G-driven budding and both led to increased budding efficiency. M budding efficiencies, on the other hand, were not significantly affected by any co-expressed cellular factor while in this combination (Fig. 5A and D). Importantly, these findings support the model depicted by our prior studies that G incorporation into VLPs

may be more tied to the budding activity of NiV F than that of M (19).

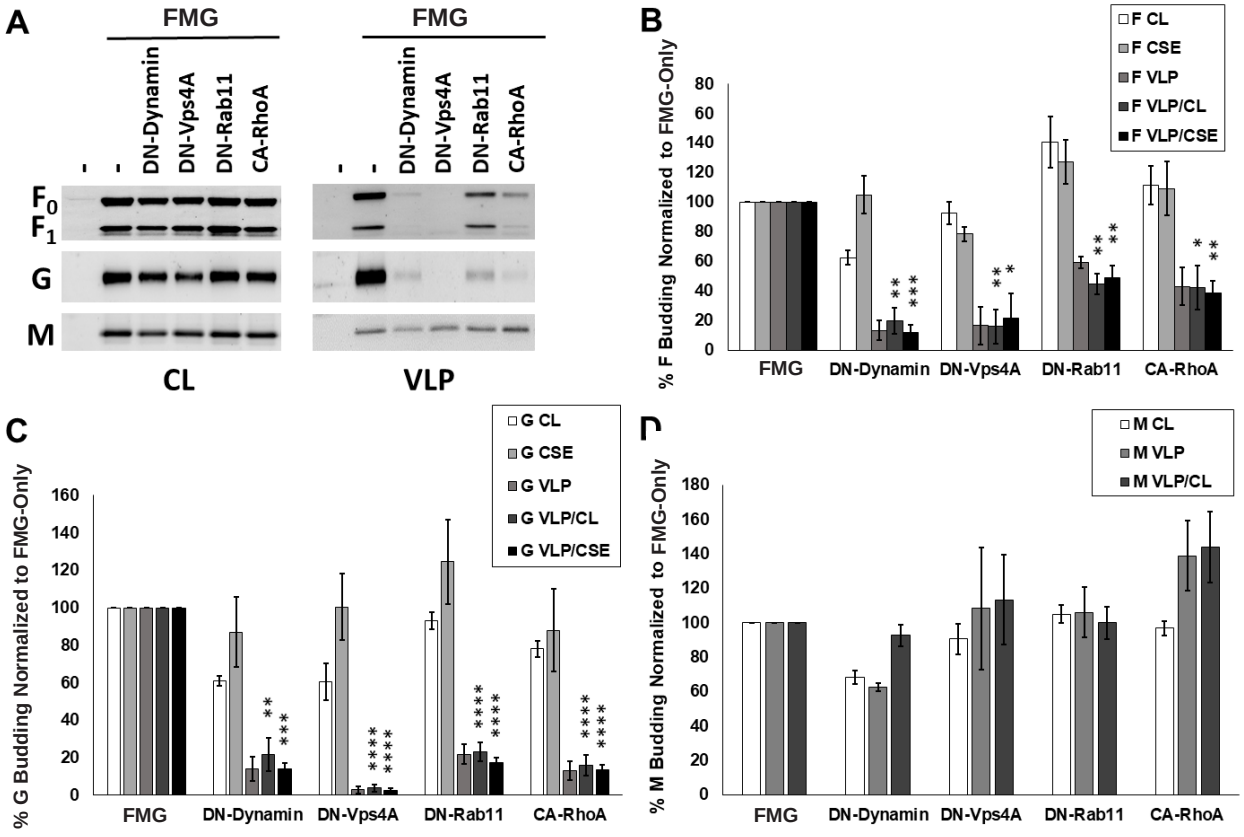

Fig. 3.5: Inhibition of Nipah virus fusion protein budding reduces attachment protein incorporation despite the presence of normally budding matrix protein. (A) To assess the effects that manipulation of vesicular trafficking (Fig. 3) and the actin cytoskeleton (Fig. 4) have on more complete budding particles, NiV F, G, and M were co-transfected with or without DN-Dynamin, DN-Vps4a, DN-Rab11, or CA-RhoA. Expression of each viral protein in cell lysates, on the cell surface for F and G, and in VLPs was quantified and used to produce budding indices as done previously. These values are summarized for (B) F, (C) G, and (D) M. Results are representative of at least three experiments with error bars indicating standard error of the mean. One-way student T-tests were used to assess significant differences in budding efficiencies for each viral protein as compared to FMG co-expression alone (*, $P < 0.05$; **, $P < 0.01$; ***, $P < 0.001$; and ****, $P < 0.0001$).

Select mutant cellular factors involved in vesicular trafficking and cytoskeletal organization affect F budding and cell-cell fusion without affecting F processing.

In the hopes of validating and expanding upon VLP proteomics, we have so far shown that mutants of several cellular factors involved in vesicular trafficking and in cytoskeletal organization impact NiV budding; however, the full importance of these major cellular processes in the lifecycle of NiV remains unclear. Since proteasomal cleavage of NiV F by endolysosomal cathepsin B or L has been shown to be essential for its fusogenic activity (73–75), we tested whether some of the constructs affected F fusogenicity using a cell-cell fusion assay. While we report that neither DN-Dynamin nor DN-Rab11 significantly affected fusion, DN-Vps4a dramatically increased (increased by 410%, $P < 0.05$) while CA-RhoA significantly decreased fusion (reduced to 16%, $P < 0.01$)(Fig.6A). Notably, data from FMG co-transfection experiments (Fig. 5) showed that none of the tested constructs significantly affected F or G CSE nor F processing levels; thus, these parameters were not responsible for the fusogenicity phenotypes observed (Fig. 6B). These findings not only suggest that NiV-F can be internalized or trafficked through the endolysosomal system through dynamin-independent means but also indicate that ESCRT and cytoskeleton machinery are able to modulate both sites of budding and fusion, either directly or indirectly.

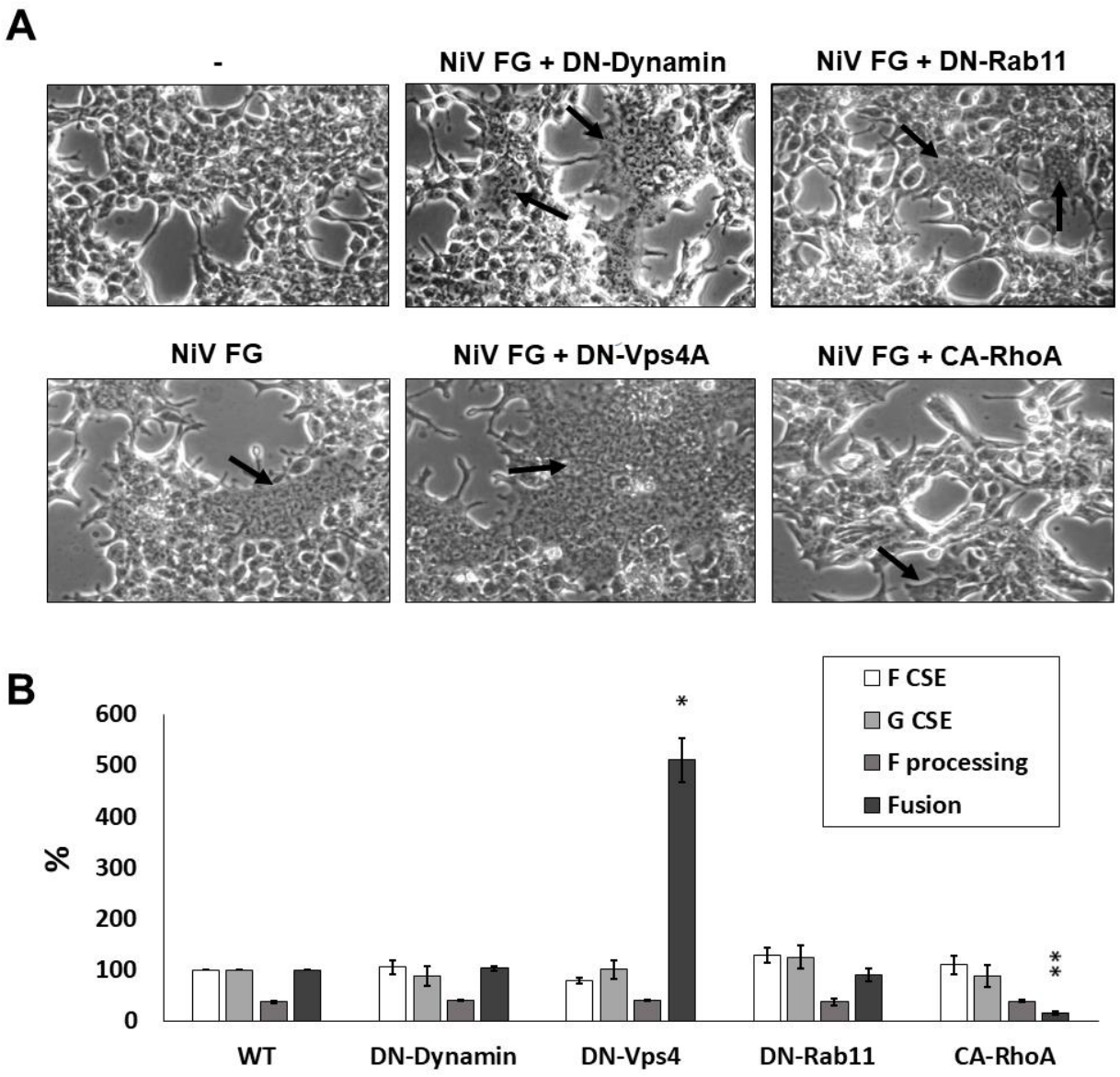

Fig. 3.6: Expression of select mutant factors that inhibit F budding does not affect processing but can modulate fusion. (A) HEK293T cells were transfected with an empty vector, or with NiV F and G with or without the listed cellular factors. Light microscope images were taken at 200x magnification. (B) By counting nuclei in fused syncytia, levels of fusion were quantified with F and G co-transfection alone set to 100%. Levels of F processing as well as F and G CSE take from experiments of FMG expression are also shown. Results are representative of at least three experiments with error bars indicating standard error of the mean. One-way student T-tests were used to assess significant differences in budding efficiencies for each viral protein as compared to FMG co-expression alone (*, $P < 0.05$; **, $P < 0.01$).

Discussion

While recent studies have helped to clarify how Nipah virus assembly and budding occur, many gaps in our understanding remain. While paramyxovirus matrix proteins are generally accepted as crucial for driving particle formation, incorporating all required viral components as well as supporting the stability and infectivity of produced virions, significantly less is understood concerning how other viral proteins may support particle formation (10, 18). Unlike most paramyxoviruses, NiV F, G, and M have all been reported to autonomously produce VLPs to various degrees upon expression alone, suggesting potential roles as supportive in budding (65). Our recent study further suggested a novel role for NiV F as capable of increasing the VLP incorporation of G (19). Moreover, our study implicated the cytoplasmic tail of NiV F as containing several specific motifs important for this budding function (38, 76). The exact function(s) of these motifs remains unclear; however, the presence of a YxxL motif may suggest interaction with the ESCRT-associated protein ALIX and/or other vesicular trafficking machinery (22, 77–79).

In a recent study published by Vera-Velasco et al., VLPs produced from co-expression of NiV F, G, and M in HEK293 cells were analyzed using LC-MS/MS-based proteomics, identifying proteins involved in vesicular trafficking as significantly incorporated (44). Here, we analyzed by proteomics VLPs produced from either individual expression or various combinations of F, G, and M co-expression, and validated the most significant processes. Corroborating the study by Vera-Velasco et al., we report that proteins incorporated into FMG VLPs were most significantly associated with vesicular trafficking (Fig. 2B). We also found that proteins involved in

the cytoskeleton showed significant incorporation as a group. Further, we reported that while M-only VLPs incorporated few cellular proteins, all VLP combinations containing F (F-alone and FM), largely recapitulated the levels and patterns of cellular factor incorporation observed during FMG expression (Fig. 2). Together these findings support a model where the matrix protein induces budding based on its ability to form higher order scaffolds, whereas the fusion protein likely relies on recruitment of cellular machinery to sites of particle formation and in some cases to virions (24, 30, 78). Future proteomics studies focused on post-translational modifications of viral and cellular factors incorporated into VLPs may further clarify the processes of assembly and budding.

To attempt to validate those VLP proteomic analyses conducted previously (44) and those described here, we targeted several aspects of vesicular trafficking and actin cytoskeletal organization. Supporting our findings that VLPs made with combinations that include F or M tend to incorporate cellular factors associated with vesicle transport (Fig. 2), we report that dominant-negative constructs of Dynamin, Eps15, and Rab11 each inhibit F and M budding when co-expressed (Fig. 3). Confirming further reports of M independence from ESCRT machinery (66), we also report that DN-Vps4A significantly reduced F but not M budding. The potential importance of ESCRTs in NiV budding is greatly supported by the identification of multiple ESCRT proteins both in this study and in Vera-Velasco et al. Very recently, live NiV infection was shown to be significantly reduced by knock-down of ESCRT machinery, with a new role for the small NiV C protein as a potential ESCRT recruitment factor through its novel mimicry of an ESCRT component. As with several retroviruses, numerous viral proteins and motifs

(80–83) can be important for ESCRT recruitment, and since neither our study nor that published previously included C, there remains a significant potential for F-driven budding to rely on the direct action of ESCRTs.

Reduced F and M budding during DN-Rab11 co-transfection are further corroborated by previous findings with the closely related Hendra virus (HeV) for which, both the F and M proteins have been shown to interact with Rab11-positive recycling endosomes and their budding is at least partially dependent on Rab11 activity (45). The full function of Rab11 during henipavirus budding is unknown; however, the importance of Rab11 and Rab11-interacting proteins has also been recently highlighted for several more distantly related enveloped viruses including influenza A and respiratory syncytial virus (34, 36).

Our findings from co-expression of constitutively active and dominant negative RhoGTPases both suggest that the actin cytoskeleton modulates NiV budding, and support the significance of cytoskeletal factor incorporation into NiV VLPs. Further studies are needed to enrich our understanding of potential roles that actin remodeling has in henipavirus particle formation. Potential involvement of the actin cytoskeleton may be in trafficking, assembly, or in the budding process itself (37, 39). Specific RhoGTPases have also been implicated as having roles in different pathways of endocytosis (84–87), which may explain the variation of effects on F, G, and M budding efficiencies (Fig. 4).

To better understand the importance of our budding phenotypes upon vesicular trafficking or cytoskeletal perturbation, FMG VLPs were characterized. We found a very clear phenotype suggesting the dependence of G incorporation on the budding of F

regardless of M budding (Fig. 5). Interestingly, these results were supported by our previous findings using a budding defective F mutant (19). Most striking was the clear shift from DN-Dynamin expression increasing G-only budding by almost seven-fold (Fig. 3) to a reduction by nearly the same magnitude when F was expressed (Fig. 5), suggesting that the budding activity of F overrides that of G when they are co-expressed. A potential explanation for this is the observed shift in trafficking profiles of these proteins when comparing individual and co-expression, however these changes require further study (77, 88).

Since vesicular trafficking has been previously associated with henipavirus F protein maturation, we also sought to understand how our constructs that most clearly altered budding would affect F-processing and fusogenic capacities (75). We found that neither processing nor levels of F or G surface expression were altered substantially after co-expression of any of the constructs tested: DN-Dynamin, DN-Vps4A, DN-Rab11, or CA-RhoA. Despite no clear change to processing or CSE, DN-Vps4A and CA-RhoA co-expression led to clear phenotypes of increased and reduced fusion, respectively (Fig. 6).

Somewhat similar reductions of fusion seen with CA-RhoA have been observed with HeV but were not consistent when assessed for parainfluenza 5, another paramyxovirus (89). Thus, the roles of actin cytoskeletal dynamics are not well understood for any aspect of the NiV lifecycle. Future study is needed to understand the functions of the cytoskeleton during the lifecycles of paramyxoviruses, though these mechanisms are likely to be obscured by differences between cell types and will vary by viral species.

Our observation of increased fusion during DN-Vps4A was completely unexpected and does not seem to be due to increased F processing nor F or G CSE increases. The cause of this phenotype is unknown, but we speculate could be explained by a change in F and G localization within the cell that is more optimal for cellular fusion. Super-resolution microscopy may shed further light into the effects of Vps4A in cell-cell fusion.

Here, we have described a VLP proteomics approach of identifying cellular factors and processes as potentially involved in NiV assembly and budding. Further, this was accomplished for VLPs produced from several combinations of NiV proteins to clarify the function of several viral proteins in cellular factor incorporation. We validated our VLP proteomics results by demonstrating that perturbation of the most significantly enriched functional groups: vesicular trafficking and the actin cytoskeleton, led to substantial modulation of VLP budding, with the clearest phenotypes being reductions in F-driven budding. The importance of functional F budding during the incorporation of the G protein into VLPs was further demonstrated using these mutant constructs. Together, these findings support a significant involvement of the NiV fusion protein and uncover the involvement of vesicular trafficking and actin cytoskeletal processes in efficient Nipah virus assembly and budding.

Experimental Design: GJ, HAC, BBT, JRT, JNA, EMC; Experimentation: GJ, BBT, BNRL, KM, NTU, LJZ, VO, HAC, PDP, HMB; Data Analysis and Statistics: GPJ, JNA, JPW; Manuscript writing: GPJ, HAC, JNA

Acknowledgements/Funding Information

This work was supported by the Department of Homeland Security (DHS) Science and Technology Directorate (S&T) under Contract HSHQPM-14-X-00238 to J.N.A and Katrina Waters, with a sub-contract to H.A.C., and by NIH grant R01 IA109022 to H.A.C. The funders had no role in study design, data collection and interpretation, or the decision to submit the work for publication.

References

1. Nipah virus outbreaks in the WHO South-East Asia Region. Surveillance and outbreak alert, World Health Organization.
2. 2015. Blueprint for R&D preparedness and response to public health emergencies due to highly infectious pathogens. World Health Organization.
3. Drexler JF, Corman VM, Müller MA, Maganga GD, Vallo P, Binger T, Gloza-Rausch F, Rasche A, Yordanov S, Seebens A, Oppong S, Sarkodie YA, Pongombo C, Lukashev AN, Schmidt-Chanasit J, Stöcker A, Carneiro AJB, Erbar S, Maisner A, Fronhoffs F, Buettner R, Kalko EKV, Kruppa T, Franke CR, Kallies R, Yandoko ERN, Herrler G, Reusken C, Hassanin A, Krüger DH, Matthee S, Ulrich RG, Leroy EM, Drosten C. 2012. Bats host major mammalian paramyxoviruses. Nat Commun 3:796.
4. Wu Z, Yang L, Yang F, Ren X, Jiang J, Dong J, Sun L, Zhu Y, Zhou H, Jin Q. 2014. Novel Henipa-like Virus, Mojiang Paramyxovirus, in Rats, China, 2012. Emerg Infect Dis 20.
5. Marsh GA, de Jong C, Barr JA, Tachedjian M, Smith C, Middleton D, Yu M, Todd S, Foord AJ, Haring V, Payne J, Robinson R, Broz I, Crameri G, Field HE, Wang L-F. 2012. Cedar Virus: A Novel Henipavirus Isolated from Australian Bats. PLoS Pathog 8:e1002836.
6. 2011. The Biology of paramyxoviruses. Caister Academic Press, Norfolk, UK.
7. Harrison MS, Sakaguchi T, Schmitt AP. 2010. Paramyxovirus assembly and budding: building particles that transmit infections. Int J Biochem Cell Biol 42:1416–1429.
8. Battisti AJ, Meng G, Winkler DC, McGinnes LW, Plevka P, Steven AC, Morrison TG, Rossmann MG. 2012. Structure and assembly of a paramyxovirus matrix protein. Proc Natl Acad Sci 109:13996–14000.
9. Coronel EC, Murti KG, Takimoto T, Portner A. 1999. Human parainfluenza virus type 1 matrix and nucleoprotein genes transiently expressed in mammalian cells induce the release of virus-like particles containing nucleocapsid-like structures. J Virol 73:7035–7038.
10. Pantua HD, McGinnes LW, Peeples ME, Morrison TG. 2006. Requirements for the assembly and release of Newcastle disease virus-like particles. J Virol 80:11062–11073.
11. Takimoto T, Murti KG, Bousse T, Scroggs RA, Portner A. 2001. Role of matrix and fusion proteins in budding of Sendai virus. J Virol 75:11384–11391.
12. Sugahara F, Uchiyama T, Watanabe H, Shimazu Y, Kuwayama M, Fujii Y, Kiyotani K, Adachi A, Kohno N, Yoshida T, Sakaguchi T. 2004. Paramyxovirus Sendai virus-like particle formation by expression of multiple viral proteins and acceleration of its release by C protein. Virology 325:1–10.
13. Li M, Schmitt PT, Li Z, McCrory TS, He B, Schmitt AP. 2009. Mumps virus matrix,

fusion, and nucleocapsid proteins cooperate for efficient production of virus-like particles. J Virol 83:7261–7272.

14. Schmitt AP, Leser GP, Waning DL, Lamb RA. 2002. Requirements for budding of paramyxovirus simian virus 5 virus-like particles. J Virol 76:3952–3964.

15. Dietzel E, Kolesnikova L, Sawatsky B, Heiner A, Weis M, Kobinger GP, Becker S, von Messling V, Maisner A. 2016. Nipah Virus Matrix Protein Influences Fusogenicity and Is Essential for Particle Infectivity and Stability. J Virol 90:2514–2522.

16. Johnston GP, Contreras EM, Dabundo J, Henderson BA, Matz KM, Ortega V, Ramirez A, Park A, Aguilar HC. 2017. Cytoplasmic Motifs in the Nipah Virus Fusion Protein Modulate Virus Particle Assembly and Egress. J Virol 91:e02150-16.

17. Park A, Yun T, Vigant F, Pernet O, Won ST, Dawes BE, Bartkowski W, Freiberg AN, Lee B. 2016. Nipah Virus C Protein Recruits Tsg101 to Promote the Efficient Release of Virus in an ESCRT-Dependent Pathway. PLOS Pathog 12:e1005659.

18. Sakaguchi T, Kato A, Sugahara F, Shimazu Y, Inoue M, Kiyotani K, Nagai Y, Yoshida T. 2005. AIP1/Alix is a binding partner of Sendai virus C protein and facilitates virus budding. J Virol 79:8933–8941.

19. Irie T, Nagata N, Yoshida T, Sakaguchi T. 2008. Recruitment of Alix/AIP1 to the plasma membrane by Sendai virus C protein facilitates budding of virus-like particles. Virology 371:108–120.

20. Ke Z, Strauss JD, Hampton CM, Brindley MA, Dillard RS, Leon F, Lamb KM, Plemper RK, Wright ER. 2018. Promotion of virus assembly and organization by the measles virus matrix protein. Nat Commun 9:1736.

21. Liu YC, Grusovin J, Adams TE. 2018. Electrostatic Interactions between Hendra Virus Matrix Proteins Are Required for Efficient Virus-Like-Particle Assembly. J Virol 92:e00143-18.

22. Dietzel E, Kolesnikova L, Maisner A. 2013. Actin filaments disruption and stabilization affect measles virus maturation by different mechanisms. Virol J 10:249.

23. Bieniasz PD. 2006. Late budding domains and host proteins in enveloped virus release. Virology 344:55–63.

24. Dilley KA, Gregory D, Johnson MC, Vogt VM. 2010. An LYPSL Late Domain in the Gag Protein Contributes to the Efficient Release and Replication of Rous Sarcoma Virus. J Virol 84:6276–6287.

25. Dolnik O, Kolesnikova L, Stevermann L, Becker S. 2010. Tsg101 Is Recruited by a Late Domain of the Nucleocapsid Protein To Support Budding of Marburg Virus-Like Particles. J Virol 84:7847–7856.

26. Freed EO. 2002. Viral Late Domains. J Virol 76:4679–4687.

27. Heidecker G, Lloyd PA, Fox K, Nagashima K, Derse D. 2004. Late Assembly Motifs of Human T-Cell Leukemia Virus Type 1 and Their Relative Roles in Particle Release. J Virol 78:6636–6648.

28. Licata JM, Simpson-Holley M, Wright NT, Han Z, Paragas J, Harty RN. 2003. Overlapping motifs (PTAP and PPEY) within the Ebola virus VP40 protein function independently as late budding domains: involvement of host proteins TSG101 and VPS-4. J Virol 77:1812–1819.

29. Schmitt AP, Leser GP, Morita E, Sundquist WI, Lamb RA. 2005. Evidence for a New Viral Late-Domain Core Sequence, FPIV, Necessary for Budding of a Paramyxovirus. J Virol 79:2988–2997.

30. Votteler J, Sundquist WI. 2013. Virus Budding and the ESCRT Pathway. Cell Host Microbe 14:232–241.

31. Rossman JS, Jing X, Leser GP, Lamb RA. 2010. Influenza Virus M2 Protein Mediates ESCRT-Independent Membrane Scission. Cell 142:902–913.

32. Chen BJ, Lamb RA. 2008. Mechanisms for enveloped virus budding: Can some viruses do without an ESCRT? Virology 372:221–232.

33. Utley TJ, Ducharme NA, Varthakavi V, Shepherd BE, Santangelo PJ, Lindquist ME, Goldenring JR, Crowe JE. 2008. Respiratory syncytial virus uses a Vps4-independent budding mechanism controlled by Rab11-FIP2. Proc Natl Acad Sci U S A 105:10209–10214.

34. Taylor MP, Koyuncu OO, Enquist LW. 2011. Subversion of the actin cytoskeleton during viral infection. Nat Rev Microbiol 9:427–439.

35. Miazza V, Mottet-Osman G, Startchick S, Chaponnier C, Roux L. 2011. Sendai virus induced cytoplasmic actin remodeling correlates with efficient virus particle production. Virology 410:7–16.

36. Gladnikoff M, Shimoni E, Gov NS, Rousso I. 2009. Retroviral Assembly and Budding Occur through an Actin-Driven Mechanism. Biophys J 97:2419–2428.

37. Fackler OT, Kräusslich H-G. 2006. Interactions of human retroviruses with the host cell cytoskeleton. Curr Opin Microbiol 9:409–415.

38. Chertova E, Chertov O, Coren LV, Roser JD, Trubey CM, Bess JW, Sowder RC, Barsov E, Hood BL, Fisher RJ, Nagashima K, Conrads TP, Veenstra TD, Lifson JD, Ott DE. 2006. Proteomic and Biochemical Analysis of Purified Human Immunodeficiency Virus Type 1 Produced from Infected Monocyte-Derived Macrophages. J Virol 80:9039–9052.

39. Radhakrishnan A, Yeo D, Brown G, Myaing MZ, Iyer LR, Fleck R, Tan B-H, Aitken J, Sanmun D, Tang K, Yarwood A, Brink J, Sugrue RJ. 2010. Protein Analysis of Purified Respiratory Syncytial Virus Particles Reveals an Important Role for Heat Shock Protein 90 in Virus Particle Assembly. Mol Cell Proteomics 9:1829–1848.

40. Ren X, Xue C, Kong Q, Zhang C, Bi Y, Cao Y. 2012. Proteomic analysis of purified Newcastle disease virus particles. Proteome Sci 10:32.

41. Vera-Velasco NM, García-Murria MJ, Sánchez del Pino MM, Mingarro I, Martinez-Gil L. 2018. Proteomic composition of Nipah virus-like particles. J Proteomics 172:190–200.

42. Cifuentes-Muñoz N, Sun W, Ray G, Schmitt PT, Webb S, Gibson K, Dutch RE, Schmitt AP. 2017. Mutations in the Transmembrane Domain and Cytoplasmic Tail of Hendra Virus Fusion Protein Disrupt Virus-Like-Particle Assembly. J Virol 91:e00152-17.

43. Ren M, Xu G, Zeng J, De Lemos-Chiarandini C, Adesnik M, Sabatini DD. 1998. Hydrolysis of GTP on rab11 is required for the direct delivery of transferrin from the pericentriolar recycling compartment to the cell surface but not from sorting endosomes. Proc Natl Acad Sci U S A 95:6187–6192.

44. Daecke J, Fackler OT, Dittmar MT, Kräusslich H-G. 2005. Involvement of Clathrin-Mediated Endocytosis in Human Immunodeficiency Virus Type 1 Entry. J Virol 79:1581–1594.

45. Benmerah A, Bayrou M, Cerf-Bensussan N, Dautry-Varsat A. 1999. Inhibition of clathrin-coated pit assembly by an Eps15 mutant. J Cell Sci 112 (Pt 9):1303–1311.

46. van der Bliek AM, Redelmeier TE, Damke H, Tisdale EJ, Meyerowitz EM, Schmid SL. 1993. Mutations in human dynamin block an intermediate stage in coated vesicle formation. J Cell Biol 122:553–563.

47. Sato T, Nakashima A, Guo L, Tamanoi F. 2009. Specific Activation of mTORC1 by Rheb G-protein in Vitro Involves Enhanced Recruitment of Its Substrate Protein. J Biol Chem 284:12783–12791.

48. Fujita H. 2003. A dominant negative form of the AAA ATPase SKD1/VPS4 impairs membrane trafficking out of endosomal/lysosomal compartments: class E vps phenotype in mammalian cells. J Cell Sci 116:401–414.

49. Aguilar HC, Matreyek KA, Filone CM, Hashimi ST, Levroney EL, Negrete OA, Bertolotti-Ciarlet A, Choi DY, McHardy I, Fulcher JA, Su SV, Wolf MC, Kohatsu L, Baum LG, Lee B. 2006. N-Glycans on Nipah Virus Fusion Protein Protect against Neutralization but Reduce Membrane Fusion and Viral Entry. J Virol 80:4878–4889.

50. Landowski M, Dabundo J, Liu Q, Nicola AV, Aguilar HC. 2014. Nipah Virion Entry Kinetics, Composition, and Conformational Changes Determined by Enzymatic Virus-Like Particles and New Flow Virometry Tools. J Virol 88:14197–14206.

51. Clair G, Piehowski PD, Nicola T, Kitzmiller JA, Huang EL, Zink EM, Sontag RL, Orton DJ, Moore RJ, Carson JP, Smith RD, Whitsett JA, Corley RA, Ambalavanan N, Ansong C. 2016. Spatially-Resolved Proteomics: Rapid Quantitative Analysis of Laser Capture Microdissected Alveolar Tissue Samples. Sci Rep 6:39223.

52. Huang EL, Piehowski PD, Orton DJ, Moore RJ, Qian W-J, Casey CP, Sun X, Dey SK, Burnum-Johnson KE, Smith RD. 2016. SNaPP: Simplified Nanoproteomics Platform for Reproducible Global Proteomic Analysis of Nanogram Protein Quantities. Endocrinology 157:1307–1314.

53. Heberle H, Meirelles GV, da Silva FR, Telles GP, Minghim R. 2015. InteractiVenn: a web-based tool for the analysis of sets through Venn diagrams. BMC Bioinformatics 16.

54. Szklarczyk D, Franceschini A, Wyder S, Forslund K, Heller D, Huerta-Cepas J,

Simonovic M, Roth A, Santos A, Tsafou KP, Kuhn M, Bork P, Jensen LJ, von Mering C. 2015. STRING v10: protein–protein interaction networks, integrated over the tree of life. Nucleic Acids Res 43:D447–D452.

55. Shannon P, Markiel A, Ozier O, Baliga NS, Wang JT, Ramage D, Amin N, Schwikowski B, Ideker T. 2003. Cytoscape: a software environment for integrated models of biomolecular interaction networks. Genome Res 13:2498–2504.

56. Boyle EI, Weng S, Gollub J, Jin H, Botstein D, Cherry JM, Sherlock G. 2004. GO::TermFinder--open source software for accessing Gene Ontology information and finding significantly enriched Gene Ontology terms associated with a list of genes. Bioinformatics 20:3710–3715.

57. Aguilar HC, Matreyek KA, Choi DY, Filone CM, Young S, Lee B. 2007. Polybasic KKR Motif in the Cytoplasmic Tail of Nipah Virus Fusion Protein Modulates Membrane Fusion by Inside-Out Signaling. J Virol 81:4520–4532.

58. Biering SB, Huang A, Vu AT, Robinson LR, Bradel-Tretheway B, Choi E, Lee B, Aguilar HC. 2012. N-Glycans on the Nipah Virus Attachment Glycoprotein Modulate Fusion and Viral Entry as They Protect against Antibody Neutralization. J Virol 86:11991–12002.

59. Bradel-Tretheway BG, Liu Q, Stone JA, McInally S, Aguilar HC. 2015. Novel Functions of Hendra Virus G N-Glycans and Comparisons to Nipah Virus. J Virol 89:7235–7247.

60. Liu Q, Stone JA, Bradel-Tretheway B, Dabundo J, Benavides Montano JA, Santos-Montanez J, Biering SB, Nicola AV, Iorio RM, Lu X, Aguilar HC. 2013. Unraveling a Three-Step Spatiotemporal Mechanism of Triggering of Receptor-Induced Nipah Virus Fusion and Cell Entry. PLoS Pathog 9:e1003770.

61. p62/SQSTM1/Sequestosome-1 is an N-recognin of the N-end rule pathway which modulates autophagosome biogenesis | Nature Communications.

62. Patch JR, Crameri G, Wang L-F, Eaton BT, Broder CC. 2007. Quantitative analysis of Nipah virus proteins released as virus-like particles reveals central role for the matrix protein. Virol J 4:1.

63. Patch JR, Han Z, McCarthy SE, Yan L, Wang L-F, Harty RN, Broder CC. 2008. The YPLGVG sequence of the Nipah virus matrix protein is required for budding. Virol J 5:137.

64. Blanchoin L, Boujemaa-Paterski R, Sykes C, Plastino J. 2014. Actin Dynamics, Architecture, and Mechanics in Cell Motility. Physiol Rev 94:235–263.

65. Engl W, Arasi B, Yap LL, Thiery JP, Viasnoff V. 2014. Actin dynamics modulate mechanosensitive immobilization of E-cadherin at adherens junctions. Nat Cell Biol 16:587–594.

66. Sit S-T, Manser E. 2011. Rho GTPases and their role in organizing the actin cytoskeleton. J Cell Sci 124:679–683.

67. Spiering D, Hodgson L. 2011. Dynamics of the Rho-family small GTPases in actin regulation and motility. Cell Adhes Migr 5:170–180.

68. Etienne-Manneville S, Hall A. 2002. Rho GTPases in cell biology. Nature 420:629–635.

69. Hodge RG, Ridley AJ. 2016. Regulating Rho GTPases and their regulators. Nat Rev Mol Cell Biol 17:496–510.

70. Diederich S, Sauerhering L, Weis M, Altmeppen H, Schaschke N, Reinheckel T, Erbar S, Maisner A. 2012. Activation of the Nipah Virus Fusion Protein in MDCK Cells Is Mediated by Cathepsin B within the Endosome-Recycling Compartment. J Virol 86:3736–3745.

71. Weis M, Maisner A. 2015. Nipah virus fusion protein: Importance of the cytoplasmic tail for endosomal trafficking and bioactivity. Eur J Cell Biol 94:316–322.

72. Vogt C, Eickmann M, Diederich S, Moll M, Maisner A. 2005. Endocytosis of the Nipah virus glycoproteins. J Virol 79:3865–3872.

73. Rohrer J. 1996. The targeting of Lamp1 to lysosomes is dependent on the spacing of its cytoplasmic tail tyrosine sorting motif relative to the membrane. J Cell Biol 132:565–576.

74. Mattera R, Farías GG, Mardones GA, Bonifacino JS. 2014. Co-assembly of Viral Envelope Glycoproteins Regulates Their Polarized Sorting in Neurons. PLoS Pathog 10:e1004107.

75. Deschambeault J, Lalonde JP, Cervantes-Acosta G, Lodge R, Cohen EA, Lemay G. 1999. Polarized human immunodeficiency virus budding in lymphocytes involves a tyrosine-based signal and favors cell-to-cell viral transmission. J Virol 73:5010–5017.

76. Lodge R. 1997. The membrane-proximal intracytoplasmic tyrosine residue of HIV-1 envelope glycoprotein is critical for basolateral targeting of viral budding in MDCK cells. EMBO J 16:695–705.

77. Garrus JE, von Schwedler UK, Pornillos OW, Morham SG, Zavitz KH, Wang HE, Wettstein DA, Stray KM, Côté M, Rich RL, Myszka DG, Sundquist WI. 2001. Tsg101 and the vacuolar protein sorting pathway are essential for HIV-1 budding. Cell 107:55–65.

78. Mercenne G, Alam SL, Arii J, Lalonde MS, Sundquist WI. 2015. Angiomotin functions in HIV-1 assembly and budding. eLife 4.

79. Sharma S, Aralaguppe SG, Abrahams M-R, Williamson C, Gray C, Balakrishnan P, Saravanan S, Murugavel KG, Solomon S, Ranga U. 2017. The PTAP sequence duplication in HIV-1 subtype C Gag p6 in drug-naive subjects of India and South Africa. BMC Infect Dis 17.

80. Strack B, Calistri A, Craig S, Popova E, Göttlinger HG. 2003. AIP1/ALIX Is a Binding Partner for HIV-1 p6 and EIAV p9 Functioning in Virus Budding. Cell 114:689–699.

81. Qualmann B, Mellor H. 2003. Regulation of endocytic traffic by Rho GTPases. Biochem J 371:233–241.

82. Curtis I de, Meldolesi J. 2012. Cell surface dynamics – how Rho GTPases orchestrate the interplay between the plasma membrane and the cortical cytoskeleton. J Cell Sci 125:4435–4444.

83. Symons M, Rusk N. 2003. Control of Vesicular Trafficking by Rho GTPases. Curr Biol 13:R409–R418.

84. Kippert A, Trajkovic K, Rajendran L, Ries J, Simons M. 2007. Rho Regulates Membrane Transport in the Endocytic Pathway to Control Plasma Membrane Specialization in Oligodendroglial Cells. J Neurosci 27:3560–3570.

85. Lamp B, Dietzel E, Kolesnikova L, Sauerhering L, Erbar S, Weingartl H, Maisner A. 2013. Nipah Virus Entry and Egress from Polarized Epithelial Cells. J Virol 87:3143–3154.

86. Schowalter RM, Wurth MA, Aguilar HC, Lee B, Moncman CL, McCann RO, Dutch RE. 2006. Rho GTPase activity modulates paramyxovirus fusion protein-mediated cell-cell fusion. Virology 350:323–334.

CHAPTER 4

Multi-platform 'omics' analyses of live Nipah virus infection of mammalian cells

Gunner P. Johnston[1], Emmie de Wit[2], Kristie Oxford[3], Jennifer Kyle[3], Jason McDermott[3], Brooke Kaiser[3], Heather Brewer[3], Jacqueline Cronin[3], Fikret Aydemir[1], Nicholas T. Usher[1], Katrina Waters[2], Heinz Feldmann[3#], Joshua Adkins[2#], Hector C. Aguilar[1#]

[1]Department of Microbiology and Immunology, College of Veterinary Medicine, Cornell University, Ithaca, New York

[2]Laboratory of Virology, Division of Intramural Research, National Institute of Allergy and Infectious Diseases, National Institutes of Health, Rocky Mountain Laboratories, Hamilton, MT

[3]Pacific Northwest National Laboratories, Richland, Washington

*Contributed equally

#Corresponding Authors

Please send correspondence to: Hector C. Aguilar (ha363@cornell.edu), Heinz Feldmann (feldmannh@niaid.nih.gov), or Joshua Adkins (Joshua.Adkins@pnnl.gov).

Key Words: Nipah virus, Paramyxovirus, Proteomics, Transcriptomics, Lipidomics, Metabolomics, Host, Metabolism, Infection

Running Title: Multi-omic Analyses of Live Nipah Virus Infection

*This manuscript was in preparation for submission as of May 3rd, 2019.

Abstract

The paramyxovirus, Nipah virus (NiV), is a biosafety level 4 and category C priority pathogen that causes encephalitis and respiratory disease with mortality rates between 40-100% for human infections. While advances have been made towards understanding individual aspects of the NiV life cycle, little is understood about major cellular changes during NiV infection. Here, we identified changes in molecular components during a NiV infection of human cells at four time points, using a multi-platform high-throughput transcriptomics, proteomics, lipidomics, and metabolomics approach. In direct contrast to what has been reported for other viruses in the same family and order, we found mitochondria-associated proteins to be very significantly enriched in abundance during infection ($p < 10^{-162}$), despite an overall decrease in the abundance of proteins involved in translation ($p = 10^{-81}$). Combining proteomic, metabolomic, and lipidomic analyses further allowed mapping of significant shifts in metabolism of glucose, lipids, and several amino acids during infection. In particular, these analyses suggest reduced glycolysis and a transition to fatty acid oxidation and glutamine anaplerosis to support mitochondrial ATP synthesis during infection. Interestingly, there was little overlap between changes in abundance of transcripts and proteins, which indicates heavy post-transcriptional modulation of the proteome during NiV infection. Such a disparity carries major implications for transcriptomic studies of paramyxovirus infections, and particularly for the rapidly growing genus *Henipavirus*.

Importance

Nipah virus (NiV) is zoonotic and highly virulent to humans. NiV belongs to a quickly growing *Henipavirus* genus that has nearly twenty newly discovered viral species and spans most continents. Because NiV requires BSL-4 containment, many studies have been conducted on individual NiV or cellular proteins at BSL-2 conditions, and relatively little is understood concerning host responses to live NiV infections. To identify cellular changes that occur in cells infected with live NiV under BSL-4 containment we combined several complementary high-throughput -omics approaches. Our results both validate and expand on the knowledge built from research on individual viral components.

Introduction

The genus *Henipavirus* in the family *Paramyxoviridae* represents a rapidly-growing group of emerging pathogens and includes Nipah virus (NiV) and Hendra virus (HeV), which are agents requiring biosafety-level four (BSL-4) containment. In the case of NiV, outbreaks have occurred nearly annually since its discovery two decades ago in Malaysia, with human mortality rates ranging between 40% and 100% and hundreds of human deaths, including the recent outbreak in India with a mortality rate of 94% (1–5). Within the last decade, over twenty novel henipa-like viruses have been identified across Asia, Oceania, Africa, and the Americas (6–9). Further, the known reservoir species for these viruses have expanded to include multiple genera of bats as well as rodents (7, 9, 10). Despite the clear potential for henipaviruses to cause future epidemics and be used as agents of bio-terrorism, approved treatments and vaccines for human use remain to be developed.

The NiV negative-sense single-stranded RNA genome contains six genes in this 3'-5' order: nucleoprotein (N), phosphoprotein (P), matrix protein (M), fusion glycoprotein (F), attachment glycoprotein (G), and large polymerase (L). For virus entry to occur, NiV G needs to bind either of the highly conserved host protein receptors, ephrinB2 or ephrinB3. Receptor binding induces a conformational cascade in G that in turn triggers a conformational cascade in F that executes viral-cell membrane fusion allowing viral entry (11–14). After entry, the viral genome is thought to be transcribed into mRNAs by the N, P, and L proteins (15, 16). These same three proteins also work together to produce positive-sense anti-genomes later during infection, which ultimately allow for viral genome replication (17).

Later during infection, NiV G and F on the infected cell surface drive extensive cell-cell fusion through a similar membrane fusion process. The large, multinucleated cells (i.e. syncytia) produced from these fusion events are a hallmark of NiV infection and contribute significantly to pathogenesis (18). Importantly, the use of highly conserved host cell protein receptors enables NiV infection in a wide range of mammalian hosts, not limited to bats, pigs, cats, dogs, horses,

rodents, and humans (2, 9, 19–25). NiV transmission to humans has been observed from infected livestock, particularly pigs, and from other humans, as well as from consumption of contaminated food, most prominently date palm sap (1, 4, 25–28).

Beyond a broad species tropism, the use of ephrinB2/B3 as entry receptors enables NiV infection in a wide variety of cell types and tissues within a host. NiV infection in humans is largely observed in the respiratory epithelia, the central nervous system (CNS), and the microvascular endothelial tissues of several major organs including spleens, kidneys and hearts (18, 21, 29, 30). Supported by animal models, infection is thought to first occur in respiratory and olfactory epithelia (20, 22, 31). Based on a Syrian hamster model, infection of the CNS is then initiated through the olfactory nerves (32). To avoid antiviral response of infected cells, the NiV P gene produces alternative products (proteins V, W, and C) that have been shown to inhibit multiple innate immune pathways through direct interaction with proteins such as STAT1/2 and TRIM25, contributing to the high levels of virulence during infection (33–36). The matrix protein, involved in assembly and egress of virions, has also been shown to directly inhibit immune responses, such as the interferon-I response via interaction with TRIM6 (37).

Cells infected with NiV undergo drastic morphological changes as they fuse readily with nearby cells into large, multinucleated syncytia, caused by G and F expression on the infected cell surface, which further contributes to pathogenesis (21, 30, 38). In addition to multi-nucleation, some infected cells also exhibit large cytoplasmic lipid droplets, mitochondrial swelling, and vacuolization (32, 39). While each of these characteristics has ties to stress responses and programmed cell death, the importance of these characteristics and their origins and timing in the context of NiV infection are unknown. Very little is known about the cellular changes that occur over the course of infection, including but not limited to the extent and types of stress and programmed cell death responses induced, and their prevalence. Understanding such features will serve to expand our understanding of pathogenesis and disease progression during NiV infection.

Significant advances in methodologies used for high-throughput analyses have allowed for an increasingly broad and complete understanding of dynamic processes such as viral infection (40–47). These high-throughput approaches; however, have largely not been applied to BSL-4 pathogens, likely due to the technical and logistical difficulties of preparing BSL-4 samples for BSL-2 analyses, while maintaining sample quality. While recently high-throughput methods have been used to elucidate several aspects of the NiV life cycle such as particle formation and protein interactions, application in the context of live infection has remained extremely limited (48, 49). Here, we describe a multi-platform 'omics' study of NiV infection of human embryonic kidney (HEK293T) cells, a widespread model for studying henipaviruses based on origins in kidney tissues relevant to NiV pathology as well as ease of ectopic gene expression (13, 48, 50–53). Specifically, we used a mass-spectrometry-compatible *irradiation* approach to assess transcriptomics, proteomics, metabolomics, and lipidomics at four time-points. Specifically, we assessed these changes at 4, 8, 12, and 16 hours post-infection (hpi). Our findings include a general timeline for detectable expression of each viral protein as well as major changes to host protein expression, bioinformatically sorted processes, and cellular locations. Further, lipidomics and metabolomics analyses, supplemented the proteomics analysis to provide unique perspectives into the metabolic dynamics of an infected cell. By using a multi-platform approach across multiple time-points, our 'omics' findings are the most comprehensive to date for the henipaviruses or the paramyxoviruses.

Methods

Biosafety Statement:

All work with infectious Nipah virus and potentially infectious materials was conducted in the biosafety level 4 (BSL4) laboratory located in the Integrated Research Facility of the Rocky Mountain Laboratories, National Institute of Allergy and Infectious Diseases (NIAID), National Institutes of Health (NIH). All infectious procedures including sample inactivation and removal were performed according to established standard operating protocols approved by the local Institutional Biosafety Committee (IBC).

Cells and Reagents

HEK293T cells were obtained from ATCC and used for all experiments, both at biosafety levels 2 and 4. These cells were grown in Dulbecco's Modified Eagle Medium supplemented with 10% Fetal Bovine Serum and 1% Penicillin/Streptomycin (Gibco) and grown at 37ºC with 5% CO_2. The Malaysia strain of NiV was used for all experiments described.

Live BSL-4 NiV Infection, irradiation, and Sample Preparation for Omics Analyses

For each of four time-points, ten 60mm and ten wells within 6-well plates were seeded with HEK293T cells. After seeding, each group of ten plates was divided into two groups of five. One group was mock infected and the other was infected with live NiV, Malaysian strain, at a multiplicity of infection (MOI) of 1. After 4, 8, 12, and 16hpi, cells from each 60 mm dish were collected with PBS and irradiated at 10 Mrads to inactivate NiV. The irradiated cells were then prepared for proteomic, metabolomic, and lipidomic analyses. Similarly, cells in the 6-well plates were treated with TRIzol for extraction of RNA to be analyzed by microarray. Prior to harvest for each experiment and time-point, representative images of infected or mock-infected cells were taken with a BioRad Zoe light microscope and prepared for publication using Fiji software.

Sample Extraction

All chemicals and solvents are from Sigma-Aldrich (St. Louis, MO) unless otherwise stated.

The infected cell pellets were processed to extract proteins, metabolites and lipids utilizing the MPLEx method (54). Briefly, each pellet was brought up to a volume of 200 uL with Milli-Q water, and 1 mL of a 2:1 Chloroform:Methanol (C:M) solution was added to each sample and vortexed for 30 seconds followed by storage on ice. The three visible layers of proteins, metabolites, and lipids were each transferred to separate vials and the protein pellet was washed with 1 mL of ice-cold methanol and dried. The lipidomic (lower, chloroform) and metabolomic (upper, methanol) layers were dried in a SpeedVac (ThermoFisher Scientific, Pittsburgh, PA), reconstituted in 500 uL 2:1 C:M and stored at -80°C.

The protein pellet was digested in a manner similar to the MPLEx method with two exceptions. After the pellets were resuspended with 100 uL of 1 mM $MgCl_2$ in 10 mM Tris-HCl, 2 uL of 2.5U/uL benzonase was added to each sample and then stored overnight at 4°C. An additional 2 uL of 2.5U/uL benzonase was added to each sample and incubated at 37°C for 30 min, 850 rpm in a thermomixer (Eppendorf, Hauppauge, New York). Urea was added to each sample to an 8M concentration and a BCA protein assay was performed. The samples were then reduced and alkylated with 5 mM dithiothreitol and 40 mM iodoacetamide. Samples were then diluted 8-fold with 50 mM ammonium bicarbonate, and $CaCl_2$ was added to achieve a concentration of 1mM per sample. The samples were digested with trypsin (Affymetrix, Santa Clara, CA) for 3 hours and desalted using a C18 solid phase column (Phenomenex, Torrance, CA) with

elution in 400 mL of 80% acetonitrile (ACN) and 0.1% trifluoroacetic acid. Samples were then dried and reconstituted in 50 uL of 5% ACN. Protein concentrations were determined by a second BCA assay and samples were normalized to a final peptide concentration of 0.1 ug/uL.

Proteomics

Peptide samples (5 uL) were analyzed by LC-MS/MS using a Waters nano-Acquity M-Class dual pumping UPLC system (Milford, MA) configured for on-line trapping at 5 µL/min for 8 min followed by gradient elution through a reversed-phase analytical column at 300 nL/min. Columns were packed in-house using 360 µm o.d. fused silica (Polymicro Technologies Inc.) and contained Jupiter C18 media (Phenomenex) in 5 µm particle size for the trapping column (100 µm i.d. x 4 cm long) and 3 µm particle size for the analytical column (75 µm i.d. x 70 cm long). Mobile phases consisted of (MP-A) 0.1% formic acid in water; and (MP-B) 0.1% formic acid in acetonitrile with the following gradient profile (min, % MP-B): 0, 1; 2, 8; 20, 12; 75, 30; 97, 45; 100, 95; 110, 95.

MS analysis was performed using a Q-Exactive HF mass spectrometer (Thermo Scientific, San Jose, CA). Electrospray emitters were prepared in-house using 150 µm o.d. x 20 µm i.d. chemically etched fused silica (Kelly et al., 2006) and subsequently attached to the column using a metal union and coupled to the mass spec via a custom built nanospray source . Electrospray voltage (2.2 kV) was applied at the metal union providing ions to the heated (325ºC) ion transfer tube entrance of the MS. Data was started 20 min after the gradient began and continued for a total acquisition time of 100 min. Precursor MS spectrum were acquired from 400–2000 *m/z* at resolution 60k (AGC target 3e6, max IT 20 ms) followed by data-dependent MS/MS spectra of the top

12 most abundant ions from the precursor spectrum with an isolation window of 2.0 *m/z* and at a resolution of 15k (AGC target 1e5, max IT 200 ms) using a normalized collision energy of 30 and a 45 sec exclusion time.

LC–MS/MS raw data were converted into dta files using Bioworks Cluster 3.2 (Thermo Fisher Scientific), and the MSGF+ algorithm was used to search MS/MS spectra against the Human Uniprot 2016-04-13 database with 20154 entries and against Uniprot entries for individual Nipah virus proteins. The key search parameters used were ±20 ppm tolerance for precursor ion masses, +2.5 Da and -1.5 Da window on fragment ion mass tolerances, MSGF+ high resolution HCD scoring model, no limit on missed cleavages but a maximum peptide length of 50 residues, partial or fully tryptic search, variable oxidation of methionine (15.9949 Da), and fixed alkylation of cysteine (carbamidomethyl, 57.0215 Da). The decoy database searching methodology was used to control the false discovery rate (FDR) at the unique peptide level to <1% and subsequent protein level to <0.5% (% FDR = ((reverse identifications*2)/total identifications)*100). Identification and quantification of the detected peptide peaks were performed by using the label-free Accurate Mass and Time (AMT) tag approach (55). Briefly, an AMT tag database was created from the MS/MS results, and in-house developed informatics tools (including algorithms for peak-picking and determining isotopic distributions and charge states, which are publicly available at ncrr.pnnl.gov/software) were used to process the LC-MS data and correlate the resulting LC-MS features to an AMT tag database. Further downstream data analysis incorporated all possible detected peptides into a visualization program, VIPER, to automatically correlate LC-MS features to the peptide identifications in the AMT tag

database. The resulting post-VIPER matching proteomics data were filtered to achieve an absolute average mass error of 1.08 ppm and an absolute average net elution time error of 0.16%.

Metabolomics

The extracted metabolite samples from the infected cells using MPLEx protocol (56) were shipped to Pacific Northwest National Laboratories (PNNL) for metabolomics analysis. The extracts were chemically derivatized for GC-MS analysis as reported previously (57). Briefly, 20 µL of methoxyamine in pyridine (30 mg/mL) were added to each sample, followed by vortexing for 30 s and incubation at 37°C with generous shaking (1,200 rpm) for 90 min To derivatize hydroxyl and amine groups to trimethylsilyated forms, 80 µL of N-methyl-N-(trimethylsilyl) trifluoroacetamide with 1% trimethylchlorosilane were then added to each vial, followed by vortexing for 10 s and incubation at 37°C with shaking (1,200 rpm) for 30 min. Samples were analyzed by Agilent GC 7890A coupled with a single quadrupole MSD 5975C (Agilent Technologies), and the samples were blocked and analyzed in random order. An HP-5MS column (30 m x 0.25 mm x 0.25 µm; Agilent Technologies) was used for global metabolomics analyses. The sample injection mode was splitless, and 1 µL of each sample was injected. The injection port temperature was held at 250°C throughout the analysis. The GC oven was held at 60°C for 1 min after injection, and the temperature was then increased to 325°C by 10°C/min, followed by a 10-min hold at 325°C. MS data were collected over the mass range 50 – 550 *m/z*. A mixture of FAMEs (C8-C28) was analyzed once per day together with the samples for retention index alignment purposes during subsequent data analysis. GC-MS raw data files were processed using

the Metabolite Detector software, version 2.5.2 beta (58). Retention indices of detected metabolites were calculated based on the analysis of the FAMEs mixture, followed by their chromatographic alignment across all analyses after deconvolution. Metabolites were initially identified by matching experimental spectra to a PNNL-augmented version of Agilent Fiehn database, containing spectra and validated retention indices for over 850 metabolites. Metabolite identifications were manually validated to reduce deconvolution errors during automated data-processing and to eliminate false identifications. The National Institute of Standards and Technology (NIST) 14 GC-MS library was also used to cross validate the spectral matching scores obtained using the Agilent library and to provide identifications of unmatched metabolites.

Lipidomics

Dried lipid extracts of plasma were shipped to PNNL for lipidomics analysis. Extracted lipids were analyzed by LC-MS/MS using a Waters NanoAcquity UPLC system interfaced with a Velos Orbitrap mass spectrometer (Thermo Scientific, San Jose, CA). The electrospray ionization emitter and MS inlet capillary potentials were 2.2 kV and 12 V, respectively. Lipid extracts were reconstituted in 200 µl of methanol, and 7 µl of each sample was injected and separated over a 90-min gradient elution (mobile phase A: ACN/H_2O (40:60) containing 10 mM ammonium acetate; mobile phase B: ACN/IPA (10:90) containing 10 mM ammonium acetate) at a flow rate of 30 µl/min. Samples were analyzed in both positive and negative ionization (full scan range of 200–2,000 *m/z*) using HCD (higher-energy collision dissociation) and CID (collision-induced dissociation) on the top 6 most abundant ions to obtain high coverage of the lipidome. A normalized collision energy of 30 and 35 arbitrary units for HCD and CID were used,

respectively. Both CID and HCD were set with a maximum charge state of 2 and an isolation width of 2 m/z units. An activation Q value of 0.18 was used for CID.

Confident lipid identifications were made by using LIQUID, which enables the examination of the tandem mass spectra for diagnostic ion fragments along with associated hydrocarbon chain fragment information. In addition, the isotopic profile, extracted ion chromatogram, and mass measurement error of precursor ions were examined for each lipid species. To facilitate quantification of lipids, a reference database for lipids identified from the MS/MS data was created, containing the lipid name, observed *m/z*, and retention time. Lipid features from each analysis were then aligned to the reference database based on their *m/z* and retention time using MZmine 2. Aligned features were manually verified and peak apex intensity values were exported for subsequent statistical analysis. Positive and negative ionization data were analyzed separately at all stages. Normalization and outlier detection were performed as described for proteomics.

Data and Statistical Analyses

Peptide, transcript, lipid, and metabolite hits were transformed to $\log_2$ fold-changes (FC) over their time-matched mock controls and assessed for statistical significance by ANOVA (quantitative) or g-test (qualitative), where applicable. From transcriptomics and proteomics, only transcripts and proteins of human origin were considered and in the case of proteomics, only genes with enough analyzed peptides for quantitative assessment (via ANOVA) of fold-change were considered. Furthermore, FC and p-value cut-offs were set as $\log_2 FC \leq -0.58$ or ≥ 0.58 (equivalent to ±1.5-fold change) and $p \leq 0.05$ for transcriptomics and proteomics. For metabolomics and lipidomics, significance was based on ANOVA ($p \leq 0.05$).

After identifying proteins and genes that were significantly altered in abundance (based on peptide peaks, see proteomics section) during infection, the gene ontology (GO) software, GOTERMFINDER (59), and the GO redundancy removal software, REVIGO (60), were used together to analyze data sets by identifying cellular pathways most associated with the affected proteins. Interactivenn (61) was used to compare between gene/protein or GO cellular process lists between time-points, as necessary. For REVIGO, medium stringency (redundancy score <0.7) was used for both proteomics and transcriptomics. For construction of the heatmap used for transcriptomics, the software heatmapper was used (62).

Due to the quantity of data produced from the proteomics experiments, another tool, Reactome (63, 64), was used to more easily visualize which cellular processes were affected during infection based on the abundance changes of proteins associated with each highlighted cellular process. The data set used for this analysis included all proteins meeting both statistical and FC cut-offs (as discussed above) for at least one time-point. For each protein, $\log_2$ FC values were given for each time-point and blank values were substituted with 0 (no fold difference over mock) as required for Reactome to run. Supplementary Table 1 includes the data in this format to support future reader analysis with the Reactome software.

Results

Overview of live Nipah virus infection multi-platform 'omics' analyses. Despite major methodological advances, studies of deadly pathogens such as NiV are limited by the logistics and costs associated with high containment requirements. Here, HEK293T cells were either mock- or NiV-infected at a MOI of 1 and collected after 4, 8, 12, or 16 hours (Fig. 1A). To maximize confidence in downstream analyses, both mock and NiV infections were conducted in five replicates for each time-point. A challenge for generating samples from human pathogens for analysis by mass spectrometry is the requirement to inactivate the pathogen with methods compatible with extraction and preservation of the desired analytes. We used a recently developed BSL-4 sample irradiation approach to successfully assess proteomics, lipidomics, and metabolomics simultaneously (56). Additional infections were carried out for transcriptomics analysis by treating samples with TRizol, an approved virus-inactivation method (65–67). The numbers of transcripts, proteins, lipids, and metabolites that met both statistical and biological thresholds ($p < 0.05$ and fold-change ≤ -1.5 or ≥ 1.5) are reported as differentially expressed for each time-point (Fig. 1B-E). For example, we report that at the 12-hour time-point, nearly equal numbers of cellular proteins met significance ($p < 0.05$) and fold-change (± 1.5) thresholds for classification as increased (1141 proteins) and decreased (1219 proteins) in abundance compared to time-matched mock controls (Fig. 1C).

A

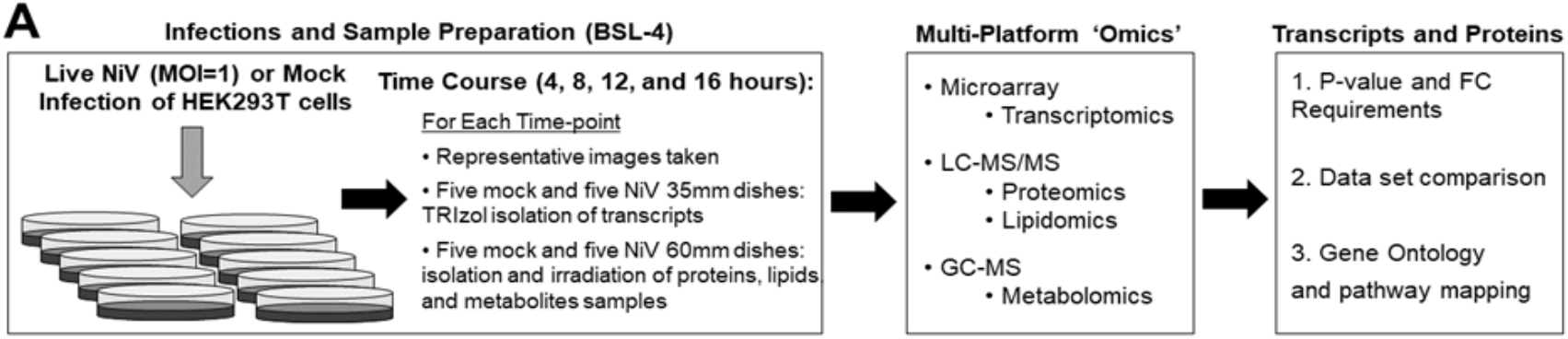

B

	Transcriptomics			
Time (Hr)	**4**	**8**	**12**	**16**
UP	0	2	12	499
DOWN	0	16	3	257

C

	Proteomics			
Time (Hr)	**4**	**8**	**12**	**16**
UP	26	165	1141	1175
DOWN	32	84	1219	1543

D

	Metabolomics			
Time (Hr)	**4**	**8**	**12**	**16**
UP	2	9	18	19
DOWN	0	7	17	19

E

	Lipidomics			
Time (Hr)	**4**	**8**	**12**	**16**
UP	40	23	9	63
DOWN	12	16	57	48

Fig. 4.1: Overview of live Nipah virus infection 'Omics' study. (A) Five pairs of mock and BSL-4 NiV infections were made at a multiplicity of infection of 1 in HEK293T cells for each of four time-points (4, 8, 12, and 16 hours post-infection). At each time-point, mock and NiV infected sample groups were irradiated, harvested, and prepared for proteomics, metabolomics, and lipidomics analyses. The same experiment was repeated separately to assess transcriptomic changes using RNA-sequencing. Resulting (B) transcripts and (C) proteins identified as significantly different based on both p-value ($p<0.05$) and fold-change requirements ($log2FC \geq 0.58$ or ≤ -0.58, which are equivalent to ±1.5 fold) are listed. Positively identified (D) metabolites and (E) lipids exhibiting statistically significant changes for any time-point were similarly counted.

Detection of Nipah virus proteins during infection. To better understand the kinetics of infection, we examined the abundance of viral and cellular proteins across time-points. Supported by previous literature for paramyxoviruses (68), NiV transcripts and proteins are made in decreasing abundance from N to L (Fig. 2A). Though 4hpi was assessed, the first statistically significant identifications of NiV protein peptides, as compared to the time-matched mock control samples, belonged to N, P (or V/W), M, and G, starting at 8hpi (Fig. 2B). The proteomic findings of the 4hpi time-point are summarized in Table 1. While individual changes to protein abundance at this time-point are likely very important during infection, few consistent patterns could be ascertained from so few changes. For this reason, the analyses described next will primarily focus on time-points 8, 12, and 16hpi.

Table 4.1: Proteins altered in abundance at 4hpi with NiV. This information is included in a supplemental spreadshet

The initial identification of viral proteins fits the expectation for the order of gene expression for similar viruses (50). Starting at the 12hpi time-point, all NiV proteins were detected. Cell-cell fusion was first noted at 8hpi (Fig. 2C), with increasing levels at 12hpi, and by 16hpi most cells were fused. Since all viral proteins were apparently highly expressed between 12 and 16hpi (Fig. 2C), the infected cells were expected to be undergoing the most drastic changes at these time-points. Despite extensive cell-cell fusion progressing after 16hpi, no

obvious cell death was observed, consistent with some evidence from a recent study of the closely related Hendra virus suggesting cell death may be inhibited during henipaviral infection of HEK293T cells (50).

A

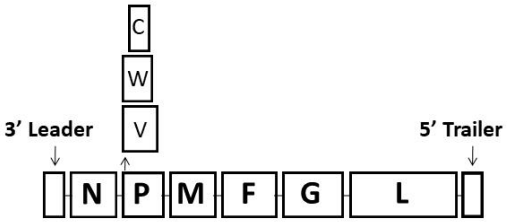

B

Viral Protein	NiV 4 hours	NiV 8 hours	NiV 12 hours	NiV 16 hours
N	-	+	+	+
P/V/W	-	+	+	+
C	-	-	+	+
M	-	+	+	+
F	-	-	+	+
G	-	+	+	+
L	-	-	+	+

C

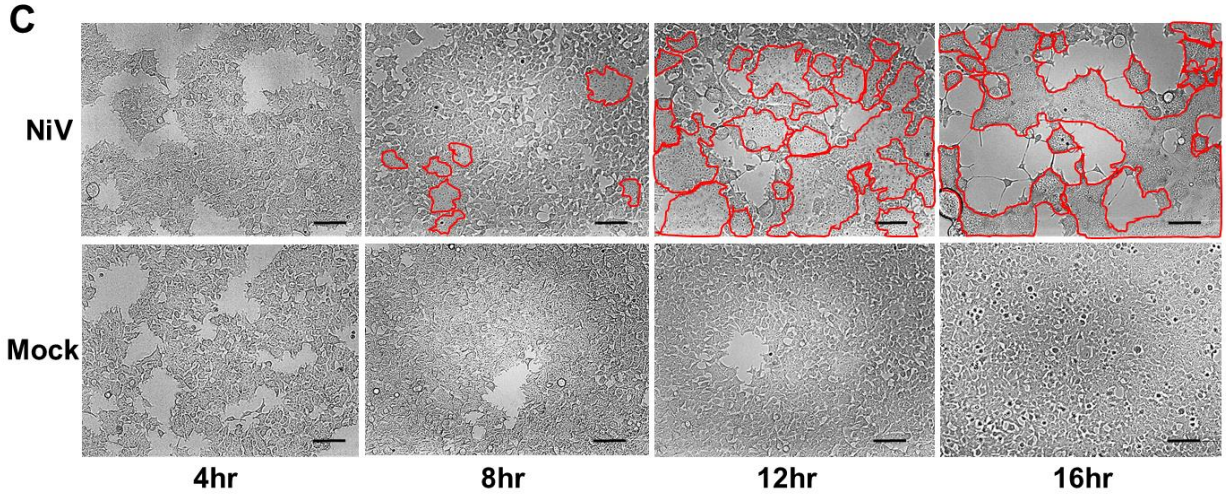

Fig. 4.2: Detection of Nipah virus proteins during infection. (A) A diagram of the 18,246 nucleotide NiV genome. The six genes encoding N, P, M, F, G, and L are shown along with V, W, and C, which are formed from the P gene as alternative products. (B) The presence or absence of each NiV protein at each time-point with a + or -, respectively, and shows detection of all proteins after 12hpi. (C) Cell-cell fusion (syncytial formation), which require F and G co-expression, is identified (outlined in red) starting at 8hpi and increases during infection to almost complete fusion at 16hpi. Scale bars indicate 100µm.

Proteomic analyses identified highly significant increases to proteins associated with RNA processing and mitochondria. Comparison of proteins of increased abundance during infection demonstrated a high degree of similarity between changes at 12 and 16hpi, not only in terms of individual proteins (Fig. 3A top) but also for gene ontology (GO) enrichment categories of cellular processes (Fig. 3A bottom). To reduce the high levels of redundancy between the plethora of GO terms enriched from our protein lists, we used another software, REVIGO, that consolidates similar terms (60). REVIGO also makes use of multi-dimensional scaling plots, which help describe complicated data normally requiring more than three dimensions, to spatially cluster similar GO terms in two dimensions. Based on the GO term overlap between 16hpi and other time-points, only 16hpi plots for processes and cellular localization were shown to increase simplicity (Fig. 3B and C). In terms of protein abundance, the most *up-regulated* cellular processes (Fig. 3B) included: RNA processing ($p=10^{-82}$), ribonucleoprotein biogenesis ($p=10^{-44}$), cellular respiration ($p=10^{-42}$), generation of precursor metabolites and energy ($p=10^{-39}$), and mitochondrial translation ($p=10^{-39}$). Increased proteins were most associated with the locations of mitochondria ($p=10^{-162}$), ribonucleoprotein complexes ($p=10^{-83}$), nuclear lumen ($p=10^{-59}$), nucleoli ($p=10^{-48}$), and spliceosomal complexes ($p=10^{-39}$) (Fig. 3C).

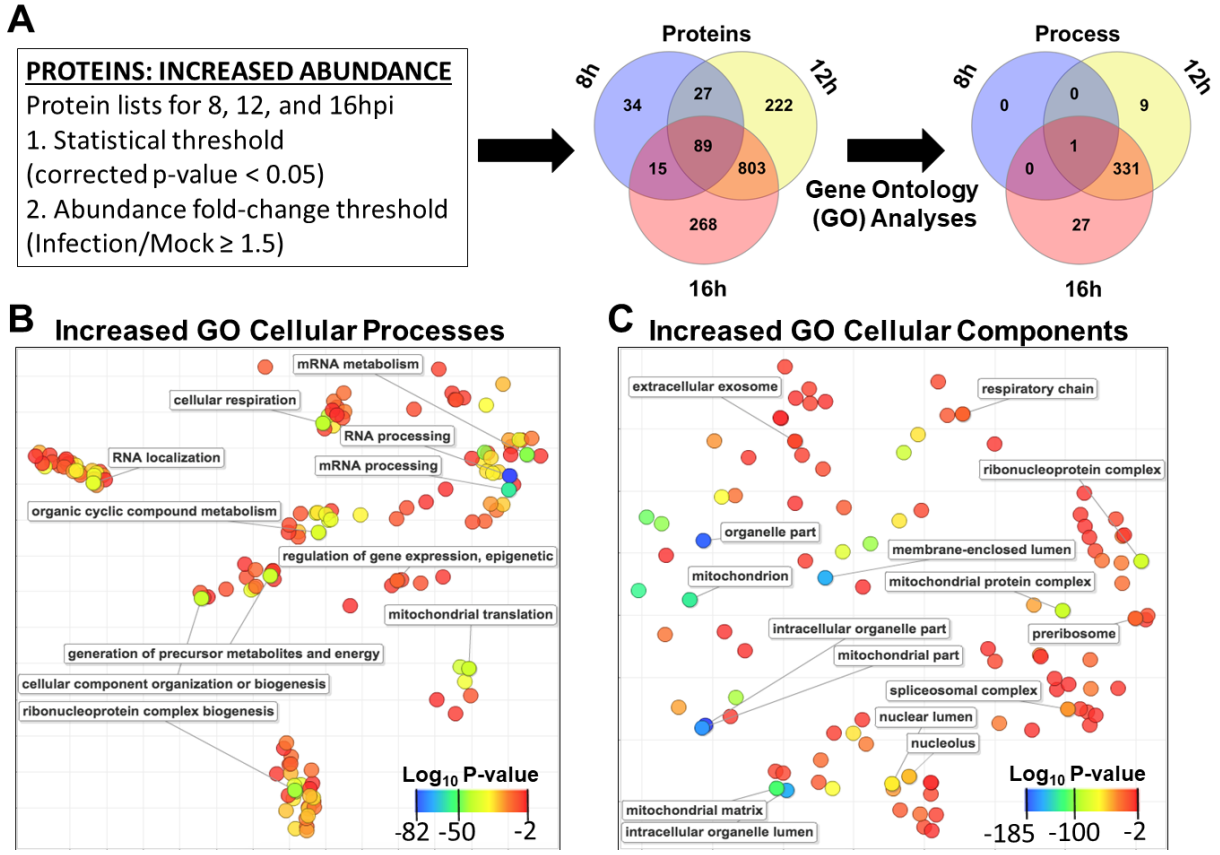

Fig. 4.3: Proteomic analyses identified highly significant increases to proteins associated with RNA processing and mitochondria. (A) For each time-point, statistically and biologically significantly increased ($p<0.05$; $log2FC \geq 0.58$) human proteins were identified and the lists for each time-point compared using InteractiVenn. These protein lists were then analyzed for gene ontology (GO) using GOTERMFINDER to identify which biological processes were affected during infection. The GO term lists were then compared across time-points as before. To reduce redundancy from GO analyses, REVIGO was then used to clarify whether proteins identified belonged to specific cellular processes or cellular locations. Based on the degree of overlap between findings from 16hpi and the other time-points, REVIGO results for cellular processes (B) and cellular locations (C) are shown here for 16hpi. Semantic similarity refers to similarity between each GO term and was used to cluster similar process or localization terms. Circles are significant GO terms with colors showing log10 p-values (Bonferroni-corrected) corresponding with each color spectrum.

Proteins associated with the cytosol, exosomes, and translation were most likely to be reduced during infection. Using similar analyses, we assessed significantly *decreased* protein abundance profiles over the course of NiV infection (Fig. 4A). As with proteins of increased abundance, the lists of proteins and GO terms identified at 8 and 12hpi overlapped substantially with and were exceeded in number by lists for the 16hpi time-point (Fig. 4A). The most down-regulated cellular processes (Fig. 4B) included: translation ($p=10^{-81}$), cellular catabolism ($p=10^{-61}$), SRP-dependent co-translational protein targeting to membrane ($p=10^{-56}$), and cell cycle ($p=10^{-35}$). In contrast to major abundance enrichment for mitochondria proteins, reduction in abundance of proteins were most associated with the cytosol ($p=10^{-299}$) and extracellular exosomes ($p=10^{-154}$) (Fig. 4C). Additional groups with significant reductions in abundance included cytosolic ribosomes ($p=10^{-60}$), nuclei ($p=10^{-51}$), proteasome complexes ($p=10^{-30}$), and the cytoskeleton ($p=10^{-30}$).

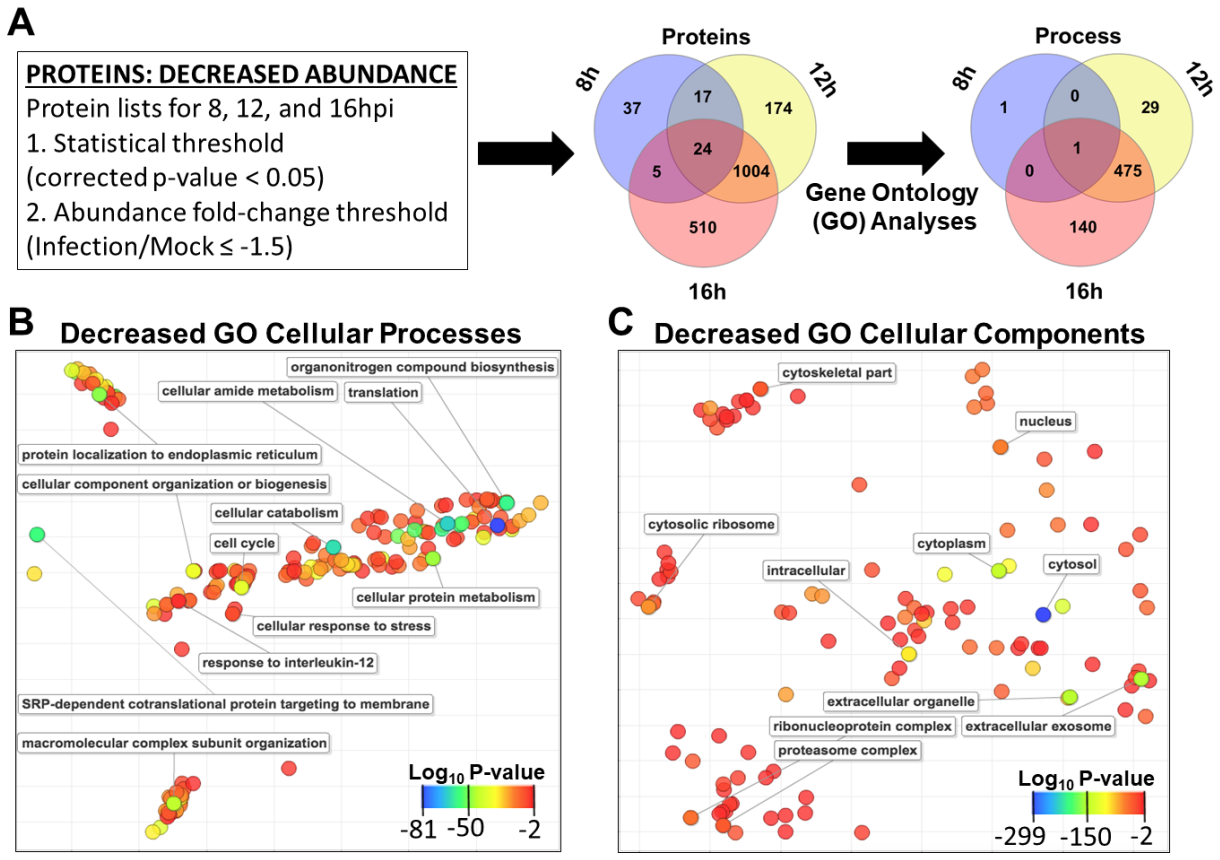

Fig. 4.4: Proteins associated with the cytosol, exosomes, and translation were most likely to be reduced during infection. The same analyses were conducted as shown in Fig. 3, except that proteins exhibiting decreased abundance ($p<0.05$; $log2FC \leq -0.58$) were identified and analyzed.

Reactome mapping of cellular proteomic changes 16 hours after NiV infection. To supplement our Gene Ontological analyses, which identified processes and cellular locations most *statistically* affected by infection, we utilized another analysis approach focused on summarizing average *fold-changes* for proteins within the cellular pathways most affected. For this purpose, the pathway analysis tool associated with the Reactome database was used (64). Specifically, all proteins identified as passing both statistical ($p \leq 0.05$) and biological thresholds ($FC \geq 1.5$ or ≤ -1.5) for at least one time-point were compiled along with their associated fold-changes for each time-point. This list is included in the supplementary file (S1) to support further reader analyses of these data in Reactome. An overview of many pathways found to be affected at 16hpi is shown in Fig. 5. This pathway overview (Fig. 5) organizes many cellular functions/pathways into several clusters of branches. Each of these branched groups have a central node, which designates the most general pathway in the center (Fig. 5 inset shows the example, “Protein Metabolism”). Related pathways that can be categorized under this central node are designated by nodes of increasing specificity further from the central node. This is clear in the case of the “Protein Metabolism” cluster (Fig. 5, inset), where one of the next most general pathways is “All Translation”. Increasing specificity once more, one of the sub-pathways under “All Translation” is “Mitochondrial Translation”. This pattern is repeated, creating the branching appearance extending from each central node/process.

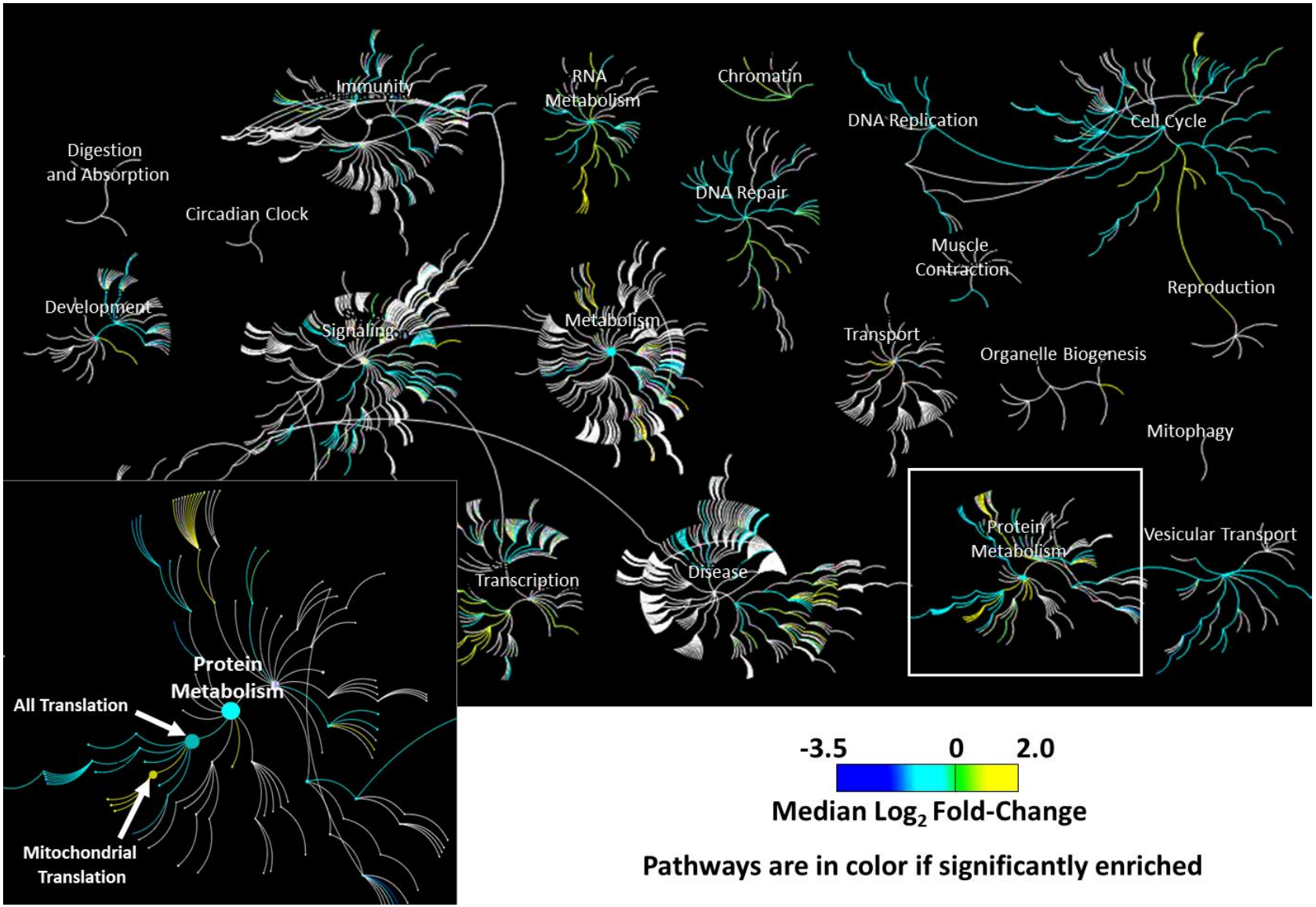
Immunity
RNA Metabolism
Chromatin
DNA Replication
Cell Cycle
Digestion and Absorption
DNA Repair
Circadian Clock
Muscle Contraction
Reproduction
Development
Signaling
Metabolism
Transport
Organelle Biogenesis
Mitophagy
Transcription
Disease
Protein Metabolism
Vesicular Transport
Protein Metabolism
All Translation
Mitochondrial Translation
-3.5
0
2.0
Median Log2 Fold-Change
Pathways are in color if significantly enriched

Fig. 4.5: Reactome mapping of cellular proteomic changes 16 hours after NiV infection. The Reactome database and map orders biological processes into branched clusters where increasingly specific processes are further from the parent process or node, as shown for the parent node, “protein metabolism” and daughter node, “all translation” (inset). Proteins identified as meeting significance thresholds at any time-point were listed along with their corresponding fold-changes to allow for proteomic expression mapping using Reactome. Significant changes specific cellular processes, based on changes in expression for associated proteins, are shown as the inclusion of any color. Color further indicates whether the median log2 fold-change of expression for proteins included in each process is positive (yellow-shifted) or negative (blue-shifted).

The Reactome pathway map (Fig. 5) indicates which cellular pathways are significantly affected through the inclusion of color. Specifically, the color of each node (i.e. pathway) corresponds to the *average* fold-change (FCs were $\log_2$ transformed for normalization) in abundance of proteins belonging to that pathway. Thus, the pathway map in Fig. 5 demonstrates that at 16hpi, NiV infection-associated proteomic changes impact many diverse cellular pathways. While discussion of every pathway affected during infection is beyond the scope of this study, Table 2 lists all affected pathways. One of the most interesting findings from this pathway map was that proteins involved in translation generally exhibited substantial decreases in abundance except in the case of mitochondrial translation machinery, which was clearly increased (Fig. 5 inset). This finding might help explain why at least some mitochondrial proteins, particularly those made within these organelles, exhibited increased abundance compared to mock infections. The consistent and substantial increases in mitochondrial proteins indicate that their function has important roles in supporting viral spread, including the provision of energy and precursors for viral replication.

Table 4.2: Summary of processes affected in Reactome map. This table lists all significantly affected processes in decreasing order of significance, along with the associated statistical family-wise detection rate (FDR) and median log2fold-changes in abundance for that process at each time-point. For easy interpretation, fold-changes are also represented by red (increased) and blue (decrease). This table will be included as a supplemental file.

Transcriptional but not proteomic changes indicate protein folding stress response during late infection. Transcriptomics (Fig. 6A) analyses also indicated increasingly dramatic changes in cellular processes from 8 to 12 to 16hpi. Changes were clearest at the 16hpi time-point, indicating increased expression of transcripts associated with the endoplasmic reticulum stress response ($p=10^{-7}$) (Fig. 6B) as well as reduced transcripts associated with DNA replication ($p=10^{-16}$) and the G1/S cell cycle transition ($p=10^{-9}$) (Fig. 6C). Of particular interest for these pathways was the identification of protein kinase R (PKR) as increasingly reduced in abundance, since PKR is centrally involved in numerous major stress and antiviral response pathways including the activation of NFkB signaling after recognition of viral dsRNA (69, 70). Importantly, several mechanisms for combatting the antiviral functions of PKR have been developed by viruses including PKR targeting by Rift Valley Fever virus proteins for degradation (71, 72). Interestingly, proteins and transcripts identified as increased or decreased in abundance exhibited very low levels of overlap (Fig. 6D). Given that this lack of overlap was also consistent when comparing cellular processes affected during infection (Figs. 3-6) post-transcriptional regulation is very likely to play major roles in shaping the proteome.

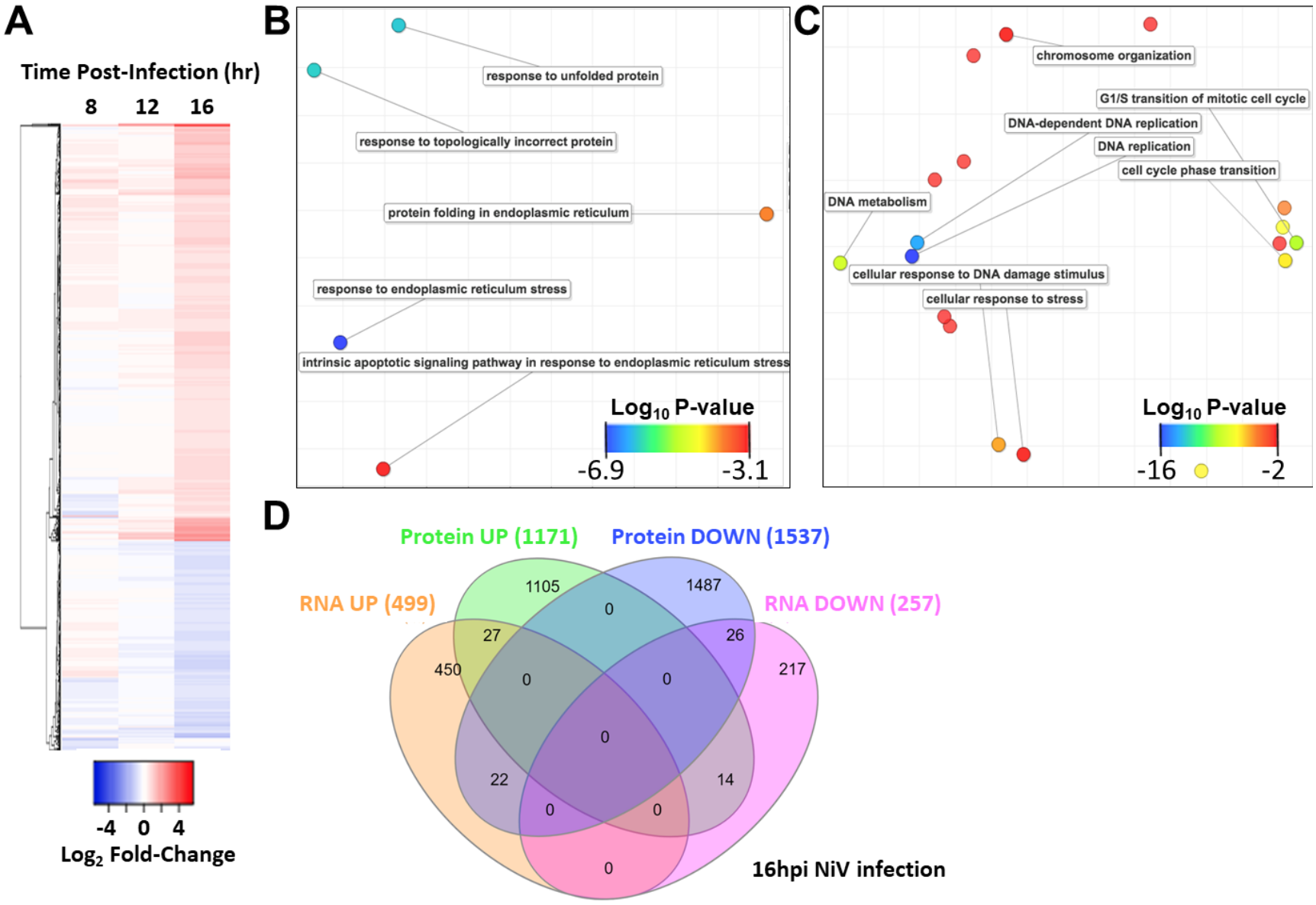
A
Time Post-Infection (hr)
8
12
16
-4
0
4
Log2 Fold-Change
B
response to unfolded protein
response to topologically incorrect protein
protein folding in endoplasmic reticulum
response to endoplasmic reticulum stress
intrinsic apoptotic signaling pathway in response to endoplasmic reticulum stress
Log10 P-value
-6.9
-3.1
C
chromosome organization
G1/S transition of mitotic cell cycle
DNA-dependent DNA replication
DNA replication
cell cycle phase transition
DNA metabolism
cellular response to DNA damage stimulus
cellular response to stress
Log10 P-value
-16
-2
D
Protein UP (1171)
Protein DOWN (1537)
RNA UP (499)
RNA DOWN (257)
1105
1487
0
27
26
450
0
0
217
0
22
14
0
0
0
16hpi NiV infection

Fig. 4.6: Transcriptional but not proteomic changes indicate protein folding stress response during late infection. Microarrays were used to identify transcriptional changes to human transcript levels across four time-points of NiV infection (4hpi exhibited no change and is not shown). (A) These enrichments are summarized in a heatmap demonstrating increasingly clear transcriptional modulation during the ongoing infection. Bonferroni-corrected P values were calculated for each GO term enrichment. For the 16hpi time-point, statistically and biologically significant ($p<0.05$ and $log2FC \geq 0.58$ or ≤ -0.58) up-(B) and down-regulated (C) transcripts were analyzed for process enrichment with GOTERMFINDER and REVIGO, as in Fig. 3. The color spectra in B and C represent the statistical significance (p-value, Bonferroni corrected) for each GO term enrichment in log10. (D) For 16hpi, lists of proteins and transcripts identified as increased or decreased are compared in a Venn diagram. These comparisons showed extremely limited overlap between these lists, indicating that proteomic changes during infection are more substantially shaped by regulation post-transcriptionally than at transcription.

Metabolomics and lipidomics indicate increased glucose and lipid metabolites. Based on proteomics (Figs. 3-5), one of the clearest cellular changes during infection was the consistent increase in proteins associated with mitochondria, an organelle with crucial functions in processes such as immune responses, apoptotic signaling, and metabolism (73, 74). While some viruses have been observed to target mitochondria for control over these processes during infections (75, 76), much less is known about how metabolite and lipid profiles are altered, particularly in the case of acute infections, such as that of NiV. From our paired mock and live BSL-4 NiV infections, samples were also taken for metabolomics and lipidomics. As shown in Fig. 7A, there were distinct metabolomic changes that occurred during infection, namely the increase of several glycolytic products, fatty acids, and monoacylglycerols as well as the clear drop in several amino acids such as L-glutamine ($p=0.012$) and L-glutamate ($p=0.003$) at 16hpi. From lipidomics analyses, changes in expression were noted for levels of all detected lipids (Fig. 7B), grouped by sub-class. From this analysis, we identified a general trend of increased lysolipid presence, particularly in the case of lysophosphatidylinositols (average $\log_2 FC = 1.95$). Cardiolipins; however, exhibited reduced levels at 16hpi (average $\log_2 FC = -1.15$). These analyses were repeated to only include lipids exhibiting statistically different expression

for at least one time-point (Fig. 7C). From this alternative analysis, the pattern seen for lysophosphatidylinositols but not for cardiolipins was conserved. This finding highlights changes to specific sub-classes and species of lipids. In some cases including human immunodeficiency virus, specific lipids such as phosphatidyl inositol are crucial during productive viral replication (77, 78). Since the biological significance of these shifts in metabolite and lipid profiles during NiV infection are unclear, these data offer an exciting new perspective into the life cycle of this virus and open many questions for future research.

Fig. 4.7: Metabolomics and lipidomics indicate up-regulation of glucose and lipid metabolites and down-regulation of several amino acids. (A) All metabolites exhibiting significantly altered levels (p-value ≤ 0.05) at 8, 12, or 16hpi, as compared to time-matched mock controls, are summarized in heat maps based on p-value and log2 fold-change. Average Log2 fold-changes for each lipid sub-class during infection are summarized here based on (B) all detected lipids as well as (C) only significantly affected lipids. Numbers in the parentheses indicate how many lipid species fall into each category. Cer – ceramide, Lcer – lysoceramide, CL – cardiolipin, CoQ10 – coenzyme Q10, DG – diacylglycerol, HexCer – hexosylceramide, GM2 – monosialic ganglioside 2, GM3 – monosialic ganglioside 3. PA – phosphatidic acid, PC – phosphatidylcholine, PCPA – plasmanyl phosphatidylcholine, PCP – phosphatidylcholine plasmalogen, LPC – lysophosphatidylcholine, LPCPA – lysoplasmanyl phosphatidylcholine, LPCP – lysophosphatidylcholine plasmalogen, PE – phosphatidylethanolamine, PEPA – plasmanyl phosphatidylethanolamine, PEP – phosphatidylethanolamine plasmalogen, LPE – lysophosphatidylethanolamine, PG – phosphatidylglycerol, LPG – lysophosphatidylglycerol, PI – phosphatidylinositol, LPI – lysophosphatidylinositol, PI – phosphatidylserine, GM2 – monosialic ganglioside 1, TG – triacylglycerol.

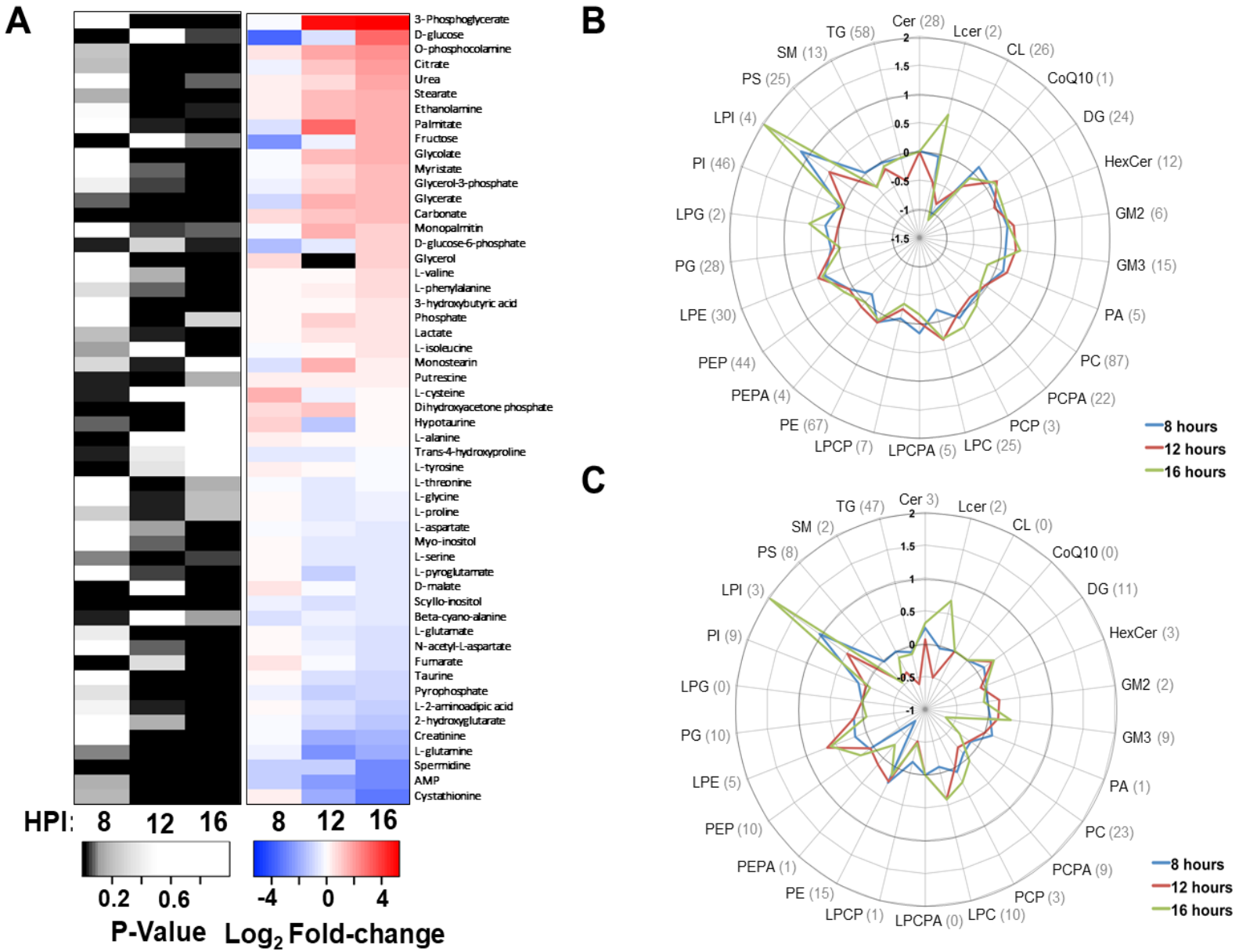
A
3-Phosphoglycerate
D-glucose
O-phosphocolamine
Citrate
Urea
Stearate
Ethanolamine
Palmitate
Fructose
Glycolate
Myristate
Glycerol-3-phosphate
Glycerate
Carbonate
Monopalmitin
D-glucose-6-phosphate
Glycerol
L-valine
L-phenylalanine
3-hydroxybutyric acid
Phosphate
Lactate
L-isoleucine
Monostearin
Putrescine
L-cysteine
Dihydroxyacetone phosphate
Hypotaurine
L-alanine
Trans-4-hydroxyproline
L-tyrosine
L-threonine
L-glycine
L-proline
L-aspartate
Myo-inositol
L-serine
L-pyroglutamate
D-malate
Scyllo-inositol
Beta-cyano-alanine
L-glutamate
N-acetyl-L-aspartate
Fumarate
Taurine
Pyrophosphate
L-2-aminoadipic acid
2-hydroxyglutarate
Creatinine
L-glutamine
Spermidine
AMP
Cystathionine
HPI: 8 12 16 8 12 16
0.2 0.6
-4 0 4
P-Value
Log2 Fold-change
B
Cer (28)
Lcer (2)
CL (26)
CoQ10 (1)
DG (24)
HexCer (12)
GM2 (6)
GM3 (15)
PA (5)
PC (87)
PCPA (22)
PCP (3)
LPC (25)
LPCPA (5)
LPCP (7)
PE (67)
PEPA (4)
PEP (44)
LPE (30)
PG (28)
LPG (2)
PI (46)
LPI (4)
PS (25)
SM (13)
TG (58)
8 hours
12 hours
16 hours
C
Cer 3)
Lcer (2)
CL (0)
CoQ10 (0)
DG (11)
HexCer (3)
GM2 (2)
GM3 (9)
PA (1)
PC (23)
PCPA (9)
PCP (3)
LPC (10)
LPCPA (0)
LPCP (1)
PE (15)
PEPA (1)
PEP (10)
LPE (5)
PG (10)
LPG (0)
PI (9)
LPI (3)
PS (8)
SM (2)
TG (47)
8 hours
12 hours
16 hours

Overall model for metabolic changes in an infected cell using a multi-'omics' approach.

To maximize the use of our findings, we summarized the major results from proteomics, metabolomics, and lipidomics analyses in a single diagram (Fig. 8). From this analysis, a few trends become clear. First, levels of glucose are significantly reduced after 8 hours ($p= 0.02$; $\log_2FC= -3.75$), rebound towards normal levels at 12 hours ($p= 0.57$; $\log_2FC= -0.70$), and increase substantially at 16hpi ($p= 0.04$; $\log_2FC= 3.13$). The same pattern, albeit weaker, was seen one step further in glycolysis for glucose-6-phosphate (G6P). Since many of the other glycolytic products past G6P were not detected this may suggest that glucose and G6P were primarily targeted for nucleotide synthesis to support viral replication. Reassuringly, this pattern was supported by our proteomic findings of concurrent, dramatic reductions in all glycolytic enzymes except hexokinases such as hexokinase 1, which is up-regulated at 12hpi ($p<0.001$; $\log_2FC= 0.77$) and 16hpi ($p<0.001$; $\log_2FC= 0.69$). Through lipidomics and metabolomics, it was also observed that triglyceride levels were reduced during infection, with the lowest levels at 12hpi, and that this reduction occurred along with increased levels of diacylglycerides, monoacylglycerides (monopalmitin and monostearin), fatty acids, glycerol, and glycerol-3-phosphate. Together, these markers may suggest an unexpected increase in triglyceride catabolism during infection. While the significance of these lipidomic changes requires further study, such broad dynamic changes are likely to affect the many functions of lipids in signaling and may have implications in several aspects of the viral life cycle.

Fig. 4.8: Overall model for metabolic changes in an infected cell using a multi-'omics' approach. Data reported from proteomics, lipidomics, and metabolomics were used to construct a simplified model for metabolic changes undergone during live NiV infection. Log2 transformed fold-changes are shown for each time-point where possible. The absence of positive detection for an item is shown in dark gray, whereas non-significant change is shown as a light gray.

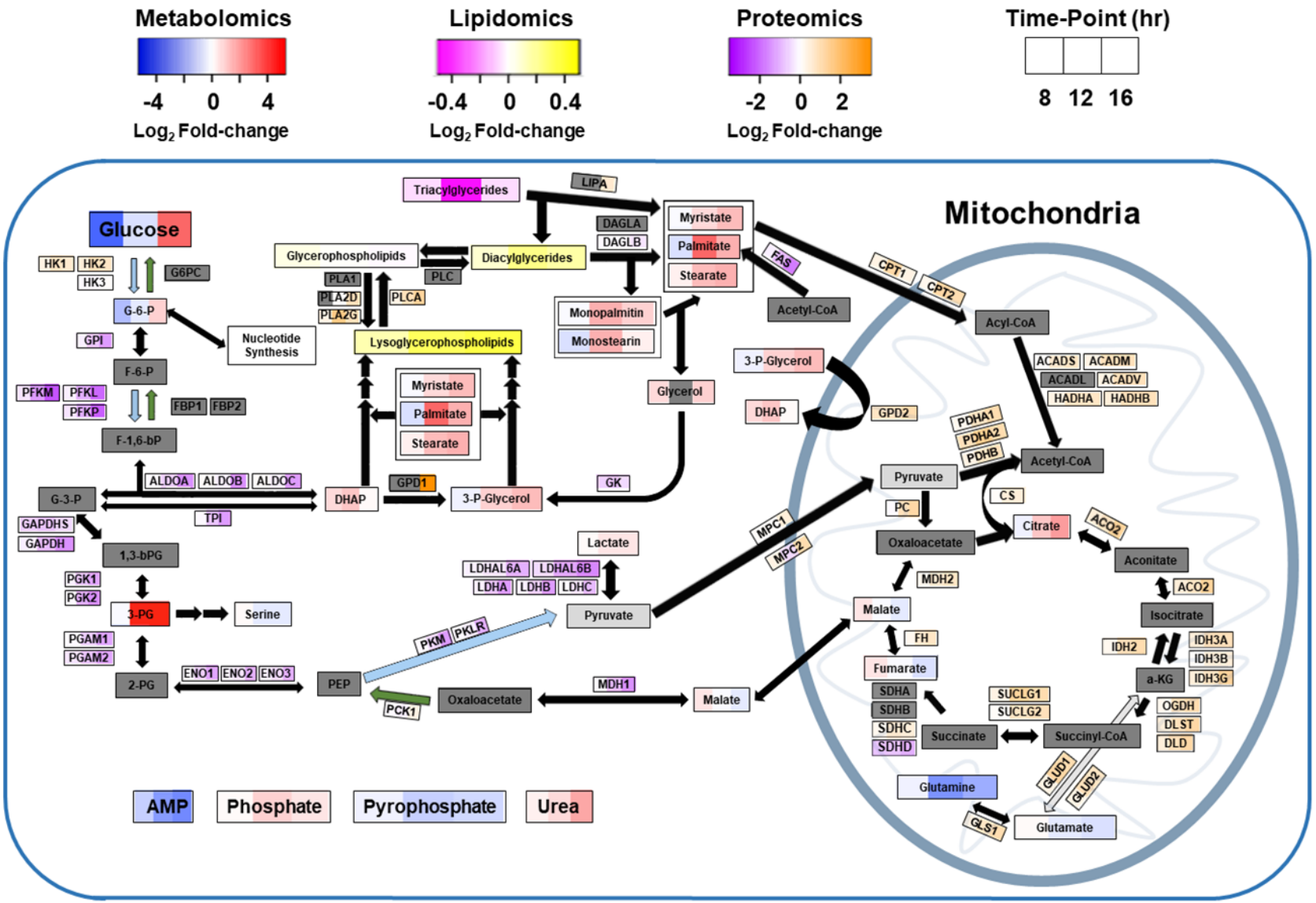
Metabolomics
-4 0 4
Log2 Fold-change
Lipidomics
-0.4 0 0.4
Log2 Fold-change
Proteomics
-2 0 2
Log2 Fold-change
Time-Point (hr)
8 12 16
Mitochondria
Glucose
HK1 HK2 HK3
G6PC
G-6-P
GPI
F-6-P
PFKM PFKL PFKP
FBP1 FBP2
F-1,6-bP
ALDOA ALDOB ALDOC
G-3-P
GAPDHS GAPDH
TPI
1,3-bPG
PGK1 PGK2
3-PG
Serine
PGAM1 PGAM2
2-PG
ENO1 ENO2 ENO3
PEP
PKM PKLR
PCK1
Pyruvate
Lactate
LDHAL6A LDHAL6B
LDHA LDHB LDHC
Oxaloacetate
MDH1
Malate
Nucleotide Synthesis
Triacylglycerides
LIPA
Glycerophospholipids
PLA1 PLA2D PLA2G
PLC PLCA
Diacylglycerides
DAGLA DAGLB
Lysoglycerophospholipids
Myristate
Palmitate
Stearate
Monopalmitin
Monostearin
Glycerol
GK
DHAP
GPD1
3-P-Glycerol
FAS
Acetyl-CoA
CPT1 CPT2
Acyl-CoA
ACADS ACADM
ACADL ACADV
HADHA HADHB
3-P-Glycerol
DHAP
GPD2
PDHA1 PDHA2 PDHB
Acetyl-CoA
Pyruvate
PC
CS
Citrate
ACO2
Aconitate
ACO2
Isocitrate
IDH2
IDH3A IDH3B IDH3G
a-KG
OGDH DLST DLD
Succinyl-CoA
SUCLG1 SUCLG2
Succinate
SDHA SDHB SDHC SDHD
Fumarate
FH
Malate
MDH2
Oxaloacetate
MPC1 MPC2
Glutamine
GLS1
Glutamate
GLUD1 GLUD2
AMP
Phosphate
Pyrophosphate
Urea

Overall model for post-transcriptional regulation of gene expression during NiV infection

One of the most striking phenotypes from all our analyses was the extreme inconsistency between proteomics and transcriptomics. First, the changes in abundance of many *individual transcripts* did not match the patterns of change for their associated proteins (Fig. 6D). Additionally, this discrepancy was also clear when contrasting between the lists of *cellular processes* identified as changed, based on proteomics as compared to transcriptomics. These findings along with proteomics analyses indicating reduced translation yet increased abundance for numerous clusters of functionally associated proteins (i.e. GO process and GO location) indicates the existence of differential post-transcriptional regulation of gene expression for specific protein groups. To aid in identifying contributing factors for these phenotypes, the proteomics data was summarized with a simplified model (Fig. 9). As shown in this model, it is clear that ribosomal proteins and those involved in translation are generally reduced; however, further inhibition of cellular capability to support cytoplasmic translation may also be induced by reductions in the proteins involved in tRNA processing as well as rRNA and tRNA but not mRNA nuclear export. Additionally, proteins translated from nuclear RNA, translated in the cytosol, and imported into mitochondria as well as those translated directly from mitochondrial RNA exhibited generally increased abundances. This consistency was unexpected and is of high interest for potential support of infection.

Another interesting finding with potential implications for the overall proteome and for immune response to NiV infection was the consistent decreased in proteasomal subunit abundance. Interestingly, we also report consistent increases in major histocompatibility complex (MHC) I proteins. Since proteasomal function is important during infection of a cell for the processing of viral antigens, which are then presented to immune cells by MHC I complexes (79, 80), future studies are needed to determine how these proteomic changes alter immune response during NiV infection.

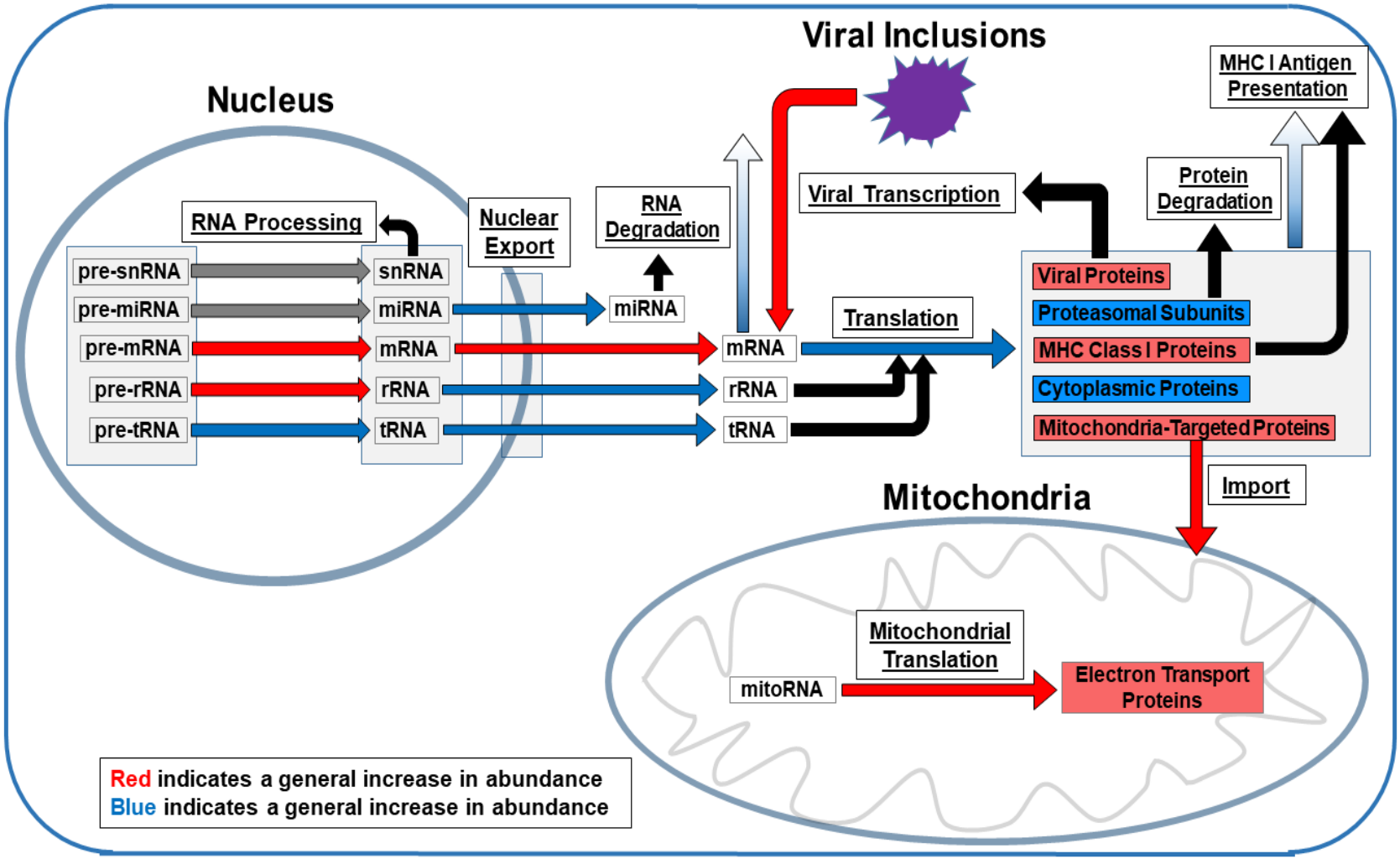
Viral Inclusions
MHC I Antigen Presentation
Nucleus
RNA Processing
Nuclear Export
RNA Degradation
Viral Transcription
Protein Degradation
pre-snRNA
pre-miRNA
pre-mRNA
pre-rRNA
pre-tRNA
snRNA
miRNA
mRNA
rRNA
tRNA
miRNA
mRNA
rRNA
tRNA
Translation
Viral Proteins
Proteasomal Subunits
MHC Class I Proteins
Cytoplasmic Proteins
Mitochondria-Targeted Proteins
Import
Mitochondria
Mitochondrial Translation
mitoRNA
Electron Transport Proteins
Red indicates a general increase in abundance
Blue indicates a general increase in abundance

Fig. 4.9: Overall model for Post-Transcriptional Regulation during NiV infection. A simplified model of major changes to post-transcriptional processes involved in gene expression as determined by proteomics. Three significant structures: the nucleus, mitochondria, and viral centers for replication and transcription (viral inclusions) are designated. Cellular and viral processes of interest, such as translation, are underlined. Each process is also associated with either a red or blue arrow, indicating that proteins involved in that process were generally increased or decreased in abundance, respectively. Similarly, while proteins involved in translation were generally decreased, proteins associated with different processes or cellular locations still exhibited substantial enrichments (red box) or reductions (blue box) in abundance compared to time-matched mock infection controls. Some types of RNA (e.g. rRNA) and proteins are also involved in specific processes, indicated here by black arrows.

Discussion

Over the last few decades, major advances in mass spectrometry software, instrumentation, and methods have dramatically improved approaches to understanding protein interactions, post-translational modifications, and changes in abundance (81). With the evolution of proteomics has come its applications to virology, yielding many advances (reviewed in 49). With the ability to quantitatively monitor changes in cellular abundance for thousands of proteins simultaneously over the course of infection, the complexity of viral infections has become clearer along with our ability to capture it. Among the viruses analyzed with this approach include hepatitis C virus, herpes simpex virus, and human cytomegalovirus (82–86).

Here, we report dramatic changes to the transcriptional and proteomic profiles of cells infected with NiV (Fig. 1). Focusing particularly at proteomic changes, infection likely alters gene expression at multiple points after transcription including mRNA splicing, translation, as well as RNA and protein degradation. From proteomics and subsequent analyses (Fig. 4B), the GO process most associated with proteins reduced in abundance was translation ($p=10^{-81}$), indicating that cellular protein expression might be generally inhibited. This expectation is further supported by our analyses with Reactome (Table 2) in which proteins associated with cytosolic tRNA aminoacylation, the process of charging tRNAs with corresponding amino acids, had among the most substantial median fold-change decreases (16hpi FC = -2.71).

While these findings suggest a global decrease in expression, we report this reduction appears to be highly dependent on sub-cellular protein localization and primarily affects cytoplasmic proteins. The most outstanding example was the large and consistent increase in mitochondrial proteins (Figs. 3-5, and 9). While several viruses have been shown to interact with individual mitochondrial proteins or complexes to influence their involvement in metabolism, cell death, and immunity, our report of highly consistent increases in mitochondrial proteins is, to our knowledge, novel for infections with viruses in the *Mononegavirales* order. The DNA virus human cytomegalovirus has been observed to induce upregulation in mitochondrial gene

expression, causing major changes in cellular metabolism (86). Infection with the unrelated *positive-sense* single-stranded RNA virus, hepatitis C virus was reported in clinical cases to induce mitochondrial dysfunction, partially through reduced abundance of mitochondrial proteins (82). Similarly, proteins of human immunodeficiency virus have been shown to induce mitochondrial alterations leading to dysfunction (87). Importantly, very little has been uncovered concerning functional interactions between henipaviruses and these organelles (75, 76). One recent study that identified cellular factor interactions for each NiV protein found that the nucleoprotein (N), essential for viral genome stability, packing, replication and transcription, interacts with mitochondrial proteins including members of the electron transport chain complex I and mitochondrial chaperones (49); however, the importance of these interactions remains entirely unelucidated. Whether these interactions alter mitochondrial function or organization are points of interest to better understand the mitochondrial changes we report during NiV infection.

The same study also identified interactions between several products of the P gene (P, V, and W) and the prp19 spliceosomal complex (49). Interestingly, several of these identified factors including prp19 itself are significantly upregulated during infection. As was previously suggested, these interactions may be important for virus-driven apoptotic avoidance or for more general influence over RNA splicing. In support of infection-associated changes to RNA splicing, our REVIGO analysis identified RNA processing ($p=10^{-82}$) and mRNA processing ($p=10^{-59}$) as the two most significantly enriched GO processes based on up-regulated proteins (Fig. 3B). Similarly, while we identified increased expression of p53 at 12 ($p<0.001$; $Log_2FC = 1.11$) and 16hpi ($p<0.01$; $Log_2FC = 1.30$), our Reactome pathway analysis suggested a trend of reduced expression for proteins associated with apoptosis (Table 2). This finding is consistent with a recent study of HeV, where infection in reservoir bat cells but not in human cells led to the induction of apoptosis (50). Based on infections with other types of viruses, the inhibition of apoptosis during NiV infection may serve to blunt the immune response and further support viral spread through cell-cell fusion (88–90).

Another finding from our Reactome analysis of proteomics was that proteins associated with small interfering RNA (siRNA) biogenesis are substantially down-regulated at 12 and 16hpi (Table 2). Based on antiviral roles of siRNAs, this could be another possible point of viral influence on cellular protein expression during infection and/or may serve as a point of inhibition of antiviral response (91–94). Supporting these possibilities, the NiV matrix protein was recently identified as a binding partner of the Dicer1 protein, which plays a central role in the formation of microRNAs and siRNAs (49, 95). A functional understanding of NiV-siRNA interactions and their importance during infection remains to be elucidated.

In the hope of validating and deepening the knowledge gained from proteomics, we also conducted lipidomics and metabolomics analyses of NiV infection. As shown in figure 8, there were highly conserved decreases in abundance for proteins involved in glycolysis, whereas protein expression of citric acid cycle enzymes was elevated. A major exception to this seemingly broad inhibition of glycolysis was that hexokinase, a key metabolic regulatory enzyme and the first of glycolysis, is up-regulated in expression at both 12 and 16hpi (Fig. 8). The clear increases in the abundance of hexokinases may serve the purpose of adding charge to glucose, thus keeping it from leaving the cell so that it may be used during infection (96). Further, phosphorylated glucose may also be shunted from glycolysis and instead utilized for nucleotide synthesis to sustain viral replication.

Our lipidomic analyses suggest that specific types of lipids are either being synthesized or removed from beta-oxidation, whereas the decreasing levels of triacyglycerols (TAGs) indicate that TAG hydrolysis and catabolism may be ongoing. This is supported by the observation that while TAG levels decrease, levels of diacyglycerols, monoacylglycerols, and free fatty acids are enriched (Fig. 7). While the average FC of glycerophospholipids does not change substantially over the course of infection, our lipidomic findings indicated a consistent increase of lysoglycerophospholipids (Figs 7 and 8); however, the purpose behind such a

change is not yet clear. One possibility is that these lipids better support the membrane curvature needed to bud new viral particles (78).

Despite the apparent inhibition of glycolysis during infection, protein expression enrichment and metabolomic findings suggest that both the citric acid cycle and oxidative phosphorylation continue functioning. The concomitant decreases in glutamine and glutamate indicate these molecules may be incorporated into the citric acid cycle to maintain it while metabolites such as malate are exported from mitochondria for use in viral replication (75, 97).

The observation that selenoamino acid metabolism and selenoprotein expression are very significantly reduced (Table 2), supports the likely roles of reactive oxygen species (ROS) and their release as involved in inflammation during NiV infection (98). Similar findings of faulty ROS removal in cells infected with human respiratory syncytial virus, a pathogen distantly related to NiV, as well as other respiratory viruses have been tied to the high levels of inflammation that occur during infection and contribute to pathology (99, 100). While the importance of ROS increases during respiratory infection have been identified as contributing to lung tissue damage, any importance in viral lifecycles has remained unclear (101). Among cellular anti-oxidant proteins identified as reduced in abundance were those involved in the synthesis and continued activity of glutathione, a crucial cellular antioxidant, including glutathione synthetase (12hpi/16hpi Log_2FC = -0.87/ -1.03) and glutathione reductase (12hpi/16hpi Log_2FC = -0.94/ -1.41). Numerous other enzymes important for directly maintaining safe ROS concentrations were also reduced: superoxide dismutase (12hpi/16hpi Log_2FC = -0.96/ -1.74), peroxiredoxin-1 (12hpi/16hpi Log_2FC = -0.90/ -1.44), and thioredoxin (12hpi/16hpi Log_2FC = -1.29/ -2.24). We thus hypothesize that ROS species continually accumulate during NiV infection due to drastic reductions in antioxidant proteins and molecules, leading to greatly exacerbated tissue damage.

Increased ROS production and other proteomic changes likely contribute to changes to mitochondrial morphology and biogenesis later during infection. Healthy mitochondrial

populations are thought to be maintained by continuous cycles of mitochondrial fusion and fission to produce unequally healthy mitochondria, where the latter is marked for degradation via macroautophagy (102). During NiV infection, the proteins involved in mitochondrial fusion, OPA1 and mitofusion-1 were increased significantly at 16hpi (Log_2FC = 1.11 and 1.04, respectively) with OPA1 also showing a trend towards similar levels of enrichment at 8hpi and 12hpi. On the contrary, the protein responsible for mitochondrial fission, Dynamin-1-like protein, exhibited statistically significant decreases in abundance from 8hpi to 16hpi (8hpi/12hpi/16hpi, Log_2FC = -0.34/-1.12/-1.94). Whether these changes are virally or cellularly driven is not clear, any ensuing mitochondrial dysregulation might have important roles in pathology and may explain a previous report of enlarged mitochondria during NiV infection of porcine cells (39).

As mentioned previously, NiV is known to inhibit activation of the type I interferon response through several means (37, 103). Similar to the influenza NS1 protein, the V protein of NiV has been shown to inhibit the RIG-I pathway through direct interaction and inhibition of TRIM25, which is crucial for RIG-I activation (36, 104). From our proteomics data, we identified statistically significant reductions in abundance of TRIM25 (8hpi/12hpi/16hpi, Log_2FC = -0.24/-0.99/-2.12) as well as another key downstream component of the RIG-I pathway, TBK1 (8hpi/12hpi/16hpi, Log_2FC = -0.47/-1.35/-2.18). While not the most significantly enriched GO terms, REVIGO analyses for 16hpi identified proteins involved in antigen processing and presentation via MHC II, and the interleukin-12 mediated signaling pathway as proteomically reduced. Similar findings were reported from reactome pathway analysis where MHC II antigen presentation as well as the interleukin-1 pathway exhibited substantial median reductions in protein expression (Table 2). Proteins involved in MHC I peptide presentation were generally increased in abundance, particularly at 12hpi; however, proteasomal subunits were drastically and consistently reduced (Fig. 9) indicating that MHC I function may still be reduced. Whether any of these processes is further targeted by specific function of NiV proteins remains unclear and of future interest. Of particular interest, is whether the reduction of proteins involved in MHC

II antigen presentation is conserved during dendritic cell infection and whether this might support the high levels of virulence during infection.

In summary, live NiV infection of mammalian cells was analyzed with a multi-omics approach across four time-points to best understand major cellular changes. Many processes including gene expression, metabolism, and immune responses were all affected over the course of infection. Among the most unexpected findings was the highly significant up regulation of mitochondrial proteins and potential changes to dynamics and organization, offering new insights into NiV pathogenicity and to the potential importance of mitochondria in the NiV lifecycle. Additionally, we report stark inconsistency between transcriptomic and proteomic changes during infection, which indicates potential post-transcriptional influence of NiV on the proteome further supported by recent reports of interactions between NiV proteins and both RNA splicing and RNAi machineries. In summary, we have described the first look with such depth into the many intracellular changes that occur during a henipavirus infection. The findings described here may serve both to identify novel mechanisms of henipaviral and cellular action as well as to provide a contextual foundation for such studies.

Contributions

Experimental Design: HAC, JA, HF; Experimentation: EDW, HAC; Data Analysis and Statistics: GPJ, NTU; Manuscript writing: GPJ, HAC

Acknowledgements

This work was funded by DHS grant to J.N.A and K.W, with a sub-contract to H.A.C, and by NIH/NIAID grant R01AI109022 to H.A.C. This study would not have been possible without the support of the NIH/NIAID and our collaborators therein at the Rocky Mountain Laboratories, E.d.W. and H.F.

“This work was supported, in part, by the Department of Homeland Security (DHS) Science and Technology Directorate (S&T) under Contract HSHQPM-14-X-00238. The funders had no role in study design, data collection and interpretation, or the decision to submit the work for publication.

References

1. Chua KB. 2000. Nipah Virus: A Recently Emergent Deadly Paramyxovirus. Science 288:1432–1435.

2. Ching PKG, de los Reyes VC, Sucaldito MN, Tayag E, Columna-Vingno AB, Malbas FF, Bolo GC, Sejvar JJ, Eagles D, Playford G, Dueger E, Kaku Y, Morikawa S, Kuroda M, Marsh GA, McCullough S, Foxwell AR. 2015. Outbreak of Henipavirus Infection, Philippines, 2014. Emerg Infect Dis 21:328–331.

3. Lam SK, Chua KB. 2002. Nipah Virus Encephalitis Outbreak in Malaysia. Clin Infect Dis 34:S48–S51.

4. Luby SP, Hossain MJ, Gurley ES, Ahmed B-N, Banu S, Khan SU, Homaira N, Rota PA, Rollin PE, Comer JA, Kenah E, Ksiazek TG, Rahman M. 2009. Recurrent Zoonotic Transmission of Nipah Virus into Humans, Bangladesh, 2001–2007. Emerg Infect Dis 15:1229–1235.

5. Nipah virus outbreaks in the WHO South-East Asia Region. Surveillance and outbreak alert, World Health Organization.

6. Drexler JF, Corman VM, Müller MA, Maganga GD, Vallo P, Binger T, Gloza-Rausch F, Rasche A, Yordanov S, Seebens A, Oppong S, Sarkodie YA, Pongombo C, Lukashev AN, Schmidt-Chanasit J, Stöcker A, Carneiro AJB, Erbar S, Maisner A, Fronhoffs F, Buettner R, Kalko EKV, Kruppa T, Franke CR, Kallies R, Yandoko ERN, Herrler G, Reusken C, Hassanin A, Krüger DH, Matthee S, Ulrich RG, Leroy EM, Drosten C. 2012. Bats host major mammalian paramyxoviruses. Nat Commun 3:796.

7. Wu Z, Yang L, Yang F, Ren X, Jiang J, Dong J, Sun L, Zhu Y, Zhou H, Jin Q. 2014. Novel Henipa-like Virus, Mojiang Paramyxovirus, in Rats, China, 2012. Emerg Infect Dis 20.

8. Marsh GA, de Jong C, Barr JA, Tachedjian M, Smith C, Middleton D, Yu M, Todd S, Foord AJ, Haring V, Payne J, Robinson R, Broz I, Crameri G, Field HE, Wang L-F. 2012. Cedar Virus: A Novel Henipavirus Isolated from Australian Bats. PLoS Pathog 8:e1002836.

9. Pernet O, Schneider BS, Beaty SM, LeBreton M, Yun TE, Park A, Zachariah TT, Bowden TA, Hitchens P, Ramirez CM, Daszak P, Mazet J, Freiberg AN, Wolfe ND, Lee B. 2014. Evidence for henipavirus spillover into human populations in Africa. Nat Commun 5:5342.

10. Breed AC, Meers J, Sendow I, Bossart KN, Barr JA, Smith I, Wacharapluesadee S, Wang L, Field HE. 2013. The Distribution of Henipaviruses in Southeast Asia and Australasia: Is Wallace's Line a Barrier to Nipah Virus? PLoS ONE 8:e61316.

11. Aguilar HC, Iorio RM. 2012. Henipavirus Membrane Fusion and Viral Entry, p. 79–94. *In* Lee, B, Rota, PA (eds.), Henipavirus. Springer Berlin Heidelberg, Berlin, Heidelberg.

12. Aguilar HC, Henderson BA, Zamora JL, Johnston GP. 2016. Paramyxovirus Glycoproteins and the Membrane Fusion Process. Curr Clin Microbiol Rep 3:142–154.

13. Liu Q, Stone JA, Bradel-Tretheway B, Dabundo J, Benavides Montano JA, Santos-Montanez J, Biering SB, Nicola AV, Iorio RM, Lu X, Aguilar HC. 2013. Unraveling a

Three-Step Spatiotemporal Mechanism of Triggering of Receptor-Induced Nipah Virus Fusion and Cell Entry. PLoS Pathog 9:e1003770.

14. Stone JA, Vemulapati BM, Bradel-Tretheway B, Aguilar HC. 2016. Multiple Strategies Reveal a Bidentate Interaction between the Nipah Virus Attachment and Fusion Glycoproteins. J Virol 90:10762–10773.

15. Curran J, Kolakofsky D. 1999. Replication of paramyxoviruses. Adv Virus Res 54:403–422.

16. Ranadheera C, Proulx R, Chaiyakul M, Jones S, Grolla A, Leung A, Rutherford J, Kobasa D, Carpenter M, Czub M. 2018. The interaction between the Nipah virus nucleocapsid protein and phosphoprotein regulates virus replication. Sci Rep 8.

17. Halpin K. 2004. Nipah virus conforms to the rule of six in a minigenome replication assay. J Gen Virol 85:701–707.

18. Wong KT, Shieh W-J, Kumar S, Norain K, Abdullah W, Guarner J, Goldsmith CS, Chua KB, Lam SK, Tan CT, Goh KJ, Chong HT, Jusoh R, Rollin PE, Ksiazek TG, Zaki SR, Nipah Virus Pathology Working Group. 2002. Nipah virus infection: pathology and pathogenesis of an emerging paramyxoviral zoonosis. Am J Pathol 161:2153–2167.

19. Geisbert TW, Daddario-DiCaprio KM, Hickey AC, Smith MA, Chan Y-P, Wang L-F, Mattapallil JJ, Geisbert JB, Bossart KN, Broder CC. 2010. Development of an Acute and Highly Pathogenic Nonhuman Primate Model of Nipah Virus Infection. PLoS ONE 5:e10690.

20. Baseler L, Scott DP, Saturday G, Horne E, Rosenke R, Thomas T, Meade-White K, Haddock E, Feldmann H, de Wit E. 2016. Identifying Early Target Cells of Nipah Virus Infection in Syrian Hamsters. PLoS Negl Trop Dis 10:e0005120.

21. Escaffre O, Borisevich V, Rockx B. 2013. Pathogenesis of Hendra and Nipah virus infection in humans. J Infect Dev Ctries 7.

22. DeBuysscher BL, de Wit E, Munster VJ, Scott D, Feldmann H, Prescott J. 2013. Comparison of the Pathogenicity of Nipah Virus Isolates from Bangladesh and Malaysia in the Syrian Hamster. PLoS Negl Trop Dis 7:e2024.

23. Mungall BA, Middleton D, Crameri G, Bingham J, Halpin K, Russell G, Green D, McEachern J, Pritchard LI, Eaton BT, Wang L-F, Bossart KN, Broder CC. 2006. Feline Model of Acute Nipah Virus Infection and Protection with a Soluble Glycoprotein-Based Subunit Vaccine. J Virol 80:12293–12302.

24. Mills JN, Alim ANM, Bunning ML, Lee OB, Wagoner KD, Amman BR, Stockton PC, Ksiazek TG. 2009. Nipah Virus Infection in Dogs, Malaysia, 1999. Emerg Infect Dis 15:950–952.

25. Looi L-M, Chua K-B. 2007. Lessons from the Nipah virus outbreak in Malaysia. Malays J Pathol 29:63–67.

26. Islam MS, Sazzad HMS, Satter SM, Sultana S, Hossain MJ, Hasan M, Rahman M, Campbell S, Cannon DL, Ströher U, Daszak P, Luby SP, Gurley ES. 2016. Nipah Virus

Transmission from Bats to Humans Associated with Drinking Traditional Liquor Made from Date Palm Sap, Bangladesh, 2011–2014. Emerg Infect Dis 22:664–670.

27. Gurley ES, Hegde ST, Hossain K, Sazzad HMS, Hossain MJ, Rahman M, Sharker MAY, Salje H, Islam MS, Epstein JH, Khan SU, Kilpatrick AM, Daszak P, Luby SP. 2017. Convergence of Humans, Bats, Trees, and Culture in Nipah Virus Transmission, Bangladesh. Emerg Infect Dis 23:1446–1453.

28. Paul L. 2018. Nipah virus in Kerala : A deadly Zoonosis. Clin Microbiol Infect.

29. Chang L-Y, Ali AM, Hassan S, AbuBakar S. 2007. Human neuronal cell protein responses to Nipah virus infection. Virol J 4:54.

30. Escaffre O, Borisevich V, Carmical JR, Prusak D, Prescott J, Feldmann H, Rockx B. 2013. Henipavirus Pathogenesis in Human Respiratory Epithelial Cells. J Virol 87:3284–3294.

31. de Wit E, Munster VJ. 2015. Animal models of disease shed light on Nipah virus pathogenesis and transmission: Nipah virus pathogenesis and transmission. J Pathol 235:196–205.

32. Munster VJ, Prescott JB, Bushmaker T, Long D, Rosenke R, Thomas T, Scott D, Fischer ER, Feldmann H, de Wit E. 2012. Rapid Nipah virus entry into the central nervous system of hamsters via the olfactory route. Sci Rep 2.

33. Basler CF. 2012. Nipah and Hendra Virus Interactions with the Innate Immune System, p. 123–152. *In* Lee, B, Rota, PA (eds.), Henipavirus. Springer Berlin Heidelberg, Berlin, Heidelberg.

34. Prescott J, de Wit E, Feldmann H, Munster VJ. 2012. The immune response to Nipah virus infection. Arch Virol 157:1635–1641.

35. Seto J, Qiao L, Guenzel CA, Xiao S, Shaw ML, Hayot F, Sealfon SC. 2010. Novel Nipah Virus Immune-Antagonism Strategy Revealed by Experimental and Computational Study. J Virol 84:10965–10973.

36. Sánchez-Aparicio MT, Feinman LJ, García-Sastre A, Shaw ML. 2018. Paramyxovirus V Proteins Interact with the RIG-I/TRIM25 Regulatory Complex and Inhibit RIG-I Signaling. J Virol 92:e01960-17.

37. Bharaj P, Wang YE, Dawes BE, Yun TE, Park A, Yen B, Basler CF, Freiberg AN, Lee B, Rajsbaum R. 2016. The Matrix Protein of Nipah Virus Targets the E3-Ubiquitin Ligase TRIM6 to Inhibit the IKKε Kinase-Mediated Type-I IFN Antiviral Response. PLOS Pathog 12:e1005880.

38. Lamp B, Dietzel E, Kolesnikova L, Sauerhering L, Erbar S, Weingartl H, Maisner A. 2013. Nipah Virus Entry and Egress from Polarized Epithelial Cells. J Virol 87:3143–3154.

39. Chang L-Y, Ali ARM, Hassan SS, AbuBakar S. 2006. Nipah virus RNA synthesis in cultured pig and human cells. J Med Virol 78:1105–1112.

40. Chan EY, Qian W-J, Diamond DL, Liu T, Gritsenko MA, Monroe ME, Camp DG, Smith RD, Katze MG. 2007. Quantitative Analysis of Human Immunodeficiency Virus Type 1-Infected CD4+ Cell Proteome: Dysregulated Cell Cycle Progression and Nuclear Transport Coincide with Robust Virus Production. J Virol 81:7571–7583.

41. Hu A, Noble WS, Wolf-Yadlin A. 2016. Technical advances in proteomics: new developments in data-independent acquisition. F1000Research 5:419.

42. Kao A, Chiu C, Vellucci D, Yang Y, Patel VR, Guan S, Randall A, Baldi P, Rychnovsky SD, Huang L. 2011. Development of a Novel Cross-linking Strategy for Fast and Accurate Identification of Cross-linked Peptides of Protein Complexes. Mol Cell Proteomics 10:M110.002212.

43. Jiang X-S, Tang L-Y, Dai J, Zhou H, Li S-J, Xia Q-C, Wu J-R, Zeng R. 2005. Quantitative Analysis of Severe Acute Respiratory Syndrome (SARS)-associated Coronavirus-infected Cells Using Proteomic Approaches: Implications for Cellular Responses to Virus Infection. Mol Cell Proteomics 4:902–913.

44. Kaake RM, Wang X, Burke A, Yu C, Kandur W, Yang Y, Novtisky EJ, Second T, Duan J, Kao A, Guan S, Vellucci D, Rychnovsky SD, Huang L. 2014. A New *in Vivo* Cross-linking Mass Spectrometry Platform to Define Protein–Protein Interactions in Living Cells. Mol Cell Proteomics 13:3533–3543.

45. Munday DC, Emmott E, Surtees R, Lardeau C-H, Wu W, Duprex WP, Dove BK, Barr JN, Hiscox JA. 2010. Quantitative Proteomic Analysis of A549 Cells Infected with Human Respiratory Syncytial Virus. Mol Cell Proteomics 9:2438–2459.

46. Vidova V, Spacil Z. 2017. A review on mass spectrometry-based quantitative proteomics: Targeted and data independent acquisition. Anal Chim Acta 964:7–23.

47. Oxford KL, Wendler JP, McDermott JE, White Iii RA, Powell JD, Jacobs JM, Adkins JN, Waters KM. 2016. The landscape of viral proteomics and its potential to impact human health. Expert Rev Proteomics 13:579–591.

48. Vera-Velasco NM, García-Murria MJ, Sánchez del Pino MM, Mingarro I, Martinez-Gil L. 2018. Proteomic composition of Nipah virus -like particles. J Proteomics 172:190–200.

49. Martinez-Gil L, Vera-Velasco NM, Mingarro I. 2017. Exploring the Human-Nipah Virus Protein-Protein Interactome. J Virol 91:e01461-17.

50. Wynne JW, Shiell BJ, Marsh GA, Boyd V, Harper JA, Heesom K, Monaghan P, Zhou P, Payne J, Klein R, Todd S, Mok L, Green D, Bingham J, Tachedjian M, Baker ML, Matthews D, Wang L-F. 2014. Proteomics informed by transcriptomics reveals Hendra virus sensitizes bat cells to TRAIL mediated apoptosis. Genome Biol 15:532.

51. Aguilar HC, Matreyek KA, Choi DY, Filone CM, Young S, Lee B. 2007. Polybasic KKR Motif in the Cytoplasmic Tail of Nipah Virus Fusion Protein Modulates Membrane Fusion by Inside-Out Signaling. J Virol 81:4520–4532.

52. Johnston GP, Contreras EM, Dabundo J, Henderson BA, Matz KM, Ortega V, Ramirez A, Park A, Aguilar HC. 2017. Cytoplasmic Motifs in the Nipah Virus Fusion Protein Modulate Virus Particle Assembly and Egress. J Virol 91:e02150-16.

53. Cifuentes-Muñoz N, Sun W, Ray G, Schmitt PT, Webb S, Gibson K, Dutch RE, Schmitt AP. 2017. Mutations in the Transmembrane Domain and Cytoplasmic Tail of Hendra Virus Fusion Protein Disrupt Virus-Like-Particle Assembly. J Virol 91:e00152-17.

54. Nakayasu ES, Nicora CD, Sims AC, Burnum-Johnson KE, Kim Y-M, Kyle JE, Matzke MM, Shukla AK, Chu RK, Schepmoes AA, Jacobs JM, Baric RS, Webb-Robertson B-J, Smith RD, Metz TO. 2016. MPLEx: a Robust and Universal Protocol for Single-Sample Integrative Proteomic, Metabolomic, and Lipidomic Analyses. mSystems 1:e00043-16.

55. Zimmer JSD, Monroe ME, Qian W-J, Smith RD. 2006. Advances in Proteomics Data Analysis and Display Using an Accurate Mass and Time Tag Approach. Mass Spectrom Rev 25:450–482.

56. Burnum-Johnson KE, Kyle JE, Eisfeld AJ, Casey CP, Stratton KG, Gonzalez JF, Habyarimana F, Negretti NM, Sims AC, Chauhan S, Thackray LB, Halfmann PJ, Walters KB, Kim Y-M, Zink EM, Nicora CD, Weitz KK, Webb-Robertson B-JM, Nakayasu ES, Ahmer B, Konkel ME, Motin V, Baric RS, Diamond MS, Kawaoka Y, Waters KM, Smith RD, Metz TO. 2017. MPLEx: a method for simultaneous pathogen inactivation and extraction of samples for multi-omics profiling. The Analyst 142:442–448.

57. Kim Y-M, Nowack S, Olsen MT, Becraft ED, Wood JM, Thiel V, Klapper I, Kühl M, Fredrickson JK, Bryant DA, Ward DM, Metz TO. 2015. Diel metabolomics analysis of a hot spring chlorophototrophic microbial mat leads to new hypotheses of community member metabolisms. Front Microbiol 6:209.

58. Hiller K, Hangebrauk J, Jäger C, Spura J, Schreiber K, Schomburg D. 2009. MetaboliteDetector: Comprehensive Analysis Tool for Targeted and Nontargeted GC/MS Based Metabolome Analysis. Anal Chem 81:3429–3439.

59. Boyle EI, Weng S, Gollub J, Jin H, Botstein D, Cherry JM, Sherlock G. 2004. GO::TermFinder--open source software for accessing Gene Ontology information and finding significantly enriched Gene Ontology terms associated with a list of genes. Bioinformatics 20:3710–3715.

60. Supek F, Bošnjak M, Škunca N, Šmuc T. 2011. REVIGO Summarizes and Visualizes Long Lists of Gene Ontology Terms. PLoS ONE 6:e21800.

61. Heberle H, Meirelles GV, da Silva FR, Telles GP, Minghim R. 2015. InteractiVenn: a web-based tool for the analysis of sets through Venn diagrams. BMC Bioinformatics 16.

62. Babicki S, Arndt D, Marcu A, Liang Y, Grant JR, Maciejewski A, Wishart DS. 2016. Heatmapper: web-enabled heat mapping for all. Nucleic Acids Res 44:W147–W153.

63. Croft D, O'Kelly G, Wu G, Haw R, Gillespie M, Matthews L, Caudy M, Garapati P, Gopinath G, Jassal B, Jupe S, Kalatskaya I, Mahajan S, May B, Ndegwa N, Schmidt E, Shamovsky V, Yung C, Birney E, Hermjakob H, D'Eustachio P, Stein L. 2011. Reactome:

a database of reactions, pathways and biological processes. Nucleic Acids Res 39:D691–D697.

64. Haw R, Hermjakob H, D'Eustachio P, Stein L. 2011. Reactome pathway analysis to enrich biological discovery in proteomics data sets. PROTEOMICS 11:3598–3613.

65. Duy J, Koehler JW, Honko AN, Minogue TD. 2015. Optimized microRNA purification from TRIzol-treated plasma. BMC Genomics 16:95.

66. Shurtleff A, Garza N, Lackemeyer M, Carrion R, Griffiths A, Patterson J, Edwin S, Bavari S. 2012. The Impact of Regulations, Safety Considerations and Physical Limitations on Research Progress at Maximum Biocontainment. Viruses 4:3932–3951.

67. Blow JA, Dohm DJ, Negley DL, Mores CN. 2004. Virus inactivation by nucleic acid extraction reagents. J Virol Methods 119:195–198.

68. Blumberg BM, Chan J, Udem SA. 1991. Function of Paramyxovirus 3′ and 5′ End Sequences, p. 235–247. *In* Kingsbury, DW (ed.), The Paramyxoviruses. Springer US, Boston, MA.

69. Rojas M, Arias CF, López S. 2010. Protein Kinase R Is Responsible for the Phosphorylation of eIF2α in Rotavirus Infection. J Virol 84:10457–10466.

70. Sadler AJ, Williams BRG. 2007. Structure and function of the protein kinase R. Curr Top Microbiol Immunol 316:253–292.

71. Habjan M, Pichlmair A, Elliott RM, Overby AK, Glatter T, Gstaiger M, Superti-Furga G, Unger H, Weber F. 2009. NSs Protein of Rift Valley Fever Virus Induces the Specific Degradation of the Double-Stranded RNA-Dependent Protein Kinase. J Virol 83:4365–4375.

72. Ikegami T, Narayanan K, Won S, Kamitani W, Peters CJ, Makino S. 2009. Rift Valley Fever Virus NSs Protein Promotes Post-Transcriptional Downregulation of Protein Kinase PKR and Inhibits eIF2α Phosphorylation. PLoS Pathog 5:e1000287.

73. Hajnóczky G, Csordás G, Das S, Garcia-Perez C, Saotome M, Sinha Roy S, Yi M. 2006. Mitochondrial calcium signalling and cell death: Approaches for assessing the role of mitochondrial Ca2+ uptake in apoptosis. Cell Calcium 40:553–560.

74. McBride HM, Neuspiel M, Wasiak S. 2006. Mitochondria: More Than Just a Powerhouse. Curr Biol 16:R551–R560.

75. Anand SK, Tikoo SK. 2013. Viruses as Modulators of Mitochondrial Functions. Adv Virol 2013:1–17.

76. Khan M, Syed GH, Kim S-J, Siddiqui A. 2015. Mitochondrial dynamics and viral infections: A close nexus. Biochim Biophys Acta BBA - Mol Cell Res 1853:2822–2833.

77. Tanner LB, Chng C, Guan XL, Lei Z, Rozen SG, Wenk MR. 2014. Lipidomics identifies a requirement for peroxisomal function during influenza virus replication. J Lipid Res 55:1357–1365.

78. Waheed AA, Freed EO. 2010. The Role of Lipids in Retrovirus Replication. Viruses 2:1146–1180.

79. Kloetzel P-M. 2004. The proteasome and MHC class I antigen processing. Biochim Biophys Acta BBA - Mol Cell Res 1695:225–233.

80. Sijts EJAM, Kloetzel P-M. 2011. The role of the proteasome in the generation of MHC class I ligands and immune responses. Cell Mol Life Sci 68:1491–1502.

81. Cox J, Mann M. 2011. Quantitative, High-Resolution Proteomics for Data-Driven Systems Biology. Annu Rev Biochem 80:273–299.

82. Diamond DL, Jacobs JM, Paeper B, Proll SC, Gritsenko MA, Carithers RL, Larson AM, Yeh MM, Camp DG, Smith RD, Katze MG. 2007. Proteomic profiling of human liver biopsies: Hepatitis C virus–induced fibrosis and mitochondrial dysfunction. Hepatology 46:649–657.

83. Scaturro P, Stukalov A, Haas DA, Cortese M, Draganova K, Płaszczyca A, Bartenschlager R, Götz M, Pichlmair A. 2018. An orthogonal proteomic survey uncovers novel Zika virus host factors. Nature 561:253.

84. Weekes MP, Tomasec P, Huttlin EL, Fielding CA, Nusinow D, Stanton RJ, Wang ECY, Aicheler R, Murrell I, Wilkinson GWG, Lehner PJ, Gygi SP. 2014. Quantitative Temporal Viromics: An Approach to Investigate Host-Pathogen Interaction. Cell 157:1460.

85. Berard AR, Coombs KM, Severini A. 2015. Quantification of the Host Response Proteome after Herpes Simplex Virus Type 1 Infection. J Proteome Res 14:2121–2142.

86. Karniely S, Weekes MP, Antrobus R, Rorbach J, Haute L van, Umrania Y, Smith DL, Stanton RJ, Minczuk M, Lehner PJ, Sinclair JH. 2016. Human Cytomegalovirus Infection Upregulates the Mitochondrial Transcription and Translation Machineries. mBio 7:e00029-16.

87. Villeneuve LM, Purnell PR, Stauch KL, Callen SE, Buch SJ, Fox HS. 2016. HIV-1 transgenic rats display mitochondrial abnormalities consistent with abnormal energy generation and distribution. J Neurovirol 22:564–574.

88. Kvansakul M. 2017. Viral Infection and Apoptosis. Viruses 9.

89. Okamoto T, Suzuki T, Kusakabe S, Tokunaga M, Hirano J, Miyata Y, Matsuura Y. 2017. Regulation of Apoptosis during Flavivirus Infection. Viruses 9.

90. Shim JM, Kim J, Tenson T, Min J-Y, Kainov DE. 2017. Influenza Virus Infection, Interferon Response, Viral Counter-Response, and Apoptosis. Viruses 9.

91. Dykxhoorn DM, Lieberman J. 2006. Silencing Viral Infection. PLoS Med 3:e242.

92. Jeang K-T. 2012. RNAi in the regulation of mammalian viral infections. BMC Biol 10:58.

93. Obbard DJ, Gordon KH., Buck AH, Jiggins FM. 2009. The evolution of RNAi as a defence against viruses and transposable elements. Philos Trans R Soc B Biol Sci 364:99–115.

94. Cullen BR. 2014. Viruses and RNA Interference: Issues and Controversies. J Virol 88:12934–12936.

95. Wilson RC, Doudna JA. 2013. Molecular Mechanisms of RNA Interference. Annu Rev Biophys 42:217–239.

96. Petit T, Diderich JA, Kruckeberg AL, Gancedo C, Van Dam K. 2000. Hexokinase Regulates Kinetics of Glucose Transport and Expression of Genes Encoding Hexose Transporters in Saccharomyces cerevisiae. J Bacteriol 182:6815–6818.

97. Owen OE, Kalhan SC, Hanson RW. 2002. The Key Role of Anaplerosis and Cataplerosis for Citric Acid Cycle Function. J Biol Chem 277:30409–30412.

98. Casola A, Rockx B, Halliday H, Escaffre O, Borisevich V. 2015. Oxidative stress in Nipah virus-infected human small airway epithelial cells. J Gen Virol 96:2961–2970.

99. Jamaluddin M, Tian B, Boldogh I, Garofalo RP, Brasier AR. 2009. Respiratory Syncytial Virus Infection Induces a Reactive Oxygen Species-MSK1-Phospho-Ser-276 RelA Pathway Required for Cytokine Expression. J Virol 83:10605–10615.

100. Garofalo RP, Kolli D, Casola A. 2013. Respiratory Syncytial Virus Infection: Mechanisms of Redox Control and Novel Therapeutic Opportunities. Antioxid Redox Signal 18:186–217.

101. Khomich OA, Kochetkov SN, Bartosch B, Ivanov AV. 2018. Redox Biology of Respiratory Viral Infections. Viruses 10.

102. Twig G, Hyde B, Shirihai OS. 2008. Mitochondrial fusion, fission and autophagy as a quality control axis: The bioenergetic view. Biochim Biophys Acta BBA - Bioenerg 1777:1092–1097.

103. Sugai A, Sato H, Takayama I, Yoneda M, Kai C. 2017. Nipah and Hendra Virus Nucleoproteins Inhibit Nuclear Accumulation of Signal Transducer and Activator of Transcription 1 (STAT1) and STAT2 by Interfering with Their Complex Formation. J Virol 91:e01136-17.

104. Molecular mechanism of influenza A NS1-mediated TRIM25 recognition and inhibition | Nature Communications.

CONCLUSION

While many viruses and other pathogens, represent threats to human and animal health, Nipah virus (NiV) and similar members of the expanding genus *Henipavirus* stand out based on very high human mortality rates, numerous modes of transmission including through aerosols, extremely broad range of mammalian hosts, and lack of approved treatments or vaccines. At the time of this dissertation, NiV is still a relatively newly discovered virus, having first been identified about twenty years ago. Together, the potential of NiV and related viruses as major threats to global health as well as how little is still understood about their life cycles has driven the research described in previous chapters.

In Chapter 2, we challenged the previous model of the NiV matrix protein as being the only protein important for viral budding. We reported that the fusion protein (F), essential for viral entry and previously reported to be capable of producing virus-like particles (VLPs), was supportive for the incorporation of the NiV attachment (G) glycoprotein. While we found that the M protein was also individually supportive of G incorporation, F and M together were most efficient. This role is important in the production of infectious particles because both F and G are absolutely essential for NiV-driven membrane fusion required for viral entry. We further found that this novel role of NiV F was dependent on individual motifs and residues within its cytoplasmic tail, indicating potential reliance on cellular factors. The importance of F in budding was made clearer when one of the faulty-budding F mutants was co-expressed with both M and G. Despite the presence of M, we found no such increase in the presence of the faulty F mutant, which suggests that the budding behavior of G is more strongly

associated with that of F. This hypothesis is supported by well-studied and strong interactions between F and G, whereas no direct interactions have been reported for either F or G with M.

In Chapter 3, we next sought to expand upon these findings by looking at the involvement of cellular machinery during budding. To do so, we produced VLPs from several combinations of F, G, and M and analyzed them proteomically. We found that VLPs derived from combinations that contained F tended to have the greatest numbers of cellular factors. By assessing our list of cellular factors incorporated into VLPs produced from F, G, and M together, we then found that most factors were associated with vesicular trafficking and/or the cytoskeleton. To better understand how these processes modulated the budding mechanisms of F, G, and M, we assessed how well each of these NiV proteins individually produced particles after co-expression of dominant-negative or constitutively-active mutants of key factors associated with vesicular trafficking and the cytoskeleton. Further supporting the model that NiV F budding requires interactions between motifs of its cytoplasmic tail and cellular machinery, we found that F was most affected by these mutant cellular factors. Specifically, the results from these studies indicated that efficient F budding is dependent on endocytosis and recycling, as well as the proper function of ESCRTs. The importance of F budding for G incorporation was further supported since co-expression of F, G, and M along with several of these mutant cellular factors led to normal M budding but greatly reduced F and G budding. Since 97 cellular proteins were identified in FMG VLPs, one major avenue of further research expanding upon these findings will be to identify which of these individual proteins are important for F, G, and M budding as

well as by which mechanisms.

While Chapter 3 utilized high-throughput proteomics to better understand NiV particle formation, we chose next to expand our focus to investigate all changes to a host cell during infection with “live” virus. Using several bioinformatic tools, we identified many, specific cellular processes that were altered over time-course of NiV infection, indicated by drastic changes in the abundances of proteins involved in said processes. Interestingly, we found that transcriptomic changes failed to predict changes in protein abundance during infection, whether on a protein-by-protein basis or based on processes affected. This discrepancy between transcriptomics and proteomics suggests that post-transcriptional regulation of gene expression may be crucial in shaping infection. Evidence for alteration to post-transcriptional regulation of gene expression was further found by consistent and significant changes in the abundances of proteins involved in RNA processing, translation, and proteasome-dependent degradation. Importantly, we reported highly consistent increases in proteins produced in the cytosol and imported into mitochondria as well as those produced within mitochondria directly. These findings, supported by lipidomics and metabolomics, strongly suggest that mitochondria are a major target of NiV to support infection; however, the means by which these organelles are modulated is unknown. While the multi-omics approach described in chapter 4, offers new insight into actual changes during infection and will support the identification of new means of cellular manipulation by NiV and related viruses, much remains unclear. Other recent studies have identified cellular factors that interact with each of the NiV proteins; however, significant work is still needed to tie those interactions with the cellular changes we have reported. Another informative

avenue of future study would be to assess NiV infection using phosphoproteomics to better understand how the actual activities of major cellular processes is affected.

Together, the described studies have offered new insights into many aspects of NiV infection, with particular interest in the budding of new virus particles. We earnestly hope that the continued use of high-throughput techniques such as proteomics in combination with more traditional methods for studying viruses will support the development of future therapeutics and particle-based vaccines capable of reducing the threats that NiV and related viruses pose to global human and animal health.